N° d'ordre : **2634**

THÈSE

présentée à

L'UNIVERSITÉ BORDEAUX I

ÉCOLE DOCTORALE DES SCIENCES PHYSIQUES ET DE L'INGÉNIEUR

par **Guillaume NEAU**

ingénieur MATMECA

POUR OBTENIR LE GRADE DE

DOCTEUR

SPÉCIALITÉ : **MÉCANIQUE**

Ondes de Lamb dans des plaques anisotropes viscoélastiques. Etude des fronts d'onde et atténuation.

Lamb waves in anisotropic viscoelastic plates. Study of the wave fronts and attenuation.

Soutenue le : 8 janvier 2003

Après avis de :

MM. O. LEROY, Professeur émérite, Institut Catholique de Louvain,
N. SAFFARI, Lecturer, University College London.

Devant la commission d'examen formée de :

MM. B. AUDOIN, Professeur, Université Bordeaux 1,
M. DESCHAMPS, Directeur de Recherche, CNRS,
O. LEROY, Professeur Emérite, Institut Catholique de Louvain,
M.J.S. LOWE, Senior Lecturer, Imperial College,
D. ROYER, Professeur, Université Paris 7,
N. SAFFARI, Lecturer, University College London.

-2003-

Remerciements

Cette thèse a le label européen et a été réalisé dans deux pays de la communauté. Les recherches se sont déroulées pour moitié au sein de l'équipe Propagation Acoustique et Ultrasons Laser du Laboratoire de Mécanique Physique de l'Université de Bordeaux 1, et au sein de l'équipe du Non-Destructive Testing Laboratory, de l'Imperial College de Londres.

Je tiens à remercier le Professeur D. Desjardins de l'Université de Bordeaux 1, ainsi que le Professeur P. Cawley de l'Imperial College, pour m'avoir accueilli dans leur laboratoire respectif.

I would like to thank Professor O. Leroy, Professor Emeritus from the Institut Catholique de Louvain and Dr. N. Saffari, from University College London, for accepting to examine my work.

Le Professeur D. Royer, de l'Université Paris 7, m'a fait l'honneur de présider le jury d'examen. Qu'il voit en ces mots toute la gratitude et le profond respect d'un étudiant qui s'est longtemps penché sur "*Ondes élastiques dans les solides*", pour comprendre de nombreux aspects de la propagation d'ondes.

Mes remerciements s'adressent également au Professeur Bertrand Audoin, de l'Université de Bordeaux 1, non seulement pour sa participation au jury de thèse mais aussi pour nos nombreuses discussions bénéfiques.

Je tiens à exprimer ma reconnaissance à Marc Deschamps, Directeur de Recherche CNRS au LMP et à Mike Lowe, Senior Lecturer à l'Imperial College, pour avoir encadré mes travaux pendant ces trois années. A cette équipe d'encadrement, j'associe Olivier Poncelet, Chargé de Recherche CNRS au LMP. Sa pédagogie et ses qualités scientifiques font de lui un modèle et un allié d'une valeur inestimable pour un étudiant. A eux trois, ils représentent l'équipe idéale sur les plans scientifiques et humains, et garantissent le succès de leurs thésards. Je réalise la chance que j'ai eue de pouvoir travailler avec eux, et je les en remercie chaleureusement.

I would like to address my warm thanks to Professor Alexander Shuvalov, AKA Sacha, for his valuable help on many scientific problems, as well as on the writing in English. I am quite sure that Mike noticed some variations in the writing style of the thesis! I also want to thank him very much for his involvement in my work.

I want to express many thanks to both NDT and LMP crews which I truly enjoy to work with. I think of Thomas Vogt, Olivier Diligent, Mark Evans, Paul Wilcox, Rob Long, Greg Gondek, Francesco Simonetti, Alex Demma, Malcolm Beard, Jon Allin, Keith Vine, Brian Pavlakovic, Dave Alleyne, Jimmy Fong, and Richard Seppings for the English side.

Du côté français, je pense à Arnaud Bernard, Nicolas Leymarie, Manu Leclézio, Fred Reverdy, Stéphanie Rousserie, Clément Rossignol, Jérome Dufaure, Matthieu Léger, Raynald Laheurte, Cécile Baron, Marie Cinquin, Hinde Meri, Guillaume Huet, Franck Le Poulain, Thomas Lubet, Sylvain Laporte, Marion Lamazouade, et une mention spéciale à Béa Desoudin pour sa disponibilité.

I finally want to thank the American side Seiji Nakagawa, Kurt Nihei, Daniel Turler and particularly Deb Hopkins for their mind-opening effect.

Merci à mes parents pour leur soutien.

Merci à ma Anne.

Contents

Introduction

De nombreuses méthodes de contrôle non-destructif (CND) ont émergé ces récentes années. Impliquant de nombreux domaines de la physique comme les rayons X, la thermique ou les ultrasons, ces méthodes ont l'avantage de permettre le suivi de la qualité d'une structure au cours de sa vie, sans avoir à l'endommager. Les domaines d'application du CND sont variés. Le besoin de détecter les défauts ou les points de corrosion éventuellement présents dans les sites de stockages de produits toxiques en est un. La conservation dans des conditions idéales des produits pétroliers dans des cuves cylindriques, aussi bien que les déchets nucléaires dans des fûts bétonnés ou dans des caves granitiques, nécessite un contrôle permanent de l'étanchéité des structures contenant ces produits. Le transport de produits dangereux ou non (pipelines, conduites d'eau) est également un sujet se prêtant à l'étude de la salubrité des canalisations transportant ces substances. L'industrie aéronautique a besoin de s'assurer de la qualité structurale des composants utilisés dans la conception des avions. Dans tous ces exemples, ces fissures, ces vides, ces délaminages peuvent être la source de défauts préjudiciables à la sécurité.

Concernant les ultrasons, les méthodes de contrôle par transmission ou réflexion ont largement été étudiées et ont prouvé leur efficacité. Ces techniques conventionnelles utilisant les ondes de volumes, restituent précisément la forme et la localisation des défauts (Hosten, B., 1991; Kundu, T., Ehsani, M. et al., 1999; Gan, T.H., Hutchins, D.A. et al., 2001) mais nécessitent un temps de contrôle assez long, et ce d'autant plus que la structure à tester est grande. Des ondes se propageant sur de longues distances permettraient un contrôle plus rapide.

Ces ondes existent, elles sont guidées par la géométrie de la structure insonifiée et sont appelées ondes de Lamb. Guidées par des plaques, des coques ou des tuyaux cylindriques, ces ondes se propagent dans des structures de faible épaisseur devant les autres dimensions. Elles existent dans les milieux isotropes et anisotropes.

Elles ont été découvertes au début du XX$^{\text{ème}}$ siècle (Lamb, H., 1917), après les études fondamentales sur les ondes de volume décrites par Christoffel (Christoffel, E.B., 1877), et sur les ondes de surface étudiées par Rayleigh (Rayleigh, L., 1885). Les ondes de volumes, solution de l'équation du mouvement en milieu infini, sont entièrement caractérisées par les propriétés du matériau insonifié et la direction de propagation. Elles sont largement utilisées dans le cadre de la caractérisation de matériau (Chu, Y.C. and Rokhlin, S.I., 1994), et pour l'imagerie des défauts de structures (Cawley, P., 1987; Gruber, J.J., Smith, J.M. et al., 1988). L'onde de surface, dont la recherche a été motivée par la géophysique dans le cadre de l'étude des séismes (Biot, M.A., 1952; Dorman, J., Ewing, M. et al., 1960), fait intervenir une interface libre du milieu semi infini considéré. L'onde de Lamb fait intervenir toute l'épaisseur du guide et présente la particularité d'être dispersive. L'étude de telles ondes a naturellement débuté sur des matériaux isotropes, pour lesquelles les ondes de Lamb (couplage entre polarisations transverses verticales et longitudinales) et les ondes transverses horizontales (SH) sont découplées. Depuis, le terme « ondes de Lamb » s'est généralisé aux ondes guidées se propageant dans les directions principales ou non de plaques anisotropes. Les ondes de Lamb sont étudiées et utilisées dans de nombreux domaines de contrôle non-destructif. Elles servent par exemple à la détection de délaminages (Rokhlin, S., 1979; Guo, N. and Cawley, P., 1993; Tan, K.S., Guo, N. et al., 1995; Leclezio, E., 2002), de corrosion (Sun, K., J., and Johnston, P., H.,, 1995; Cawley, P. and Alleyne, D., 1996), à tester l'adhésion de structures collées (Lowe, M.J.S. and Cawley, P., 1994; Nagy, P.B., 1994; Challis, R.E., Bork, U. et al., 1996; Kundu, T., Maji, A. et al., 1998), et à la caractérisation de matériaux (Nagy, P.B. and Adler, L., 1989; Bar-Cohen, Y. and Mal, A.K., 1990; Chimenti, D.E., 1997).

Grâce à leur bon compromis masse-robustesse, l'utilisation des composites dans l'industrie aéronautique s'est répandue. En conséquence, l'étude de la propagation des ondes guidées dans les matériaux anisotropes s'est développée (Nayfeh, A.H. and Chimenti, D.E., 1988; Dayal, V. and Kinra, V.K., 1989; Ditri, J.J. and Rose, J.L., 1994). La synthèse des matériaux composites, par empilement de fibres pré-imprégnées dans des orientations particulières, privilégie certaines directions pour la propagation de l'énergie. Le phénomène de déviation de faisceau, connu pour les ondes de volumes, est également observé pour les ondes guidées se propageant dans les directions non-principales des plaques anisotropes. En plus de la dispersion fréquentielle des ondes de Lamb se propageant en milieu isotrope, il faut prendre en compte la dispersion angulaire induite par l'anisotropie. La connaissance des propriétés de phase et d'énergie des ondes de guidées dans ces matériaux est primordiale pour une bonne utilisation de leur potentiel de contrôle. C'est l'objet du travail présenté.

Le chapitre 1 détaille le cadre théorique des ondes de Lamb dans une plaque orthotrope. Les courbes de dispersion (variation de la vitesse de phase avec la fréquence), ainsi que les propriétés de groupe (vitesse et angle de déviation) y sont décrites. Ces paramètres sont également étudiés en fonction de la direction de phase, variant entre les axes principaux du matériau. Faisant référence aux travaux de (Simon, C., 1997), la difficulté de nommer les modes de Lamb pour toutes les directions de propagations est abordée. En effet, les propriétés des modes guidés varient en fonction de la fréquence et de la direction de phase, y compris la polarisation. Ainsi, il apparaît que les propriétés de chaque mode de Lamb généralisé peuvent être représentées en 3D. Cette visualisation est nouvelle et constitue l'apport de cette première section. L'étude se restreint toutefois au cas purement élastique, le cas absorbant étant abordé au chapitre suivant.

Le chapitre 2 étend donc l'étude théorique des ondes de Lamb aux matériaux anisotropes viscoélastiques. Les modèles rhéologiques les plus communs y sont décrits, ainsi que leur conséquence sur la propagation des ondes guidées. L'atténuation des ondes guidées y est étudiée, à la fois en fonction de la fréquence et de la direction de phase. Toutefois, seule l'atténuation causée par la viscosité du matériau est étudiée dans ce chapitre. D'un point de vue expérimental, la diffraction du faisceau due à la taille finie de la source et la diffusion causée par les fibres de verre ou de carbone sont en partie responsable de l'atténuation des ondes. Pour les fréquences utilisées dans ce travail, les longueurs d'onde seront de l'ordre de quelques centimètres. Dans ces conditions le matériau insonifié est perçu comme homogène et la diffusion par les fibres du composite peut être négligée. En ce qui concerne la diffraction, les mesures d'atténuation seront réalisées assez loin de la source, dans une zone où la décroissance en fonction de la distance a une importance moindre. Ces phénomènes ne sont donc pas pris en compte dans cette étude, qui se focalise sur l'atténuation causée par la viscosité du matériau. Comme pour les vitesses de phase et de groupe décrites dans le 1er chapitre, il est également possible de représenter l'évolution de l'atténuation en 3D, ce qui est la nouveauté apportée par cette étude. En milieu viscoélastique, il n'est cependant pas simple de définir une vitesse de groupe qui ait un sens physique. Pour compléter l'étude des ondes de Lamb, il est nécessaire de décrire la propagation de l'énergie. C'est un des thèmes du chapitre 3.

Le chapitre 3 s'attache en effet à définir la vitesse d'énergie des ondes de Lamb en milieu anisotrope viscoélastique, à partir du vecteur de Poynting. En se rapprochant de la configuration expérimentale « source ponctuelle/récepteur ponctuel », les propriétés des ondes de Lamb sont étudiées le long de la direction d'observation. Cette représentation se distingue de la dispersion du module de la vitesse de groupe, présentée pour une seule direction de front de phase, qui nécessite, pour une information complète sur le vecteur vitesse d'énergie, l'association de la dispersion de la direction d'énergie. Les dispersions de la vitesse d'énergie, ainsi que de l'atténuation sont présentées le long de la direction d'énergie. Cela permet de suivre la naissance et la disparition de cornes sur les surfaces d'ondes des modes guidées, en fonction de la fréquence. De plus, l'étude théorique de l'atténuation le long du rayon met en lumière la signification physique de la projection de l'atténuation de phase sur la direction d'énergie. Autant que l'auteur le sache, ce domaine n'a pas été étudié et constitue la nouveauté apportée par cette partie.

Le chapitre 4 se concentre sur l'illustration expérimentale des propriétés décrites dans les précédents chapitres. Les expériences sont réalisées sur des composites uni-directionnels de verre et de carbone époxy. Elles portent successivement sur la mesure de la vitesse d'énergie pour toutes les directions d'observation, la mise en évidence de la déviation de faisceau pour une direction de phase particulière et sur l'atténuation le long de la direction de phase et d'énergie des ondes de Lamb. Il faut noter dans cette partie la nouveauté apportée par les mesures de vitesse d'énergie dans la zone de corne, ainsi que les mesures d'atténuation des ondes guidées se propageant dans des directions non-principales. Au travers des résultats obtenus, la prise en compte de tous les paramètres des ondes de Lamb se propageant dans des matériaux anisotropes viscoélastiques s'avère essentielle. Une attention particulière est portée sur le potentiel d'application des ondes guidées à la caractérisation de tels matériaux.

Introduction

Numerous non-destructive evaluation (NDE) methods have emerged in recent years. Involving various domains of Physics, such as X-rays, heat-transfer, or ultrasound, the advantage of these methods is that they enable the monitoring of the integrity of structures during their life, without having to destroy them.

The applications field of NDE is varied. The aeronautic industry needs to ensure the structural integrity of components used in the manufacturing of aircraft. The need to detect defects or corrosion zones which may occur in toxic chemicals storage sites is also important. The preservation in ideal conditions of oil in cylindrical tanks, as well as of nuclear wastes in concrete containers or in granite caves, requires frequent inspection of the waterproofness of the structures containing these chemicals. The transport of material which may be dangerous, is also a topic for which the study of the integrity of pipes is required. For all these examples, defects such as cracks, voids, and delaminations can be prejudicial to safety.

Concerning ultrasound, the transmission and reflection testing methods have been studied extensively and have proved to be very effective. These conventional techniques enable the rendering of the shape and location of the defects, but are time-demanding, especially for large structures. Waves which are able to propagate over these large distances would facilitate faster inspection.

Such waves exist. They are guided by the geometry of the insonified structure and are called Lamb waves. Guided by plates, cylindrical pipes or shells, these waves propagate in structures for which the thickness is small compared to other dimensions. They can propagate in isotropic or anisotropic media.

Lamb waves were discovered at the beginning of the XXth century (Lamb, H., 1917), after fundamental studies on bulk waves described by Christoffel (Christoffel, E.B., 1877), and suface waves studied by Rayleigh (Rayleigh, L., 1885). Bulk waves, being the solution of the equation of motion in infinite media, are entirely characterised by the properties of the insonified material and the direction of propagation. They are widely used in the context of material characterisation (Hosten, B., 1991; Chu, Y.C. and Rokhlin, S.I., 1994), and for the imaging of defects in structure (Cawley, P., 1987; Gruber, J.J., Smith, J.M. et al., 1988). The surface wave, for which the research has been motivated by geophysics for earthquake studies (Biot, M.A., 1952; Dorman, J., Ewing, M. et al., 1960), involves a free interface of a semi-infinite medium. The Lamb wave involves the whole thickness of a layer of material (the waveguide) and has the particularity of being dispersive. The study of such waves naturally began with isotropic materials, for which the Lamb waves (coupling between the transverse vertical and longitudinal polarisations) and the shear horizontal waves (SH) are uncoupled. Since then, the term “Lamb waves” has been generalised to include guided waves propagating in principal or non-principal directions of anisotropic plates. Lamb waves are studied and applied in numerous domains of NDE. For instance, they are useful for the detection of delaminations (Rokhlin, S., 1979; Guo, N. and Cawley, P., 1993; Tan, K.S., Guo, N. et al., 1995; Leclezio, E., 2002), of corrosion (Sun, K., J., and Johnston, P., H.,, 1995; Cawley, P. and Alleyne, D., 1996), for the testing of adhesion of bonded structures (Lowe, M.J.S. and Cawley, P., 1994; Nagy, P.B., 1994; Challis, R.E., Bork, U. et al., 1996; Kundu, T., Maji, A. et al., 1998), and for material characterisation (Nagy, P.B. and Adler, L., 1989; Bar-Cohen, Y. and Mal, A.K., 1990; Chimenti, D.E., 1997).

Thanks to their good strength-weight ratio, the use of fibre composites in aeronautics has increased. Consequently, the study of the propagation of guided waves in anisotropic materials has been developed (Nayfeh, A.H. and Chimenti, D.E., 1988; Dayal, V. and Kinra, V.K., 1989; Ditri, J.J. and Rose, J.L., 1994). Due to the manufacturing process of composites, using the piling of pre-impregnated fibres in particular orientations, some directions are privileged for the transport of energy of the guided waves. The phenomenon of beam deflection (or skewing), well-known for bulk waves in anisotropic materials, occurs for the guided waves which propagate in non-principal directions of anisotropic plates. On top of the frequency dispersion of the Lamb waves, which is already a property of waves in isotropic media, angular dispersion, caused by the anisotropy, has to be taken into account. The knowledge of the phase and energy properties of the guided waves travelling in such materials is of primary importance for the full exploitation of their inspection potential. This is the topic of the thesis.

The first chapter presents the theoretical framework of Lamb waves in an orthotropic plate. The dispersion curves (dependence of the phase velocity with the frequency), as well as the group properties (velocity and deviation angle), are described. Those parameters are also studied as a function of the phase front direction, varying between the principal axes of the material. Referencing the work of Simon (Simon, C., 1997), the problem of naming the Lamb modes for all directions is addressed. The properties of guided modes vary as a function of the frequency and as a function of the phase direction, and of their polarisation. Thus, as the originality of the work produced in this chapter, the properties of each generalised Lamb mode are represented using a 3D view. The study is however limited to the purely elastic case, the absorbing case being the focus of the following chapter.

Chapter 2 expands the theoretical study to the Lamb waves in anisotropic viscoelastic materials. The most common rheological models are described, along with their consequences on the propagation of guided waves. The attenuation of guided waves is studied, both as a function of the frequency and of the phase direction. However, only the attenuation caused by the viscosity is taken into account; attenuation caused by beam spreading and diffraction are neglected. The beam spreading is due to the finite size of the source and the diffraction is caused by the glass or carbon fibres. At the frequencies used in this work, the wavelengths are approximately in the order of a few centimetres. Under these assumptions, the insonified material is seen as homogeneous, and this allows the fibre diffraction to be neglected. Concerning the beam spreading, the measurements are realised quite far from the source, in a zone where the amplitude decrease as a function of the distance has relatively little effect. As for the phase and group velocities described in the first chapter, it is also possible to represent the dependence of the attenuation in a 3D plot, which is the novelty brought by this chapter. In a viscoelastic medium, it is however not straightforward to define the group velocity with a strict physical interpretation. In order to complete the study of the Lamb waves, it is necessary to describe the energy propagation. It is one of the topics of Chapter 3.

The third chapter is centred on the definition of the energy velocity of the Lamb modes in an anisotropic viscoelastic medium, from the Poynting vector. Getting closer to the “point source-point receiver” experimental configuration, the properties of the Lamb modes are studied along the observation direction. This representation is opposed to the dispersion of the group velocity modulus, presented in Chapter 1 for a fixed phase direction, which needs, for a complete description of the energy velocity vector, the association of the deviation angle dispersion. The dispersions of the energy velocity as well as the attenuation are now represented for a given energy direction. It enables the possibility of following the appearance and the vanishing of cusps on the wave surfaces, as a function of the frequency. Moreover, the theoretical study of the attenuation along the ray direction casts light on the physical interpretation of the projection of the phase attenuation onto the energy direction. To the best of the author’s knowledge, this part is new and has not been explored in the literature.

Chapter 4 is centred on the experimental illustration of the previously described properties. Experiments are realised on unidirectional glass and carbon-epoxy composites. They concern successively the measure of the energy velocity in all observation directions, the determination of the beam skewing angle for a selected phase direction, and the attenuation along the phase and energy directions of the Lamb waves. It is to be noted that the experimental observation of the energy velocities in the cusp region, as well as the attenuation measurements in non-principal direction of generalised Lamb modes is new. Through the obtained results, the knowledge of all the parameters of the Lamb waves propagating in an anisotropic viscoelastic medium are revealed to be essential. Particular attention is brought to the potential of using guided modes for materials characterisation.

Chapter 1

Lamb wave propagation in non-absorbing plates

1.1 Introduction

This chapter aims to review the equations and solutions of bulk waves propagating in an infinite anisotropic medium, before introducing the guided waves in plates, the so-called Lamb modes. In the first part of this chapter, solutions of the equation of motion for an anisotropic infinite medium are described. Studies of bulk waves have been published by many authors, and general works from (Auld, B.A., 1973; Royer, D. and Dieulesaint, E., 1996) and (Balasubramaniam, K. and Whitney, S.C., 1996) can be cited for instance. Through their use in material characterisation (Hosten, B., 1989; Audoin, B., Baste, S. et al., 1991; Castagnède, B., Kim, K.Y. et al., 1991), bulk modes are well exploited and referenced. The role of these so-called bulk mode solutions, that are eigenvalues and eigenvectors of the Christoffel equation, in the phenomenon of guided waves in a bounded geometry is then detailed. In the case of an anisotropic medium, the Lamb modes are indeed seen as the superposition of successive reflections of bulk modes inside the plate (Solie, L.P. and Auld, B.A., 1973), as the scalar and vector potentials commonly used in the isotropic case (Lamb, H., 1917) are too complicated to derive.

The equations of the Lamb modes as well as their solution are presented. Due to the increasing use of Lamb modes for non-destructive applications, many publications concerning Lamb wave modelling in both isotropic and anisotropic materials, are provided by the literature. Works from (Chimenti, D.E., 1997), (Simon, C., Kaczmarek, H. et al., 1997), that concern Lamb waves in general, as well as studies of their use on anisotropic material have been used. Publications on the use of Lamb waves for Non-Destructive-Testing (NDT) (Alleyne, D.N. and Cawley, P., 1991; Lowe, M.J.S., 1993), for paper characterization (Bonnin, A., Huchon, R. et al., 1999) or for material characterisation (Chimenti, D.E., 1997) have been of great help in writing the derivation section.

Having the characteristics of the Lamb modes, the third section focuses on their group velocity. The propagation properties of guided modes, such as the steering angle, the frequential and spatial dispersions developed in (Simon, C., Kaczmarek, H. et al., 1997; Poncelet, O., Deschamps, M. et al., 2000; Potel, C., Gatignol, P. et al., 2001) are detailed in this last section of the chapter.

1.2 Infinite media

An infinite orthotropic medium is considered. The elasticity tensor is described by the fourth rank tensor C_{ijkl}, and ρ is its mass density. The generalised Hook's law expresses the stress tensor σ_{ij} as a function of the stain tensor ε_{ij}. This well-known relationship is described by:

$$\sigma_{ij} = C_{ijkl}\varepsilon_{kl}. \tag{1.1}$$

In the case of a purely elastic medium, a small perturbation of the equilibrium of the particles, caused by a source, results in an endless motion of the particles. This motion, infinitely far and after the perturbation, is governed by:

$$\sigma_{ij,j} = \rho\,\partial_t V_i, \tag{1.2}$$

where V_i are the components of the particle velocity vector. Solutions of Eq. (1.2) are searched in the form of monochromatic waves with an angular frequency ω, a phase slowness vector $\boldsymbol{S}$, a polarisation vector $\boldsymbol{P}$ and an amplitude A. The displacement field $\boldsymbol{U}$ of this type of wave at a location $\boldsymbol{M}\left(x_1, x_2, x_3\right)$ can be expressed as:

$$U_i = AP_i \exp i\omega\left(t - S_1x_1 - S_2x_2 - S_3x_3\right), \tag{1.3}$$

where U_i are the components of the displacement field and S_i are the components of the slowness vector in the $\left(\boldsymbol{e}_1, \boldsymbol{e}_2, \boldsymbol{e}_3\right)$ coordinate system, see Fig.(1.1). Since the derivation of bulk solutions is going to be used for the Lamb solutions derivation, let us introduce the orientations of the coordinate system. The slowness vector can be decomposed into the component $\boldsymbol{S}_1$ and the component $\boldsymbol{S}_{//}$.

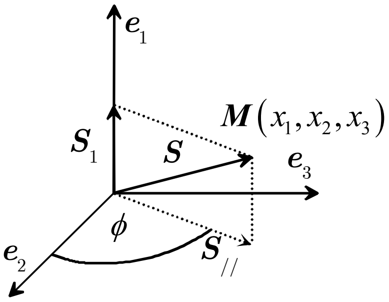

Figure 1.1: coordinate system.

The direction of $\boldsymbol{S}_{//}$ is ruled by the direction ϕ. The slowness vector can therefore be expressed as:

$$\boldsymbol{S} = \begin{pmatrix} S_1 \\ S_2 \\ S_3 \end{pmatrix} = \begin{pmatrix} S_1 \\ S_{//} \cos\phi \\ S_{//} \sin\phi \end{pmatrix}, \tag{1.4}$$

where $S_{//}$ designates the modulus of $\boldsymbol{S}_{//}$. (In this work all vectors are denoted using bold font and their modulus or components are expressed in normal font.)

Inserting the type of solution described in Eq.(1.3) into the equation of motion results in the well-known Christoffel equation. This system can be expressed in a matrix form, where the eigenvalues and eigenvectors of the Christoffel matrix fully provide the bulk modes (Auld, B.A., 1973; Royer, D. and Dieulesaint, E., 1996). The eigenvalues are indeed the squared phase velocities and the eigenvectors are the polarisation of these bulk solutions. Another expression can be obtained if the solutions are searched in terms of slowness rather than velocity. Writing the slowness vector $\boldsymbol{S}$ as the inverse of the phase velocity $\boldsymbol{V}_{ph}$ (inverse of the phase velocity modulus, collinear to the velocity direction), the solving of the equation of motion leads to nullifying the determinant of the matrix $\boldsymbol{\Gamma}_C$ described as:

$$\boldsymbol{\Gamma}_C = \begin{bmatrix} C_{11}S_1^2 + a_1 S_{//}{}^2 - \rho & a_{12} S_1 S_{//} & a_{13} S_1 S_{//} \\ & C_{66}S_1^2 + a_2 S_{//}{}^2 - \rho & a_{23} S_{//}{}^2 \\ & & C_{55}S_1^2 + a_3 S_{//}{}^2 - \rho \end{bmatrix}, \tag{1.5}$$

with

$$\begin{aligned} & a_1 = C_{66}\cos^2\phi + C_{55}\sin^2\phi;\ a_2 = C_{22}\cos^2\phi + C_{44}\sin^2\phi; \\ & a_3 = C_{44}\cos^2\phi + C_{33}\sin^2\phi;\ a_{12} = \left(C_{12} + C_{66}\right)\cos\phi; \\ & a_{13} = \left(C_{13} + C_{55}\right)\sin\phi;\ a_{23} = \left(C_{23} + C_{44}\right)\sin\phi\cos\phi. \end{aligned} \tag{1.6}$$

The determinant of $\boldsymbol{\Gamma}_C$ can be viewed as the sixth order polynomial form in S_1 or the third order polynomial form in S_1^2. This polynomial has to be solved to fully characterise the bulk modes able to propagate in the considered medium.

Having the solutions for the phase slowness, the polarisation can be obtained. Both the determinant of $\boldsymbol{\Gamma}_C$ and the polarisations of the solutions are expressed using the minors of $\boldsymbol{\Gamma}_C$. They are described as:

$$\begin{aligned} & \Delta_{11} = \Gamma_{22}\Gamma_{33} - \Gamma_{23}\Gamma_{23},\ \Delta_{12} = \Gamma_{12}\Gamma_{33} - \Gamma_{13}\Gamma_{23}, \\ & \Delta_{13} = \Gamma_{12}\Gamma_{23} - \Gamma_{13}\Gamma_{22}, \Delta_{22} = \Gamma_{11}\Gamma_{33} - \Gamma_{13}\Gamma_{13}, \\ & \Delta_{23} = \Gamma_{11}\Gamma_{23} - \Gamma_{13}\Gamma_{12},\ \Delta_{33} = \Gamma_{11}\Gamma_{22} - \Gamma_{12}\Gamma_{12}, \end{aligned} \tag{1.7}$$

where Γ_{ij} are the components of the matrix $\boldsymbol{\Gamma}_C$. The determinant of $\boldsymbol{\Gamma}_C$, denoted γ_C can be expressed as:

$$\gamma_C = \Gamma_{11}\Delta_{11} - \Gamma_{12}\Delta_{12} + \Gamma_{13}\Delta_{13}. \tag{1.8}$$

It is to be noted that there are two other forms to express γ_C. An arbitrary choice is made to use Eq.(1.8). Consistently with this choice, the polarisation vectors for each solution are described by:

$$\boldsymbol{P}^i = \begin{pmatrix} \Delta_{13}\left(S_1^i\right) \\ -\Delta_{23}\left(S_1^i\right) \\ \Delta_{33}\left(S_1^i\right) \end{pmatrix}, \tag{1.9}$$

where S_1^i are the solutions of $\gamma_C = 0$, and P_k^i are the components of the polarisation vector $\boldsymbol{P}^i$. Now being able to solve the equation of motion for a given component $S_{//}$ and a given phase direction ϕ, it is possible to plot the bulk solutions in polar coordinates.

Anticipating the interface geometry that is going to be developed in the next section, the plane $\left(\boldsymbol{e}_2, \boldsymbol{e}_3\right)$ of Fig.(1.2 e) can be seen as the azimuthal plane and the planes $\left(\boldsymbol{e}_1, \boldsymbol{e}_\phi\right)$ as zenithal planes. Solutions of the Christofel equation can be described using slowness surfaces. Cuts of these surfaces can be made. When the involved coordinates are S_1^i and $S_{//}$ the solution plot is called a slice of the slowness surface. When the involved coordinates are S_2 and S_3, the resulting plot concerns those skimming waves, for which the S_1^i component is null (Bescond, C. and Deschamps, M., 1998; Wu, T.T. and Liu, P.L., 1998). It is to be noted that these waves can also exist with the out of plane components, when the slowness surface exhibits a vertical tangent plane.

For an anisotropic material, the slowness surface does depend on the azimuthal angle ϕ. For instance, the example of a unidirectional carbon-epoxy is taken, for which the elasticity tensor is shown in Table (2.3) of Chapter 2. Fig.(1.2) represents the slowness surfaces for each type of the polarisation at different directions in plots a) to d), as well as the skimming waves in plot e). These plots do not depend on the frequency in the case of a purely elastic solid. In this figure, the polarisations are represented using a dashed line for the longitudinal mode, solid and dotted line for the transverse modes. The connection between plots a)-d) and e) is obvious since they correspond respectively to zenithal and azimuthal views of bulk modes. The intersections of plots a)-d) with the vertical axis do not depend on the phase direction. They are represented with trapezoids remaining at the same values for all phase directions. The intersections of plots a)-d) with the horizontal axis for phase direction of 0, 20, 60 and 90 degrees, represented respectively with discs, triangles, stars and squares, can be visualised on the skimming waves plot e) that lies in the azimuthal plane. As opposed to the variation of these values with the direction of the phase, the intersections with vertical axis are constant for any phase direction.

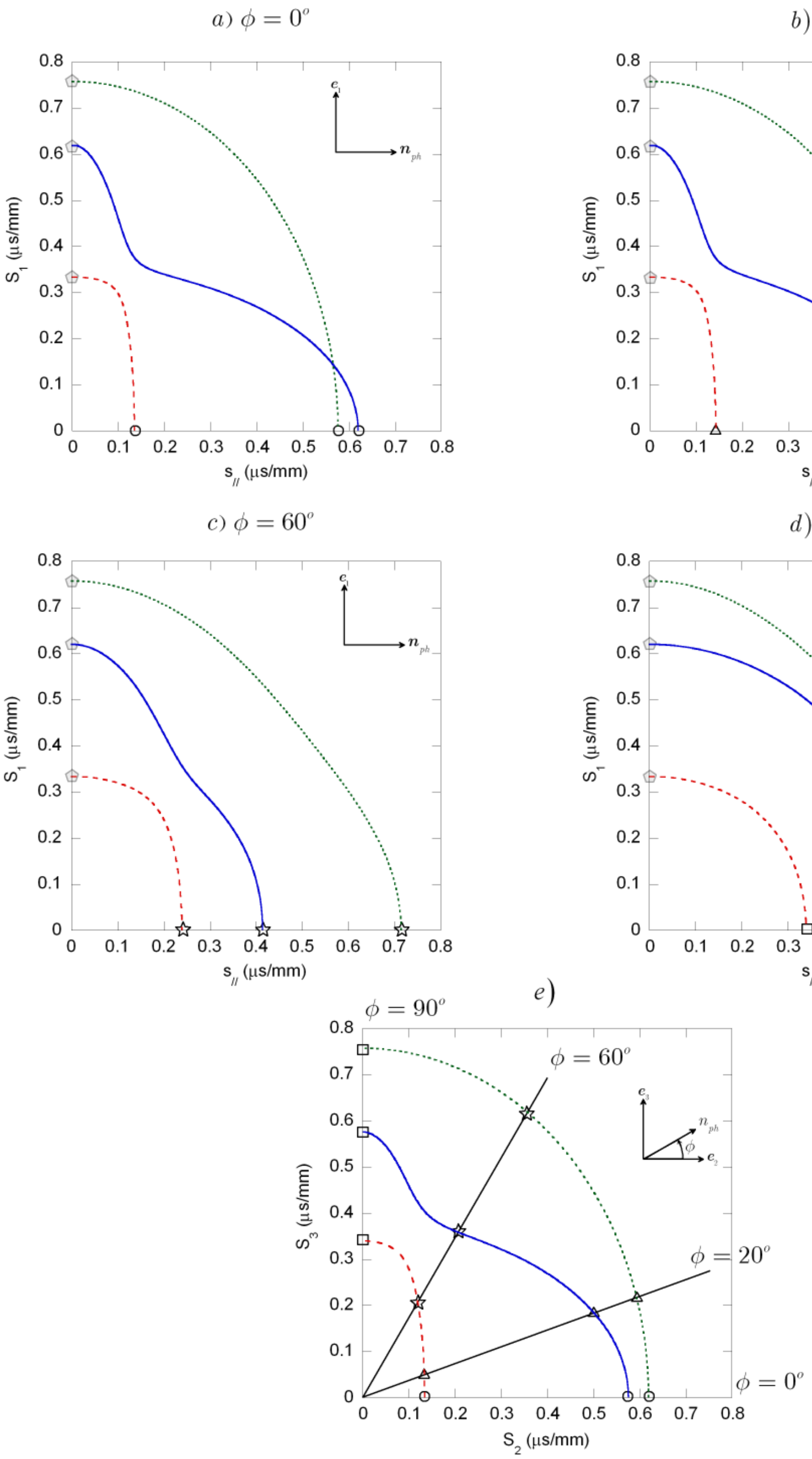

Figure 1.2: Slowness surfaces slices for the unidirectional carbon-epoxy plate. Plots a) to d) represent cuts of the bulk slowness surfaces for ϕ = 0 (fibres direction), 20, 60 and 90 degrees. Plot e) represents the solutions for which S_1 is null. Projections of the wave slownesses of plots a) to d) are indicated in plot e) with circles, triangles, stars and squares respectively.

This illustration of the calculation of bulk solutions of the Christoffel equation concludes this first section. The solutions of waves propagating in a purely elastic, infinite anisotropic medium have been described. Their role in the propagation of Lamb wave is detailed in the next section.

1.3 Lamb waves in an elastic orthotropic plate.

The geometry of the system is now a plate of finite thickness h and infinite other dimensions. This plate is bordered by vacuum. In an orthotropic material, the three kinds of bulk modes existing in an anisotropic medium must be considered.

One way to model Lamb wave is to describe them as the superposition of partial solutions (Solie, L.P. and Auld, B.A., 1973). Due to the bounded geometry of the plate, the bulk waves can indeed be reflected by the upper and lower interfaces of the structure, see Fig.(1.3). The combination of these successive reflections, going towards the upper or the lower interfaces, results in guided modes propagating along the phase front direction, lying in the $\left(\boldsymbol{e}_2, \boldsymbol{e}_3\right)$ plane.

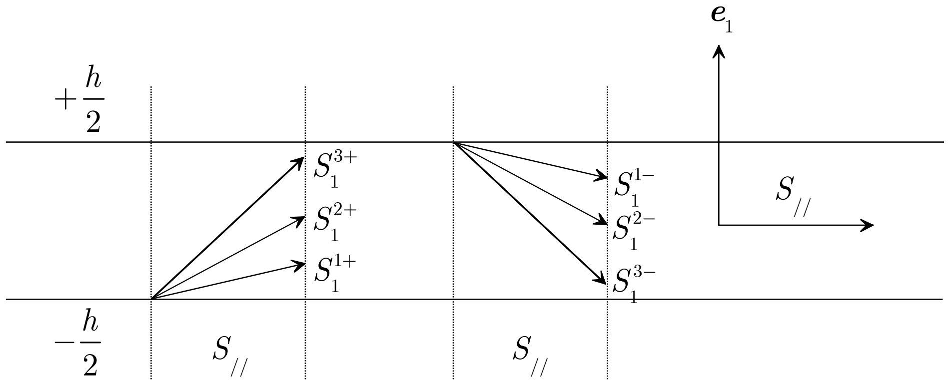

Figure 1.3: Lamb wave modelling. The combination of bulk wave reflections results in guided modes propagating at the slowness $S_{//}$.

The superposition of these partial solutions must satisfy the boundary conditions, i.e. no tensile stress at both interfaces, since the surrounding medium is the vacuum. In order to express the stress tensor of these partial waves, their displacement fields are expressed as follows:

$$\begin{aligned}
\boldsymbol{U}_1^+ &= A_1^+ \boldsymbol{P}_1^+ e^{i\omega S_1^1 x_1} e^{i\omega(t - S_2 x_2 - S_3 x_3)}; \boldsymbol{U}_1^- = A_1^- \boldsymbol{P}_1^- e^{-i\omega S_1^1 x_1} e^{i\omega(t - S_2 x_2 - S_3 x_3)} \\
\boldsymbol{U}_2^+ &= A_2^+ \boldsymbol{P}_2^+ e^{i\omega S_1^2 x_1} e^{i\omega(t - S_2 x_2 - S_3 x_3)}; \boldsymbol{U}_2^- = A_2^- \boldsymbol{P}_2^- e^{-i\omega S_1^2 x_1} e^{i\omega(t - S_2 x_2 - S_3 x_3)} \\
\boldsymbol{U}_3^+ &= A_3^+ \boldsymbol{P}_3^+ e^{i\omega S_1^3 x_1} e^{i\omega(t - S_2 x_2 - S_3 x_3)}; \boldsymbol{U}_3^- = A_3^- \boldsymbol{P}_3^- e^{-i\omega S_1^3 x_1} e^{i\omega(t - S_2 x_2 - S_3 x_3)}
\end{aligned} \tag{1.10}$$

where $+$ designates waves propagating in the $\boldsymbol{e}_1$ direction, $-$ in the -$\boldsymbol{e}_1$ direction. For an orthotropic material, the symmetry plane $\left(S_1^{i+} = -S_1^{i-}\right)$ exists and two cases are possible: symmetrical or anti-symmetrical modes. Based on the displacement field, this choice depends on the polarisations for "plus" and "minus" modes. If $\left(A^+ = A^-\right)$, the solution is symmetrical, if $\left(A^+ = -A^-\right)$, the solution is anti-symmetrical. From the displacement fields, the stress tensor is derived using the following relation:

$$2\varepsilon_{ij} = u_{i,j} + u_{j,i}. \tag{1.11}$$

The stress field is then obtained using Hook's law. To satisfy boundary conditions the following equations must hold:

$$\begin{pmatrix} \sigma_{11} \\ \sigma_{12} \\ \sigma_{13} \end{pmatrix}_{x_1=\pm\frac{h}{2}} = \begin{pmatrix} 0 \\ 0 \\ 0 \end{pmatrix}. \tag{1.12}$$

This system can be expressed in a matrix form :

$$\boldsymbol{\Omega}\left(S_{//},\omega,\phi\right)\begin{pmatrix} A_1 \\ A_2 \\ A_3 \end{pmatrix} = \begin{pmatrix} 0 \\ 0 \\ 0 \end{pmatrix}, \tag{1.13}$$

where $\boldsymbol{\Omega}\left(S_{//},\omega,\phi\right)$ is a 3×3 matrix, and A_i is the amplitude of the i$^{\text{th}}$ partial mode. In order to find non-trivial solutions of Eq.(1.13), the determinant of $\boldsymbol{\Omega}\left(S_{//},\omega,\phi\right)$ must be null. This determinant can be factorised in the product of amplitude term and the quantity noted $\Omega_{S,A}\left(S_{//},\omega,\phi\right)$ (for symmetric and anti-symmetric case respectively). The problem of nullifying the Lamb determinant is therefore equivalent to the problem of nullifying the quantity $\Omega_{S,A}\left(S_{//},\omega,\phi\right)$. This term, sometimes called the Lamb determinant in this work, is described in the symmetric case by:

$$\Omega_S\left(S_{//},\omega,\phi\right) = \alpha_1\left(\beta_2\gamma_3 - \beta_3\gamma_2\right)\theta_1 - \alpha_2\left(\beta_1\gamma_3 - \beta_3\gamma_1\right)\theta_2 + \alpha_3\left(\beta_1\gamma_2 - \beta_2\gamma_1\right)\theta_3, \tag{1.14}$$

with :

$$\begin{aligned} &\alpha_j = C_{11}P_1^jS_1^j + C_{12}P_2^jS_2 + C_{13}P_3^jS_3; \\ &\beta_j = C_{66}\left(S_2P_1^j + S_1^jP_2^j\right); \gamma_p = C_{55}\left(S_3P_1^j + S_1^jP_3^j\right); \\ &\theta_j = \cot\left(\omega S_1^j\frac{h}{2}\right); j = 1,2,3, \end{aligned} \tag{1.15}$$

where j stands for the polarisations, and $P_{1,2,3}^j$ are the components of the polarisation vectors. To obtain the Lamb determinant for the anti-symmetrical case, the cotangent function is to be replaced by tangent function. The aim now is to find triplets $\left(S_{//},\omega,\phi\right)$ solutions of:

$$\Omega_{S,A}\left(S_{//},\omega,\phi\right)=0. \tag{1.16}$$

A classical zero-finding algorithm such as the Newton-Raphson algorithm is used to find the solutions and so plot the dispersion curves. For this purpose, the derivatives of $\Omega_{S,A}\left(S_{//},\omega,\phi\right)$ with respect to the phase slowness $S_{//}$, the phase front direction ϕ, and to the angular frequency ω are needed. It implies the knowledge of the derivative of S_1 , contained in $\Omega_{S,A}\left(S_{//},\omega,\phi\right)$, with respect to $S_{//}$ and ϕ. To calculate these partial derivatives, the implicit function theorem is used on the Christoffel determinant.

At a fixed phase front direction, γ_C is considered as depending only on S_1 and $S_{//}$. For S_1 and $S_{//}$ solutions, γ_C is zero and remains constant, its total differential is therefore zero:

$$d\gamma_C=\frac{\partial\gamma_C}{\partial S_{//}}dS_{//}+\frac{\partial\gamma_C}{\partial S_1}dS_1=0. \tag{1.17}$$

Hence, for S_1 and $S_{//}$ solutions of:

$$\gamma_C\left(S_1,S_{//}\right)\Big|_{\phi=\text{constant}}=0, \tag{1.18}$$

the derivative of S_1 with respect to $S_{//}$ is:

$$\frac{dS_1}{dS_{//}}=-\frac{\dfrac{\partial\gamma_C}{\partial S_{//}}}{\dfrac{\partial\gamma_C}{\partial S_1}}. \tag{1.19}$$

Following the same pattern, at a fixed $S_{//}$ and for S_1 and ϕ solutions of:

$$\gamma_C\left(S_1,\phi\right)\Big|_{S_{//}=\text{constant}}=0, \tag{1.20}$$

the derivative of S_1 with respect to ϕ is deduced:

$$\frac{dS_1}{d\phi}=-\frac{\dfrac{\partial\gamma_C}{\partial\phi}}{\dfrac{\partial\gamma_C}{\partial S_1}}. \tag{1.21}$$

Derivatives of $\Omega_{S,A}\left(S_{//},\omega,\phi\right)$ with respect to the frequency are much easier to obtain, since no composite functions are involved with the frequency argument. All the tools are now present to perform the Newton-Raphson algorithm with analytical derivatives. The advantages of the analytical formulation are the precision and quicker computation times.

To initialise the search, the Newton-Raphson algorithm needs an initial guess of the solution to ensure the convergence. In order to get this initial value, the modulus of the Lamb determinant is calculated as a function of the slowness, at a given frequency. The minima of this function correspond to solutions existing at this frequency. One particular mode is chosen to launch the search. Thus, at a given frequency, the root can be found using this algorithm.

To find the solution corresponding to the neighbouring value of the frequency, the result of the previous search is used as the initial guess, and so on. With such an implementation, the dispersion curves of Lamb modes can be calculated. The programming has been written in C++, under Windows platform.

It is to be noted when calculating the dispersion curves that particular care has to be taken at the beginning of the high dispersion zones. In these zones, it is observed that the algorithm fails sometimes to remain on the same mode and finds a different one. This phenomenon of "mode jumping" has been discussed in the literature (Lowe, M., 1995; Pavlakovic, B., Lowe, M. et al., 1997). Refinements on the search have therefore to be done in the vicinity of such zones to avoid this problem.

The model has been validated using several material properties. Lamb modes have been calculated for a graphite-epoxy plate, for the 0 and 45 degrees phase directions. Results superpose perfectly with those published in Nayfeh's book (Nayfeh, A.H., 1995). The model has also been compared with Disperse, a multipurpose software developed at the Imperial College by B. Pavlakovic and M.J.S Lowe (Pavlakovic, B., Lowe, M. et al., 1997; Lowe, M.J.S. and Pavlakovic, B., N., 2001). Rigorously the same dispersion plots have been obtained by the two programs, for glass and carbon-epoxy plates, both in principal and non-principal directions. Moreover, the analytical approach developed here extends the possibilities of analysis in non-principal directions. As seen later in this work, the dependences of the steering angle on the frequency and the energy velocity on the observation direction, which are not calculated by Disperse, can be plotted using the developed program.

Taking again the example of the unidirectional carbon-epoxy (material properties in Table 2.3), the dispersion curves of the main Lamb modes propagating in a 3.6 mm thick plate are displayed in Figs.(1.4a and 1.4b), for several phase front directions (0 degree being the direction of the fibres).

A digression is brought here concerning the names of guided modes: it is chosen to extend the names of fundamental modes existing in the 0 degree principal direction to any direction. Therefore the SH_0 mode that rigorously exists in principal directions only, is named the same way when it couples with other displacement components in non-principal directions. For higher order modes however, the segregation is more difficult and their name will be deduced from their order and nature only (symmetric or not). In that case, the mode SH_i existing only in principal directions is named S_i in an other direction, i being the number of this now coupled mode. It is to be noted that i is not the order of the mode any longer. The modes are labelled in order of appearance, and not with respect to the number of nodes in the plate thickness as they would conventionally be. In principal directions, where the Lamb modes and the SH modes are not coupled, their dispersion plots intersect with each other (even orders correspond to symmetric SH modes, odd orders to anti-symmetric SH modes).

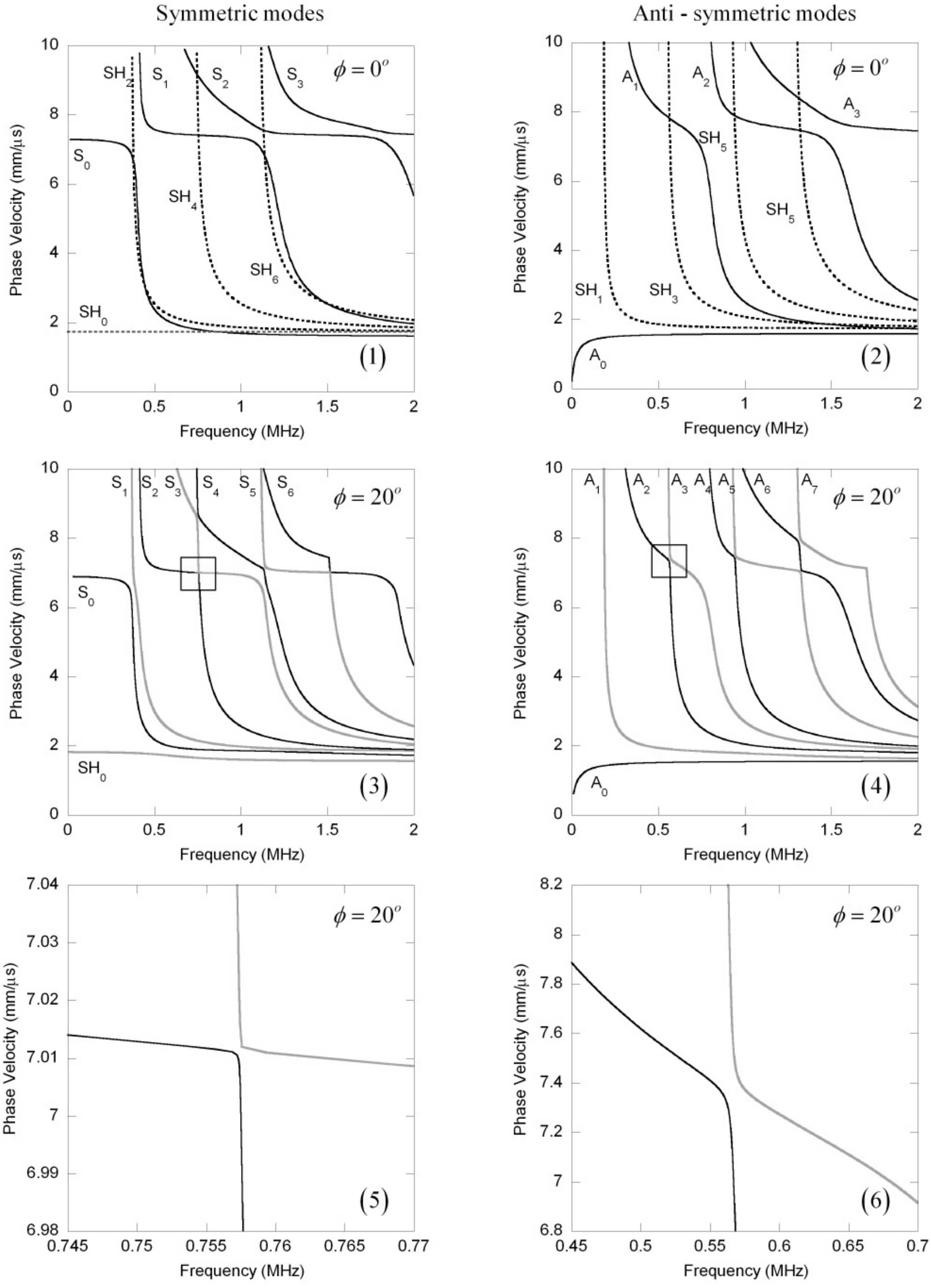

Figure 1.4a: Phase velocity dispersion for 0 and 20 degrees phase front directions, for the 3.6 mm thick carbon-epoxy plate. Dotted and lines of plots (1) and (2) represent the SH and the Lamb modes respectively. Grey and black lines of plots (3) and (4) are used to distinguish the guided modes. As seen on the close-up views for the 20 degrees direction (plots (5) and (6)), Lamb and SH modes are coupled and do not intersect in non-principal directions.

In non-principal directions, for which these formerly different type of modes are coupled together, branches of the same nature (i.e. symmetric or anti-symmetric) do not intersect any longer (Solie, L.P. and Auld, B.A., 1973; Simon, C., Kaczmarek, H. et al., 1997).

It can be noticed that velocities of the S_0 and A_0 mode are decreasing from their maximum value in the 0 degree direction to their minimum value at 90 degrees. At low frequency, these variations are consistent with the shapes of these modes.

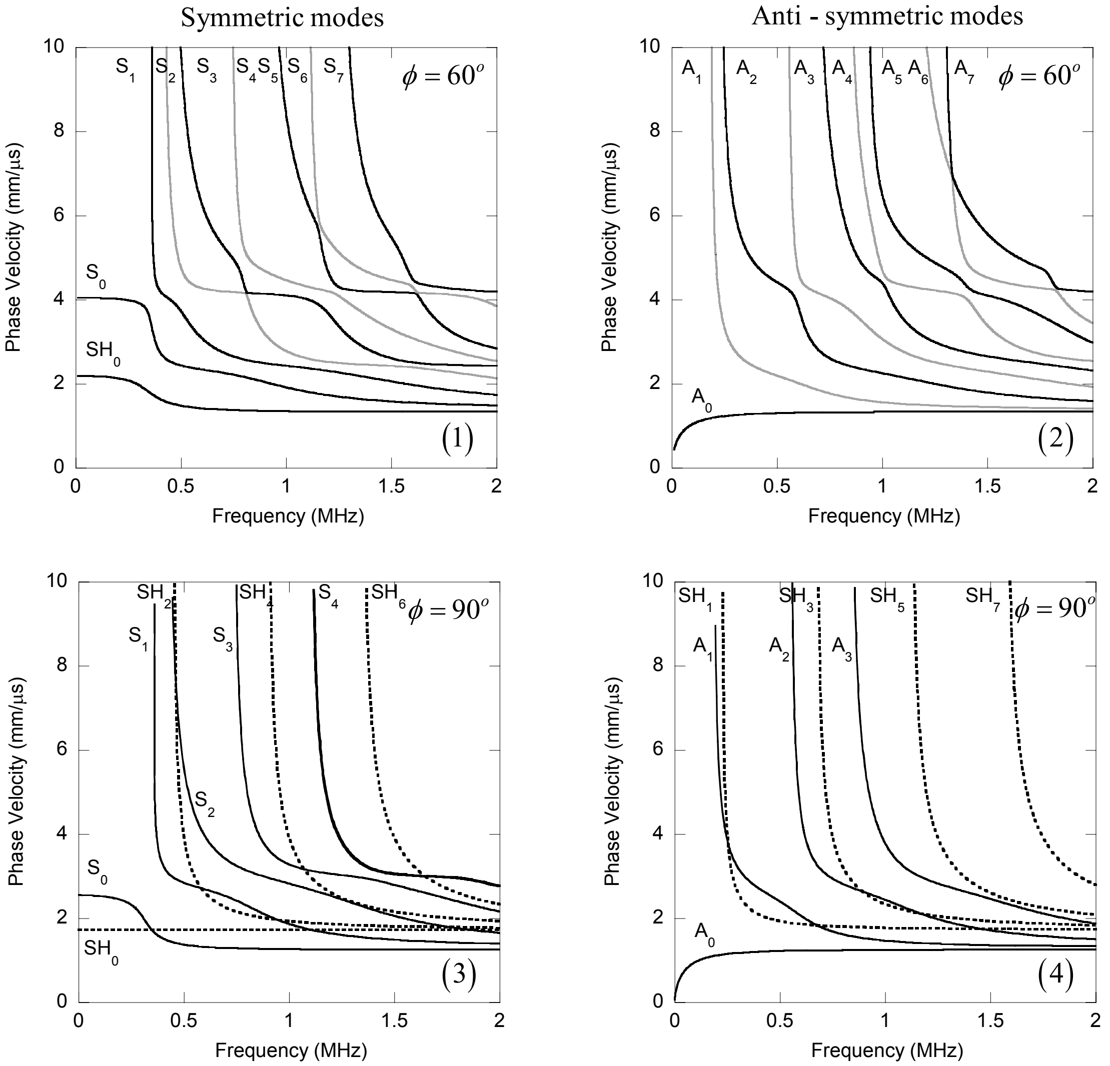

Figure 1.4b: Phase velocity dispersion for 60 and 90 degrees phase front directions, for the 3.6 mm thick carbon-epoxy plate. For the 60 degrees direction, dispersion curves do not intersect. Grey and black lines of plots (1) and (2) are used to distinguish the guided modes. At 90 degrees (principal direction), Lamb (solid lines) and SH modes (dotted lines) are uncoupled and the dispersion curves do intersect in plots (3) and (4).

The S_0 mode at low frequency is indeed essentially a compression mode, it propagates therefore faster in a direction where it involves stiffer C_{ijkl}. A similar comment can be made on the A_0 mode, which is a bending mode at low frequency.

In parallel to calculating the dependence of the phase velocity on the frequency for a given phase front direction, it is also possible to compute the variation of the phase velocity with the phase front angle, for a given frequency. For several frequencies, the variation of the first Lamb modes with the phase front direction is displayed in Fig.(1.5). Again, it can be seen that the anisotropy affects drastically the value of the phase velocity of the guided modes and it does this in a different way at different frequencies. The dependence of the phase velocity on the frequency does vary with the phase front direction as well.

The solution branches are labelled SH or S according to their polarisation in the principal direction 0°. Changing the phase front direction ϕ varies the Lamb modes polarisation. At low frequency, this variation is such that the branch, which is SH or S_0 at 0 degrees principal direction, retains the same type at 90 degrees. In Fig.(1.5) at 0.1 MHz for instance (plots (1) and (2)), only three modes are present, their polarisations are "normal", i.e. depend on the phase direction so that they present the same relative characteristics for any phase front direction. At 0 degrees (along the horizontal axis of these plots), the S_0 mode is mostly compressional, the SH_0 mostly a shear mode and A_0 mostly a bending mode. At 90 degrees (vertical axis), they do present the same characteristics. In this case, this is what is called by Simon a "normal" dependence of the polarisation on the phase front direction.

However, at higher frequency (plots (3) and (4)), the branch which is, say, SH_0 (dotted line) at 0 degree, on its angular variation arrives at 90 degrees as the S_0 branch (same velocity and polarisation), whereas the S_0 branch (solid line) at 0 degrees becomes, correspondingly, the SH_0 one at 90 degrees (same velocity and polarisation). As described in (Simon, C., 1997), it is observed in Fig.(1.5), that the polarisation transfer occurs, to paraphrase the author. While they keep their name given in the 0 degree direction, these two modes have swapped their polarisation while rotating the phase front direction.

Another general comment can be made to this figure. The number of modes increases with the frequency as there are more Lamb modes at higher frequency. Moreover many of the modes present inflexion points on their slowness surface, that imply cusps on their associated wave surface. This feature is described in the next section where the energy velocity of guided modes is detailed.

One way to visualise all these dependencies at one glance is to use a 3D view of one mode. A convenient projection is proposed here, using cylindrical coordinates for which the elevation axis represents the frequency, the polar angle represents the phase front direction, and the polar modulus represents the phase velocity. Some example plots are displayed in Fig.(1.6).

Symmetric modes *a*) $f = 0.1\, MHz$ Anti - symmetric modes

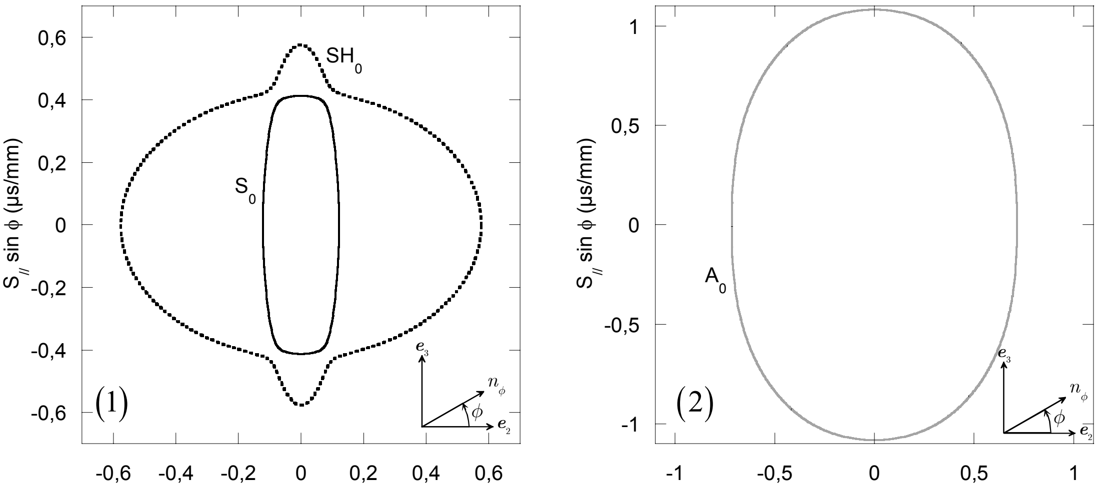

b) $f = 0.5\, MHz$

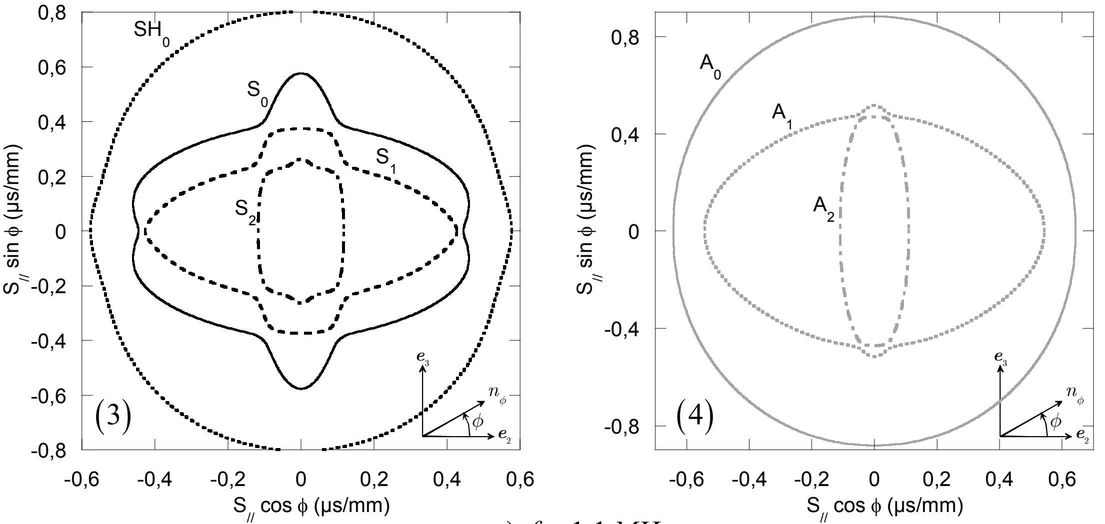

c) $f = 1.1\, MHz$

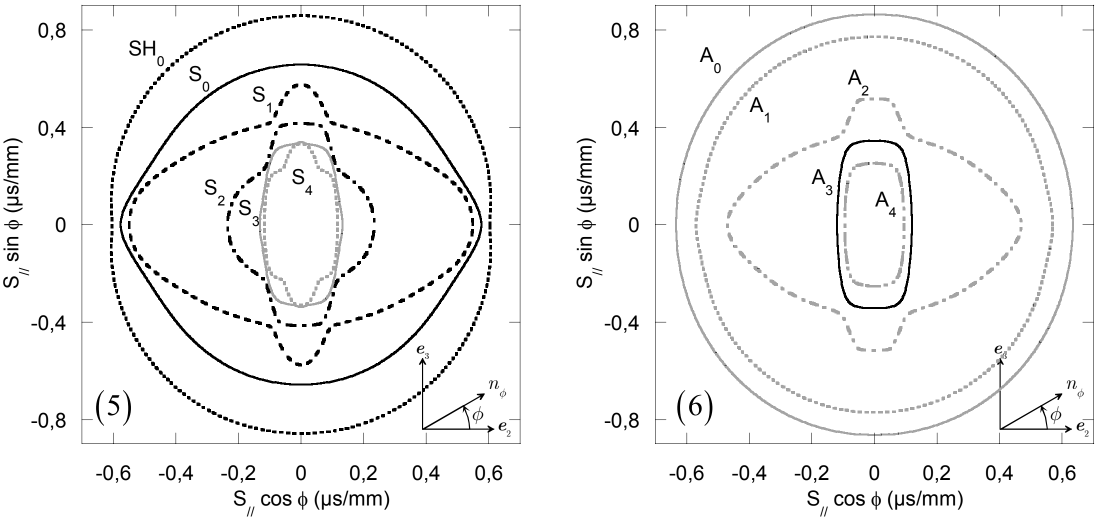

Figure 1.5: Slowness surfaces cuts of the Lamb modes at a) 0.1, b) 0.5 and c) 1.1 MHz, for the 3.6 mm thick carbon-epoxy plate.

Concerning the A_0 mode, remarks made earlier on its dispersion curves for different phase directions are observable. Indeed, along the 0 degree direction, its velocity is greater than its phase velocity at 90 degrees. The smooth dependence of the phase velocity of this mode with the phase direction and the frequency is illustrated by this plot.

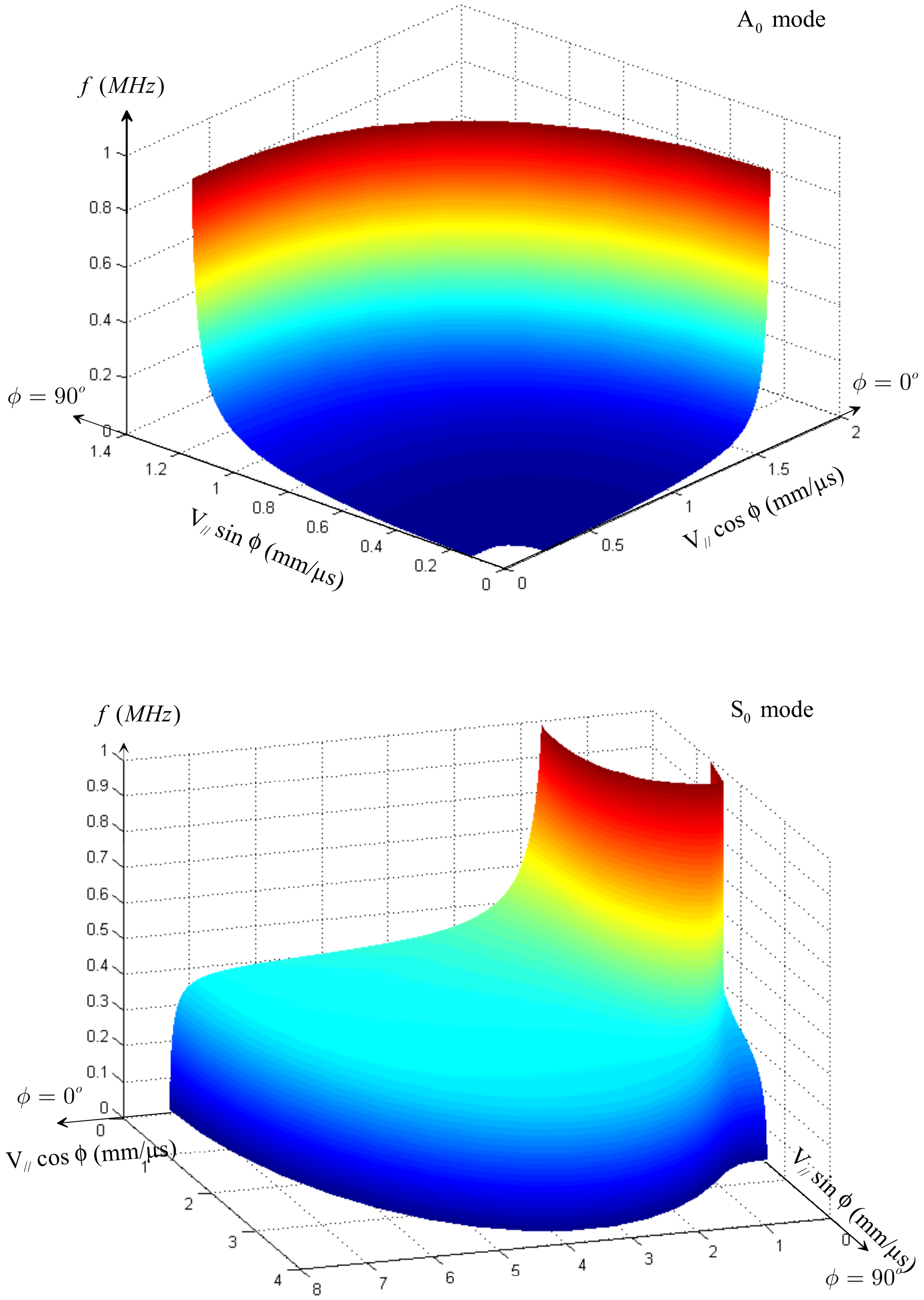

Figure 1.6: 3D views of the A_0 and the S_0 mode, for the 3.6 mm thick carbon-epoxy plate. Cylindrical coordinates: the elevation is the frequency, the polar modulus is the phase velocity and the azimuthal angle is the phase front direction.

In the bottom plot of Fig.(1.6) the S_0 mode is displayed. Similar comments can be made on its phase velocity values depending on the phase direction. The variations are however steeper than for the A_0 mode. According to its phase dispersion plots at 0 and 90 degrees respectively, its phase velocity does vary from more than 7 to less than 3 mm/µs at zero frequency. Slices of this 3D view made respectively at 0, 60 or 90 degrees correspond to the phase velocity dispersion plots displayed in Figs.(1.4a) and (1.4b).

Having these characteristics of the guided modes at hand, it is now possible to study their energy velocity. As shown in (Auld, B.A., 1973), in the case of non-absorbing media, the energy velocity is rigorously equal to the group velocity. The next section describes the calculation of the group velocity of guided modes, as well as the steering angle phenomenon that occurs for anisotropic materials.

1.4 Group velocity and steering angle of Lamb modes.

The group velocity $\boldsymbol{V}_g$ corresponds to the wave packet velocity. For dispersive waves, it is expressed as the derivative of the angular frequency with respect to the wave vector $\boldsymbol{k}_{//}$:

$$\boldsymbol{V}_g = \frac{\partial \omega}{\partial \boldsymbol{k}_{//}}. \tag{1.22}$$

Using once more the implicit function theorem, the expression of the group velocity vector as a function of the Lamb determinant can be obtained. This is the aim of the following derivation.

At a fixed phase front direction ϕ, for $S_{//}$ and ω solutions of the Lamb equation (Eq. 1.16), $\Omega_{S,A}$ is null. Its total differential is therefore null:

$$d\Omega_{S,A} = \frac{\partial \Omega}{\partial S_{//}} dS_{//} + \frac{\partial \Omega}{\partial \omega} d\omega = 0. \tag{1.23}$$

Expressing the phase slowness vector as a function of the wave vector $\boldsymbol{k}_{//}$ and the frequency as:

$$\boldsymbol{S}_{//} = \frac{\boldsymbol{k}_{//}}{\omega}, \tag{1.24}$$

the differential of $\boldsymbol{S}_{//}$ reads:

$$d\boldsymbol{S}_{//} = \frac{\partial \boldsymbol{S}_{//}}{\partial \boldsymbol{k}_{//}} d\boldsymbol{k}_{//} + \frac{\partial \boldsymbol{S}_{//}}{\partial \omega} d\omega = \frac{1}{\omega} d\boldsymbol{k}_{//} - \frac{\boldsymbol{k}_{//}}{\omega^2} d\omega. \tag{1.25}$$

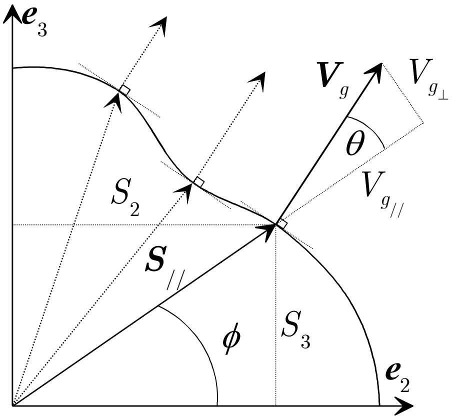

Fig. 1.7: Lamb mode slowness surface cut and group velocity at fixed frequency, θ *is the steering angle.*

Hence from Eq. (1.23), it can be obtained:

$$\left(\frac{\partial\Omega}{\partial\omega}-\frac{\partial\Omega}{\partial \boldsymbol{S}_{//}}\cdot\frac{\boldsymbol{S}_{//}}{\omega}\right)d\omega+\frac{1}{\omega}\frac{\partial\Omega}{\partial \boldsymbol{S}_{//}}d\boldsymbol{k}_{//}=0. \tag{1.26}$$

The previous equation yields (Auld, B.A., 1973; Simon, C., Kaczmarek, H. et al., 1997; Poncelet, O., Deschamps, M. et al., 2000):

$$\frac{d\omega}{d\boldsymbol{k}_{//}}=\boldsymbol{V}_g=\frac{\dfrac{\partial\Omega}{\partial \boldsymbol{S}_{//}}}{\dfrac{\partial\Omega}{\partial \boldsymbol{S}_{//}}\cdot\boldsymbol{S}_{//}-\omega\dfrac{\partial\Omega}{\partial\omega}}. \tag{1.27}$$

The components of the group velocity vector are as follows:

$$V_{g_{//}}=\frac{\dfrac{\partial\Omega}{\partial S_{//}}}{\dfrac{\partial\Omega}{\partial \boldsymbol{S}_{//}}\boldsymbol{S}_{//}-\omega\dfrac{\partial\Omega}{\partial\omega}}, \tag{1.28}$$

and:

$$V_{g_\perp}=\frac{\dfrac{\partial\Omega}{\partial\phi}}{S_{//}\left(\dfrac{\partial\Omega}{\partial \boldsymbol{S}_{//}}\cdot\boldsymbol{S}_{//}-\omega\dfrac{\partial\Omega}{\partial\omega}\right)}. \tag{1.29}$$

The direction of the group velocity may be characterised by θ, the deviation angle measured from the phase direction reference:

$$\theta=\arctan\frac{V_{g_\perp}}{V_{g_{//}}}. \tag{1.30}$$

The steering or deviation angle, is also defined as the algebraic difference between the group direction Ψ and the phase direction ϕ.

$$\theta = \Psi - \phi. \tag{1.31}$$

This concludes the derivation of the group velocity of the Lamb modes. As seen in Eq.(1.27) where the denominator of the group velocity contains two derivatives of the Lamb determinant, the dispersion acts through two variables: the frequency and the direction of propagation. Compared to the group velocity of bulk waves, where the dispersion is only angular, the dispersion of Lamb modes is a more involved phenomenon since it is both angular and frequential.

It is known that for anisotropic material, the direction of the group velocity differs from the phase front direction. As for bulk waves in a purely elastic material (Auld, B.A., 1973; Nayfeh, A.H., 1995; Balasubramaniam, K. and Ji, Y., 2000; Potel, C., Gatignol, P. et al., 2002), the group velocity vector is normal to the phase slowness surface, as seen in Fig.(1.7). However the relation (Auld, B.A., 1973) for bulk waves reads:

$$\boldsymbol{S}_{//} \cdot \boldsymbol{V}_g = 1, \tag{1.32}$$

Eq. (1.32) is modified in the case of frequency dispersive waves such as Lamb modes. Using the previous expression of the group velocity, it can be obtained:

$$\boldsymbol{S}_{//}.\boldsymbol{V}_g = 1 + \frac{\omega \, \partial_\omega \Omega}{\boldsymbol{S}_{//}.\partial_{\boldsymbol{S}_{//}} \Omega - \omega \, \partial_\omega \Omega}. \tag{1.33}$$

The scalar product of the phase slowness vector with the energy (or group) velocity vector, described in Eq. (1.33), is affected by a frequential dispersion term that is absent in the case of bulk modes. The fact that the group velocity of the guided modes can be greater or lower than its associated phase velocity, is explained by role of the dispersion term. The consequences of that expression will be analysed later in Chapter 3, in the context of viscoelastic media.

It is interesting that the phenomenon of energy focusing, well-known for bulk waves (Auld, B.A., 1973; Maznev, A.A. and Every, A.G., 1995; Bescond, C. and Deschamps, M., 1998; Wolfe, J.P., 1998), occurs for the Lamb modes as well. Lamb mode slowness surfaces can indeed have many inflexion points in a 90 degrees sector. It implies that the same group velocity direction may correspond to many phase front directions. These particular shapes are responsible for the cusps of the associated group velocity (or wave surface). Moreover, the slowness surfaces of Lamb modes, and therefore their associated wave surfaces, vary with the frequency as well.

It is understood now that for a complete information on the group velocity of a Lamb mode, the variation of its velocity modulus with the frequency must be complemented by the variation of its steering angle with the frequency (Simon, C., Kaczmarek, H. et al., 1997; Poncelet, O., Deschamps, M. et al., 2000).

To illustrate these features the unidirectional carbon-epoxy example has been used. The particular case of the 0 degree (principal direction) is given in Fig.(1.8). There is indeed no steering angle for principal directions. In Fig.(1.9), the associated group velocity of Lamb modes propagating in the phase direction of 60 degrees are displayed, along with their associated steering angle.

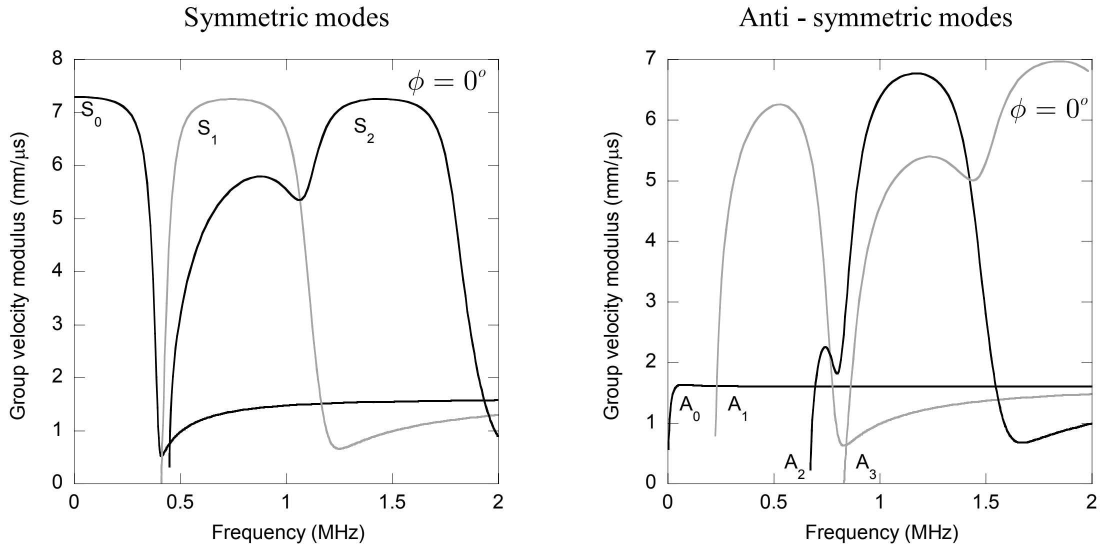

Figure 1.8: Group velocity of the symmetric and anti-symmetric modes in the 0 degree principal direction for the 3.6 mm thick carbon-epoxy plate.

Regarding Fig.(1.9), it is to be stressed that the direction of the group velocity depends on the frequency. Whereas the phase velocity dispersion plots concern only one phase direction, the group velocity plots displayed in Fig.(1.9) are to be associated with phase front directions varying with the frequency. The variations of the steering angle with the frequency are substantial. For instance, the S_0 mode propagating in the 60 degrees phase direction has a steering angle around –50 degrees at low frequency. It means that its energy travels approximately along the 10 degrees direction at this frequency. Moreover, the steering angle dispersion follows the frequency dispersion. Each high dispersion zone of either the group or phase velocity implies a strong variation of the deviation angle with the frequency and vice versa. Looking at the A_0 mode for instance, its steering angle is stabilised after 0.15 MHz; its group velocity plot correspondingly presents little dispersion after this frequency.

A digression is brought here concerning the S_1 mode displayed in Fig.(1.9). This mode presents a steering angle greater than $\pi/2$ in absolute value. It can be explained that this mode is actually the combination of two modes. If one mode is defined by a single-valued function describing the dependence of the phase velocity on the frequency, the phase dispersion of S_1 in Fig.(1.4) involves two modes. The threshold between the two modes is the point of infinite dispersion, so that the solutions found below and above that threshold belong to the two different modes, one for which the group velocity component along the phase direction is negative, the other for which this component is positive (Auld, B.A., 1973). This feature is illustrated in Fig.(1.10).

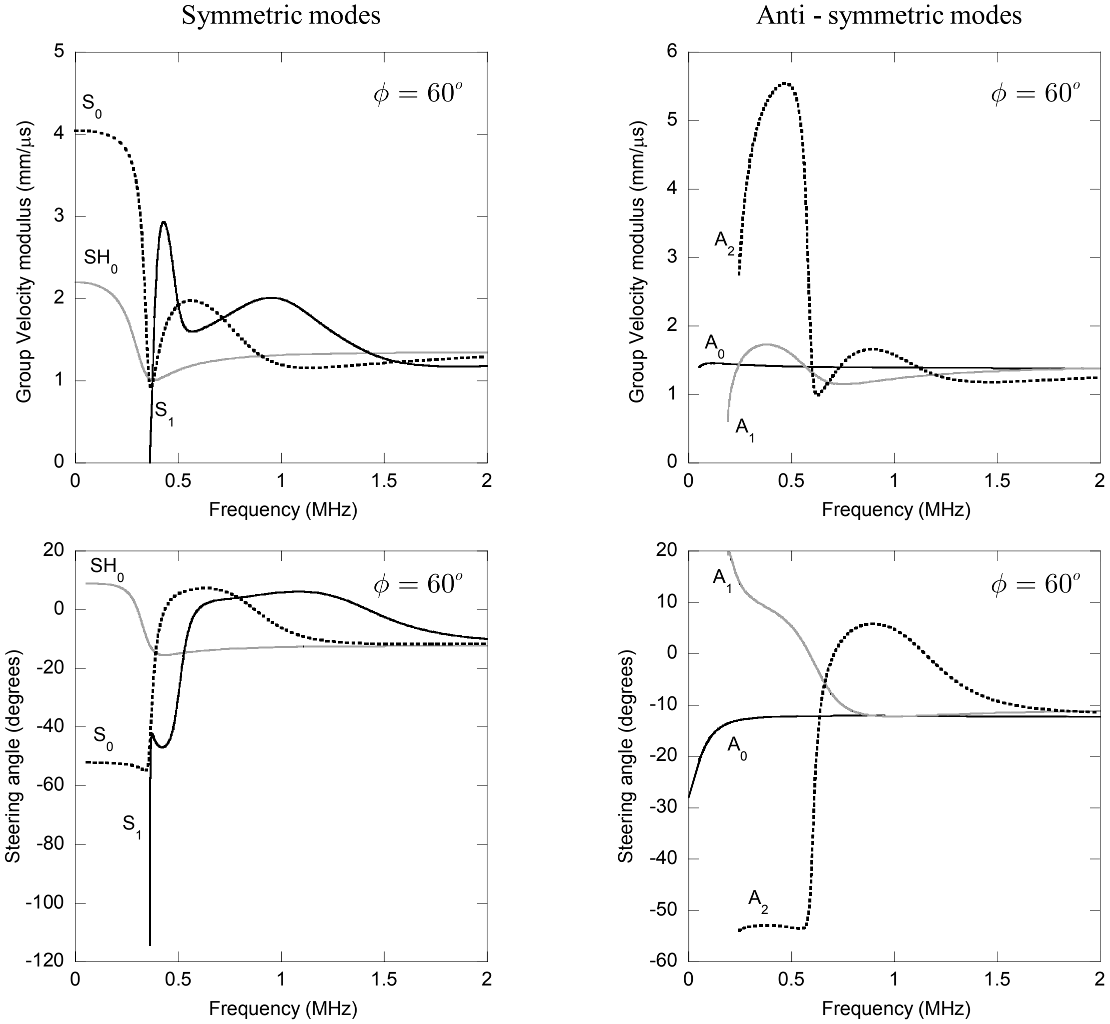

Figure 1.9: Group Velocity modulus (top plots) and steering angle (bottom plots for a 60 degrees phase direction for the 3.6 mm thick carbon-epoxy plate.

The group velocity of a guided mode can be studied for a fixed frequency as well. Corresponding to the bulk wave case, such plots showing the group velocity modulus as a function of the group direction are called wave surfaces. Such plots for the example material at 1.1 MHz are displayed in Figs.(1.11) and (1.12) and represent the associated wave surfaces of the slowness surfaces shown in Fig.(1.5).

Due to the number of modes present at 1.1 MHz, wave surfaces at this frequency have been separated in two plots for clarity. In these figures, for which the horizontal axis represents the 0 degree direction (direction of the carbon-epoxy fibres in this case), it can be observed that some modes which were cusp free at 0.1 MHz, acquire cusps at higher frequencies, and *vice versa*.

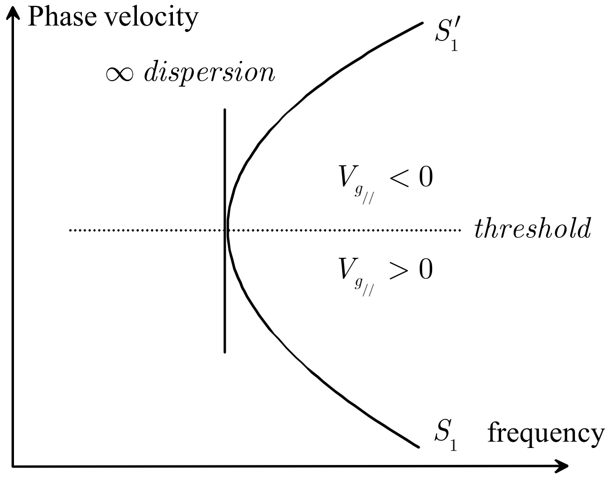

Figure 1.10: S_1 mode case of infinite dispersion. Above the point of infinite dispersion, the component of the group velocity along the phase direction becomes negative.

For instance the SH_0 mode has a cusp at 0.1 MHz but not at either 0.5 or 1.1MHz. Another example can be pointed out for the S_0 mode that has no cusps at 0.1 MHz and 1.1 MHz and has one at 0.5 MHz. The presence or absence of these cusps implies arrival or vanishing of the inflexion points on the slowness surfaces at these frequencies, as shown in Fig.(1.5).

The influence of anisotropy, which entails the angular dispersion and affects the frequency dispersion is visible on all Lamb modes displayed in Figs.(1.11, 1.12). The frequency dependence of slowness surfaces of the guided modes and the associated wave surfaces will be studied in detail in Chapter 3, when dealing with the Lamb mode properties along the direction of energy propagation.

As it has been done for phase quantities, it is possible to summarise the dispersions of the group velocity with a 3D view of a mode, shown in Figs.(1.13, 1.14). These figures are displayed in cylindrical coordinates, as for the previous 3D plots. For the two top plots of these figures, the polar modulus represents the modulus of the group velocity, the elevation the frequency and the azimuthal angle is the phase angle. All iso-frequency cuts have the same colour scale. The interpretation of the 3D group velocity plot is however more intricate. It is indeed necessary to bear in mind that the polar angle is the phase direction. To have the complete information, the 3D view of the steering angle is necessary. For the two bottom plots of Figs.(1.13, 1.14), the axes are in Cartesian coordinates, with labelled axes. The two principal axes that are the 0 and the 90 degrees direction are clearly visible since there is no steering in these directions. The group velocity of one point of the phase dispersion curve

$\left(S_{//},\omega,\phi\right)$ picked on Fig.(1.6) is completely defined by taking the elevation of the point $\left(\omega,\phi\right)$ in the top plots of either Fig.(1.13) or (1.14), and the associated $\left(\theta,\omega,\phi\right)$ point on the associated bottom plots, i.e. the modulus and the steering angle of the group velocity respectively.

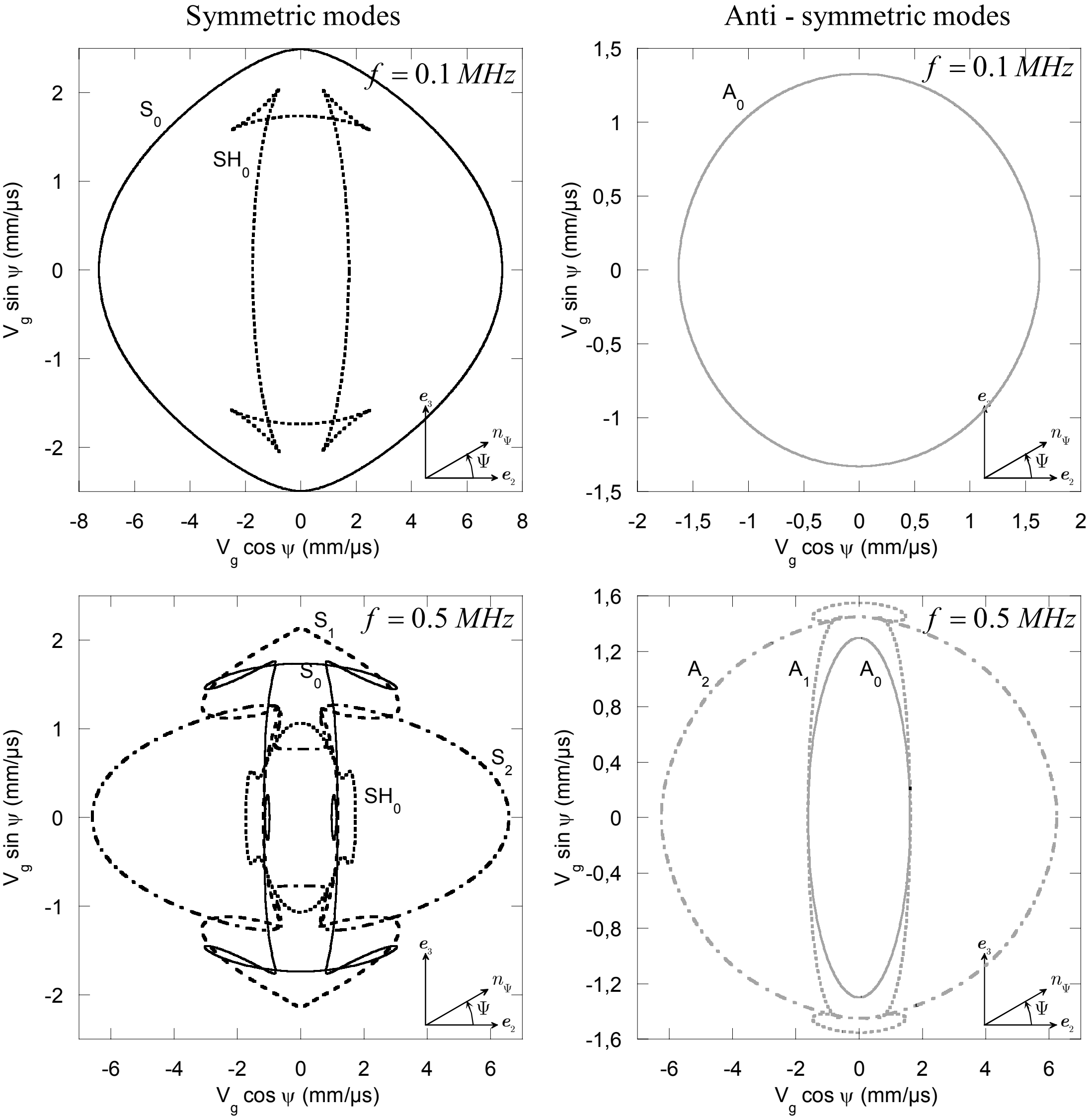

Figure 1.11: Wave surface cuts of the Lamb modes at 0.1 and 0.5 MHz. The horizontal axis represents the 0 degree direction (direction of the carbon-epoxy fibres in this case). Accordingly the vertical axis represents the direction perpendicular to the fibres (the plane of visualisation is the azimuthal plane). The left and right hand side plots concern respectively the symmetric and the anti-symmetric modes. The wave surface represents the wave energy front of a guided mode in the unidirectional carbon-epoxy plate.

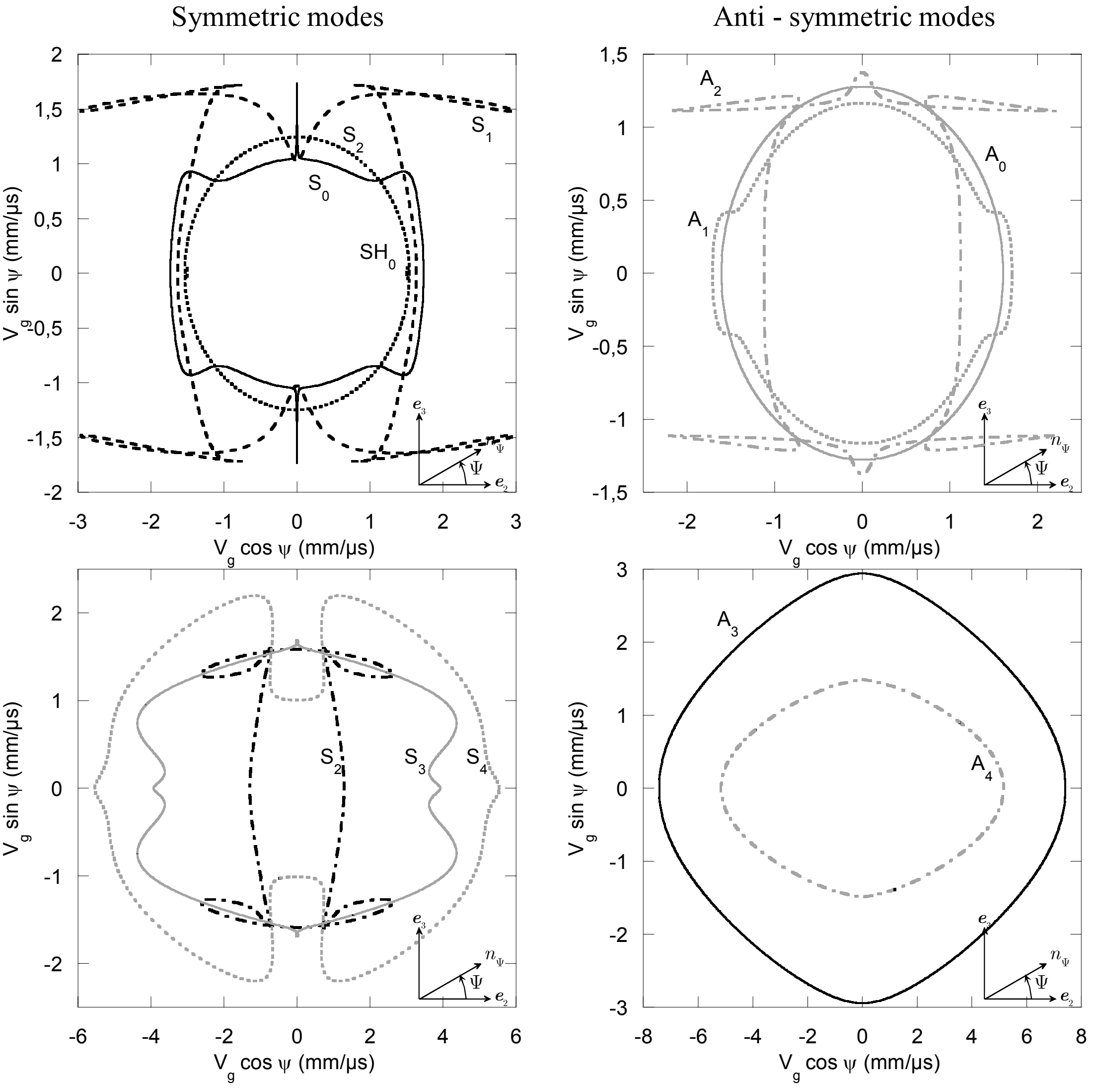

Figure 1.12: Wave surface cuts of the Lamb modes at 1.1 MHz. The horizontal axis represents the 0 degree direction (direction of the carbon-epoxy fibres in this case). Accordingly the vertical axis represents the direction perpendicular to the fibres (the plane of visualisation is the azimuthal plane). The left and right hand side plots concern respectively the symmetric and the anti-symmetric modes. The wave surface represents the wave energy front of a guided mode in the unidirectional carbon-epoxy plate.

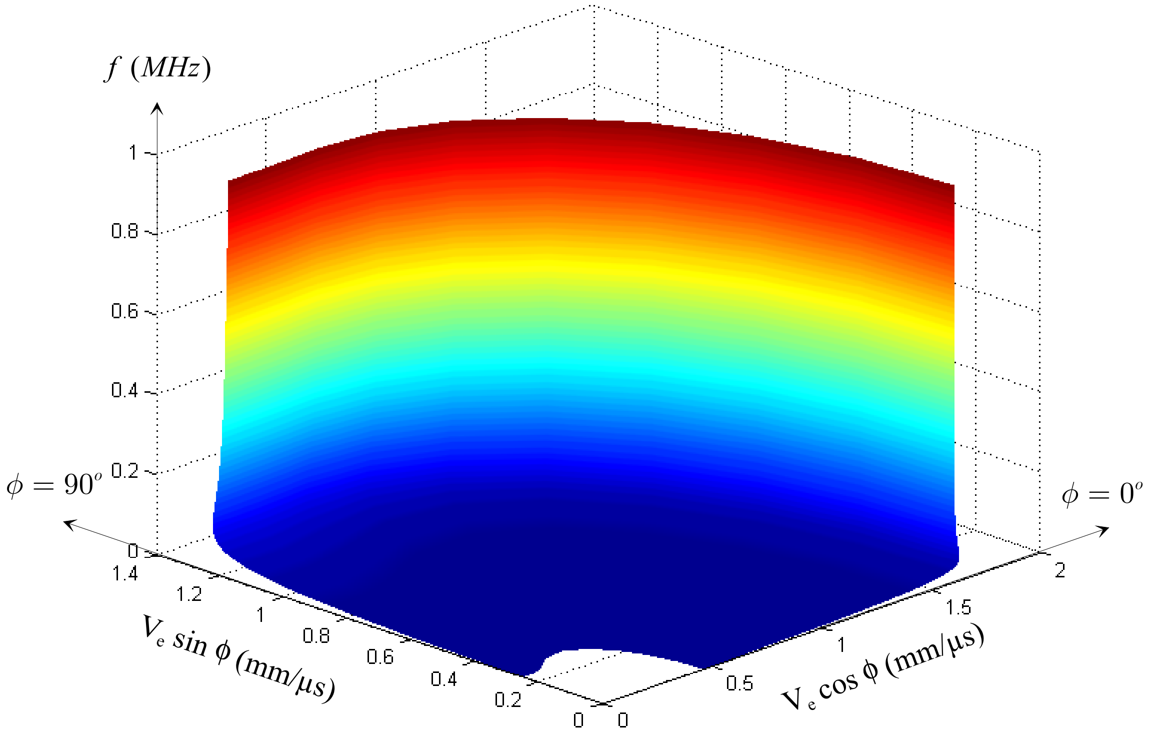

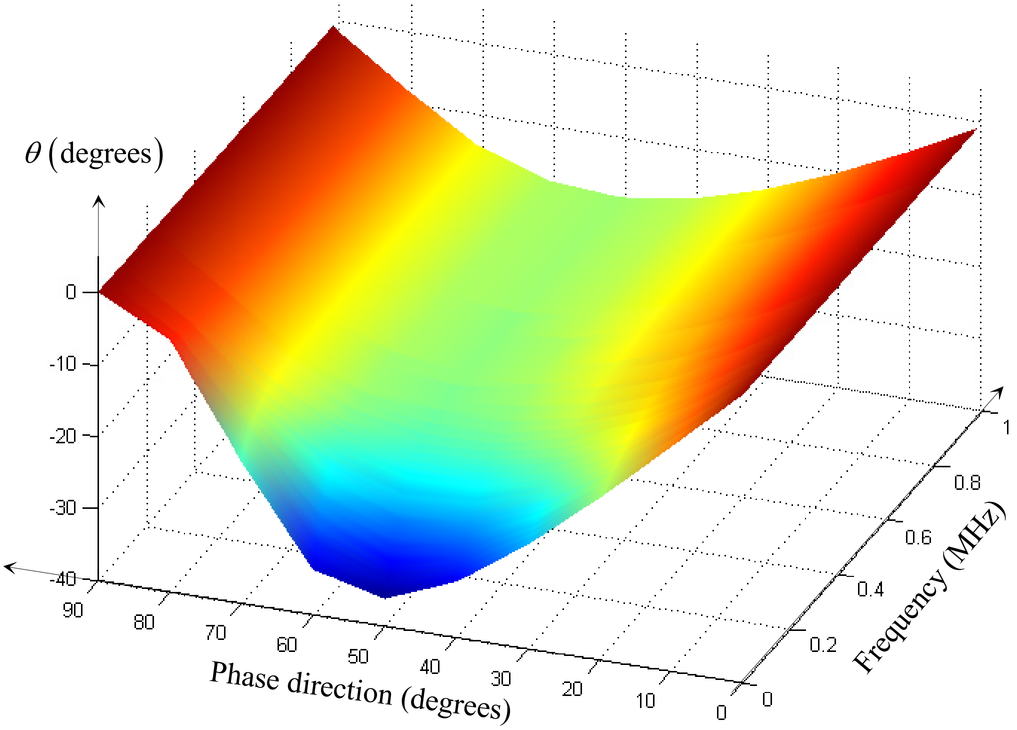

Figure 1.13: 3D view of the energy (group) velocity (above) and steering angle (below) for the A_0 branch. For the energy velocity plot, the azimuthal angle is the phase front direction in degrees, the elevation is the frequency in MHz and the polar radius is the group velocity modulus in mm/μs. For the steering angle plot, axes are denoted in the figure.

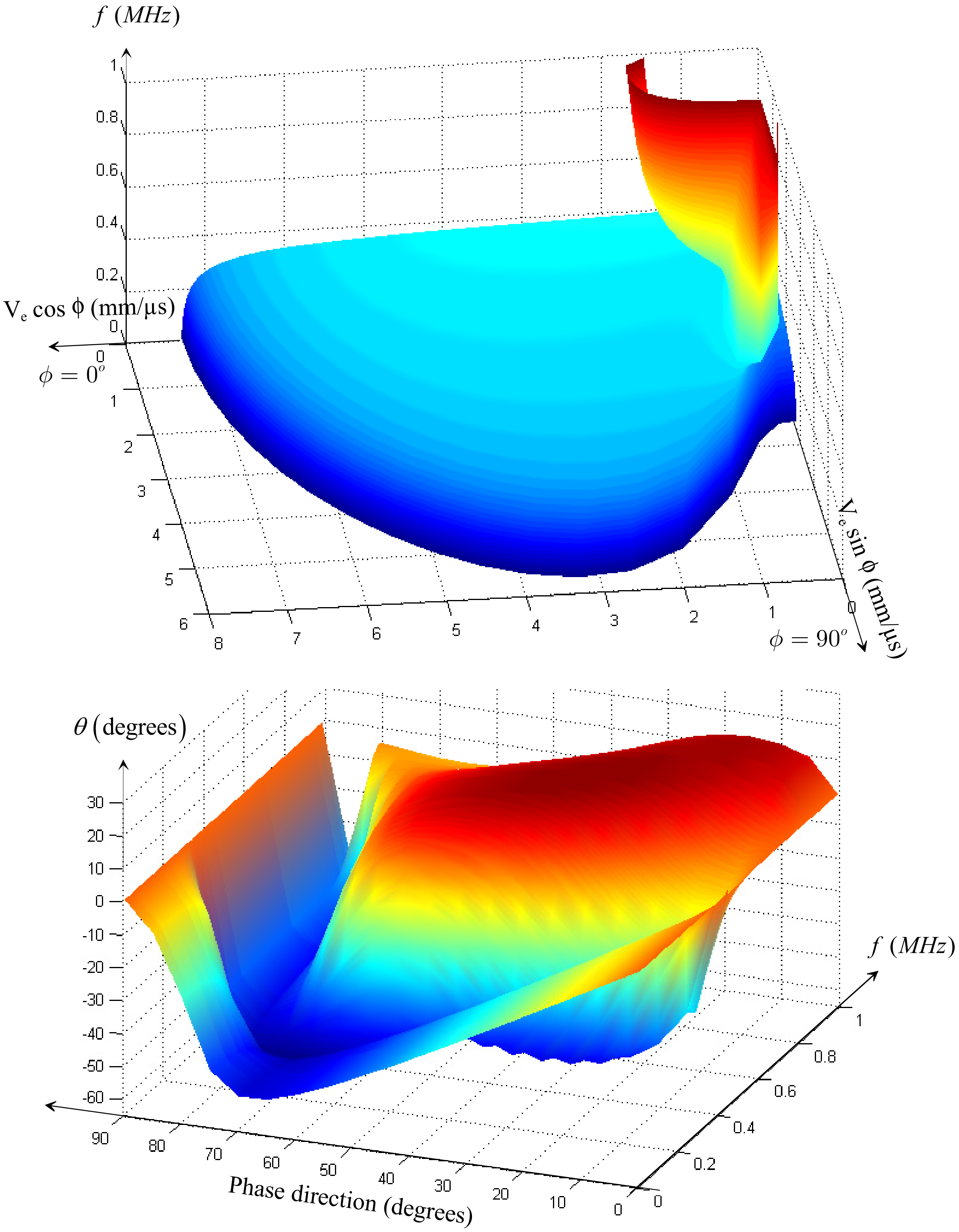

Figure 1.14: 3D view of the energy (group) velocity (above) and steering angle (below) for the S_0 branch. For the energy velocity plot, the azimuthal angle is the phase front direction in degrees, the elevation is the frequency in MHz and the polar radius is the group velocity modulus in mm/μs. For the steering angle plot, axes are denoted in the figure.

1.5 Conclusion

This first chapter presented the theoretical background concerned with the propagation properties of the Lamb modes in elastic anisotropic materials. The detailed derivation exposed in this chapter aimed to introduce the notations for the following chapters as well as to describe the approach exploited in this work.

Properties concerning phase as well as group quantities have been described and illustrated through the example of a unidirectional carbon-epoxy plate. Both angular and frequential dispersion have been taken into account in the description of the energy velocity. It has been demonstrated that the knowledge of a Lamb mode can be displayed using 3D plots, revealing the dependence on both the frequency and the phase front direction.

The complexity of the group velocity of Lamb modes propagating in anisotropic media has been emphasised with the interpretation of the 3D view of group velocity dispersion and its associated steering angle. Even though this information is useful when exciting a chosen phase direction, it is not suitable for the inverse case when the energy direction is chosen from the beginning. This point is going to be detailed in Chapter 3, concerned with the properties of Lamb modes along the observation direction.

Moreover, the effects of anisotropy on phase and group velocities have been described, in the case of a purely elastic material. The natural next step is to study the more general case of a visco-elastic anisotropic material. The validity of the equations derived for the elastic case are discussed in the next chapter.

Chapter 2

Lamb waves in viscoelastic anisotropic plates

2.1 Introduction

Whilst the first chapter was focused on the purely elastic case and reviewed the basics of guided mode propagation, this part of the thesis puts the emphasis on viscoelastic materials. A purely elastic material is indeed a simplification of the physical reality. There always exist phenomena acting in the process of wave propagation which induce energy losses and therefore affect the amplitude of the particle motion. In composite materials specifically, such as carbon or glass fibre-reinforced epoxy resins, the fibres act as scatterers for the bulk acoustic waves. Moreover, the composite matrix material is responsible for the viscous damping that causes the absorption of some of the wave energy (Auld, B.A., 1973; Chandra, R., Singh, S.P. et al., 1999; Biwa, S., Watanabe, Y. et al., 2001). On top of these phenomena, beam spreading occurs. For guided modes, losses due to beam spreading are lower than for the waves propagating in an infinite medium. The geometrical structure, usually a cylinder or a plate, guides the waves so that the losses due to diffraction are small compared to the losses caused by the absorption.

In this chapter the attention centres on the latter type of attenuation. The attenuation of the Lamb modes in composite plates is significant and affects their measurability after a propagation over a long distance. For the development of NDT methods using guided waves, it is essential to know about the properties consequent to the material viscosity. But so far, the studies of all researchers of Lamb waves in composites have depended on the assumption of elastic materials, mainly because of the limitations of the current modelling tools and the difficulty to obtain the complete viscoelastic tensor of the material under investigation. This lack of works taking the material viscosity into account stresses the need for such a study.

In the first section the wave modelling is described, i.e. the usual mathematical formulation of the slowness taking the attenuation into account. Then the viscoelastic medium is studied using most common rheological models. Their influence on the wave propagation and attenuation is described as well. In this section, the characterisation using conventional techniques of a unidirectional carbon-epoxy panel is described. The Lamb wave formulation in this particular case is then compared with the purely elastic case, and differences are explained and illustrated. The attenuation of Lamb modes is described in the same way as the phase velocity, i.e. with frequential and spatial dispersion plots.

2.2 Wave modelling

The waves propagating in a viscoelastic medium are losing some energy, so there is a need for a term to represent this attenuation. The choice of a complex slowness vector is classical and is described as follows (Carcione, J.M., Cavallini, F., 1995):

$$\boldsymbol{S}_{//} = \boldsymbol{S}'_{//} - i\boldsymbol{S}''_{//}, \tag{2.1}$$

where $\boldsymbol{S}'_{//}$ and $\boldsymbol{S}''_{//}$ stand for the propagation term (real part of the slowness vector) and for the damping term (imaginary part of the slowness vector) respectively. The propagation term is related to the phase velocity V_{ph} of the wave in the same way as for the elastic case:

$$S'_{//} = \frac{1}{V_{ph}}. \tag{2.2}$$

The damping term is related to the wave attenuation $\boldsymbol{k}''_{//}$ (imaginary part of the in-plane wave vector) through the relation:

$$\boldsymbol{S}''_{//} = \frac{\boldsymbol{k}''_{//}}{\omega}, \tag{2.3}$$

where ω is assumed to be real. These two components of the complex slowness vector can be collinear or not, in accordance with the homogeneous or heterogeneous model of the wave solution, respectively. There is no assumption made here on the homogeneity of the waves. In the implementation, $\boldsymbol{S}'_{//}$ and $\boldsymbol{S}''_{//}$ are two collinear vectors, as displayed in Fig.(2.1). If the waves are homogeneous, then $\boldsymbol{S}''_{//}$ stands for the total damping term. If they are heterogeneous, this term stands for the projection of the total damping term onto the phase direction.

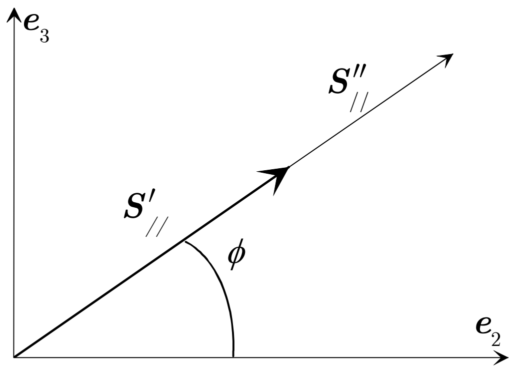

Figure 2.1: Complex slowness vector.

2.3 Material damping models

Two models are often used to describe absorbing media. One of them expresses the dynamic behaviour of the hysteresis shaped stress-strain relationship by means of the complex viscoelastic tensor C^*_{ijkl} (Lakes, R.S., 1999).

$$C^*_{ijkl} = C'_{ijkl} + i\, C''_{ijkl}, \tag{2.4}$$

where C'_{ijkl} and C''_{ijkl} are the real and imaginary part of the viscoelastic tensor. In this hysteretic model, the imaginary part of each viscoelastic constant does not depend on the frequency. In contrast, the Kelvin-Voigt model (Rose, J.L., 1999) assumes a linear dependence of C''_{ijkl} on the frequency.

$$C''_{ijkl} = \omega\, \eta_{ijkl}, \tag{2.5}$$

where η_{ijkl} is the viscosity tensor. When used in the equation of motion, the first model has lesser consequences on the implementation. Compared to a non-absorbing propagation model, the only modification is that the viscoelastic tensor becomes complex. All derivations using formerly the real elastic tensor remain the same with this viscoelastic model. On the other hand, the effect of the Kelvin-Voigt model, bringing about the frequency dependence of the tensor C^*_{ijkl}, is more drastic, the imaginary part of the viscoelasticity tensor being re-calculated at each frequency.

The impact of both models has been thoroughly investigated. From the Christoffel equation, the attenuation of bulk waves, assuming $C'_{ijkl} << C''_{ijkl}$, can be expressed as a function of the complex C^*_{ijkl} (Auld, B.A., 1973; Hosten, B., Deschamps, M. et al., 1987). It appears that the attenuation is proportional to the frequency times the imaginary part of the viscoelastic tensor. It is obvious from Eqs.(2.4 and 2.5) that the attenuation of bulk waves, being the loss per unit distance travelled, is a linear function of the frequency in the case of the hysteretic model and a quadratic function of the frequency in the case of the Kelvin-Voigt model.

Materials used in this study have been characterised using interferometry methods, at a given frequency. For that particular frequency, the attenuation in either model must therefore be the same. As seen in Fig.(2.2), this point constitutes the reference point for both viscoelastic models. Further away from this characterisation frequency, differences in attenuation predicted by the two models increase in the measure of the linear and the quadratic functions of the frequency. Thus, from a practical point of view, the difference between the models matters only if the working frequency is very different from the characterisation frequency.

Bearing in mind that the attenuation plots shown in Fig.(2.2) concern bulk waves, it is expected that similar differences will be obtained for the attenuation of Lamb waves. This matter is discussed in the derivation of Lamb waves in lossy and anisotropic plates.

The materials used in this work have been characterised using conventional ultrasonic interferometry methods (Castaings, M., Hosten, B. et al., 2000). In this process, a small sample of the unidirectional carbon-epoxy is immersed into water. Signals going through the sample are compared with signals travelling in the water only, for several incidence angles. Bulk waves velocities are measured for each configuration.

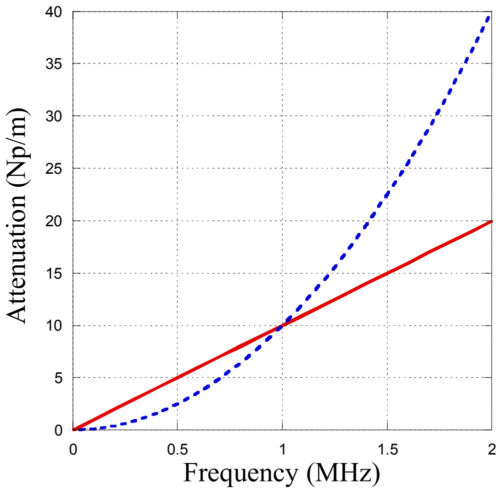

Figure 2.2: Comparison between the hysteretic model (solid line) and the Kelvin-Voigt model (dotted line). The arbitrary material is characterized at 1 MHz. The figure represents the attenuation per meter of a bulk mode using the two rheological models, as a function of the frequency.

$C'_{11} = 14.00$	$C''_{11} = 0.28$
$C'_{12} = 6.40$	$C''_{12} = 0.60$
$C'_{13} = 6.80$	$C''_{13} = 0.25$
$C'_{22} = 86.60$	$C''_{22} = 7.50$
$C'_{23} = 9.00$	$C''_{23} = 0.30$
$C'_{33} = 13.50$	$C''_{33} = 0.60$
$C'_{44} = 4.70$	$C''_{44} = 0.28$
$C'_{55} = 2.72$	$C''_{55} = 0.10$
$C'_{66} = 4.06$	$C''_{66} = 0.12$

Table 2.3: Viscoelastic components of the unidirectional carbon-epoxy panel. All quantities are given in GPa. The material density is 1.56 g.cm^{-3}. The thickness of the sample is 3.6 mm. Characterisation frequency is 2 MHz (*). Axes are those described in Chapter 1. $\mathbf{e}_1$ is the normal to the plate and $\mathbf{e}_2$ is the direction of the fibres.

Using an inverse problem formulation on the recorded information, it is possible to get back to the real and imaginary part of the viscoelastic tensor of the material. This has been performed on the Carbon-epoxy panel and the results are shown in Table (2.3).

The hysteretic model has proved to be more frequently used in composites NDE literature, reviewed in (Lakes, R.S., 1999). Rheological models have been discussed in (Leymarie, N., Aristégui, C. et al., 2002; Leymarie, N., Aristégui, C. et al., 2002) and further investigations on the material behaviour are under development. Some authors choose the attenuation law depending on the nature of modes: attenuation of the longitudinal modes manifests a different dependence on the frequency than that of the shear modes (Szabo, T.L. and Wu, J., 2000).

Even though the characterisation of specifically the viscoelastic materials is partly an issue and a possible application of this work, it is not the primary topic of this study. It suffices to mention that the theoretical framework developed for describing the propagation properties of the Lamb modes in viscoelastic anisotropic materials can adapt to any rheological model. For clarity, the choice is made to use the hysteretic model.

(*) the author is thankful to Dr. M. Castaings for his help on material characterisation.

2.4 Attenuation of Lamb modes

In the case of viscoelastic materials, the expressions for the Lamb determinant and its derivatives remain the same, except that the variable $S_{//}$ is now a complex quantity. Roots are therefore complex as well, and constitute the propagation and damping terms of the searched solution. A particular feature of the Newton-Raphson algorithm is that it is working the same way for both real and complex variables, as long as all computed functions are holomorphic functions of a complex variable. In other words , on solving Eq.(1.16), a mode is now characterized not only by its phase velocity as a function of the frequency, as in the purely elastic case, but also by the dependence of its attenuation on the frequency.

As seen on Fig.(2.4), the attenuation of the guided modes does not follow an explicit mathematical function. It is mode shape and frequency dependent. Large and sudden increases in attenuation are connected to the mode shapes changing with the frequency. For example, the S_0 mode, which is essentially compressional at low frequencies, has a very low attenuation in this range of the spectrum. As the frequency increases its displacement gets more and more out of plane and its attenuation changes drastically. Most of the modes follow this pattern. Their attenuation is strongly related also to the phase velocity dispersion: the greater the frequential dispersion is, the larger is the change of attenuation. As the frequency tends to infinity, the Lamb modes converge to bulk solutions. Accordingly, their attenuation become a linear function of the frequency. Focusing on the behaviour of the S_2 mode in Fig. (2.4), it can be seen that in the vicinity of its former cut-off frequency (former = in the non-absorbing case), the attenuation is very high and decreases along with the dispersion when the frequency raises. Further away in the frequency range (around 1.2 MHz), the attenuation increases again, along with the dispersion of the phase velocity.

A noteworthy point is the fact that there are no cut-off frequencies of the guided wave dispersion curves any longer. Event though it is not evident from Fig.(2.4), all modes start at zero frequency, like the S_1 mode. The scale is not large enough to observe all the dispersion curves of the guided modes going back to zero frequency and velocity. The former propagating mode solutions ($S_{//}$ real), are extended for values of the frequency lower than their cut-off frequency in highly attenuated or purely imaginary (non-propagating) solutions.

When the viscosity of the material is small, it has very little effect on the value of the phase velocity. Even so, some modes that were distinct in the purely elastic case become connected with each other in the absorbing case. However, this connection is actually true for the phase velocity only (linked to the real part of the slowness), whereas the attenuations of two "crossing" modes are different. Since a mode is completely defined by the quadruplet $\left(S'_{//}, S''_{//}, \omega, \phi\right)$, there is therefore no crossing of guided modes. The same phenomenon has been observed in the isotropic case by (Bernard, A., Deschamps, M. et al., 1999). For an illustration, some computations have been performed for the unidirectional Carbon-epoxy plate, and results are shown in Fig.(2.4).

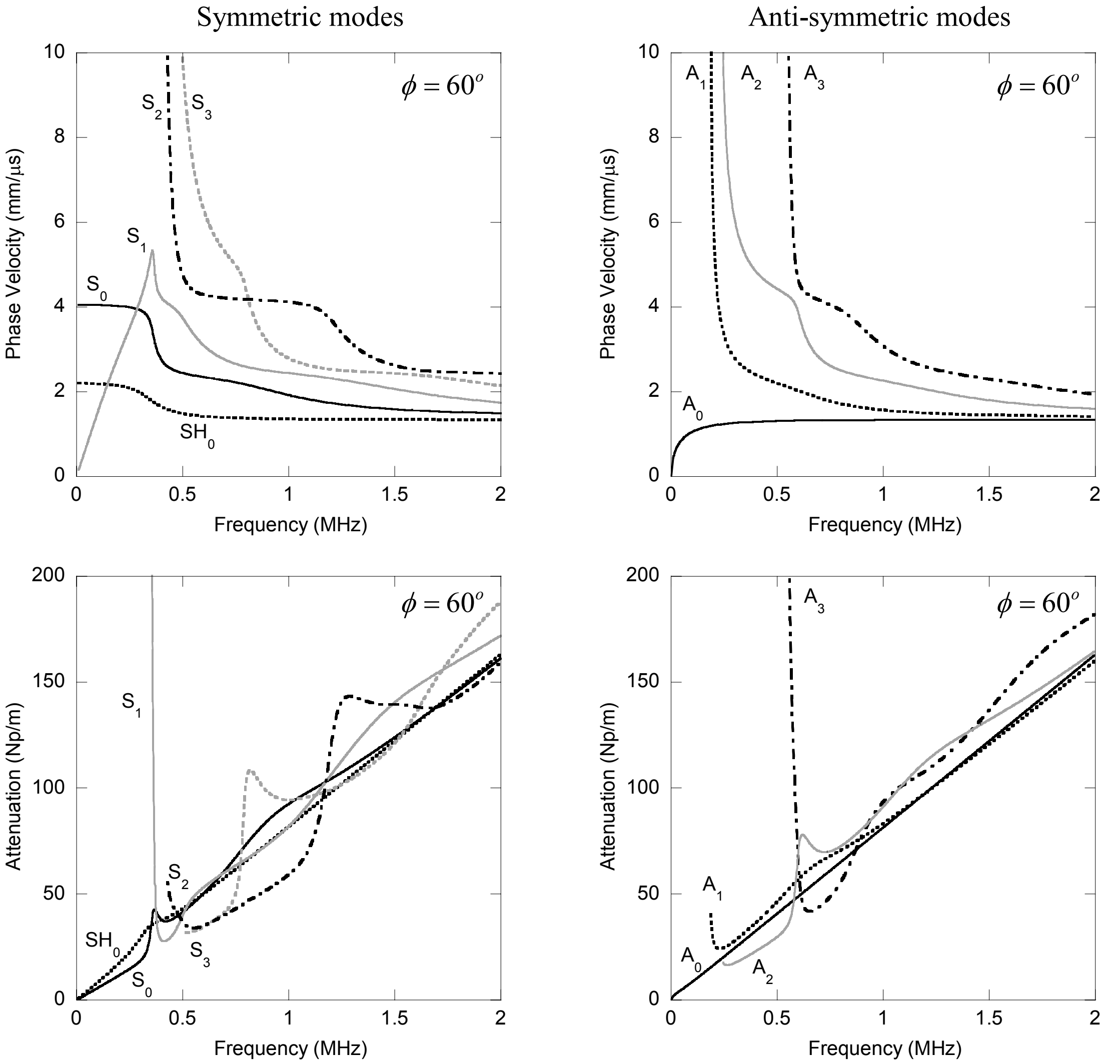

Symmetric modes

Anti-symmetric modes

Figure 2.4: Lamb mode dispersion and attenuation for a 60 degrees phase direction, for the 3.6 mm thick carbon-epoxy plate. The first row displays phase velocity (mm/µs) as a function of the frequency (MHz), for symmetric and anti-symmetric modes respectively. The second row displays their associated attenuation (Np/m) as a function of the frequency (Hysteretic model).

As said in the previous section, the rheological model affects drastically the value of attenuation of wave modes. Assuming the same rheological models as in Fig.(2.2), the attenuation prediction for the Lamb modes is described by the following pattern: far below the characterisation frequency, the Kelvin-Voigt model gives a substantially lower attenuation than the hysteretic model, at the characterisation frequency both models imply the same attenuation, and above this frequency the Kelvin-Voigt model provides a much larger attenuation than the hysteretic model.

In Fig.(2.5), the dispersions of phase velocity are compared with and without attenuation. The phenomenon of modes “crossing” described above applies for this case. For the 20 degrees phase direction, the S_0 mode in the attenuative case is a combination of the S_0 and S_1 modes existing for the purely elastic case.

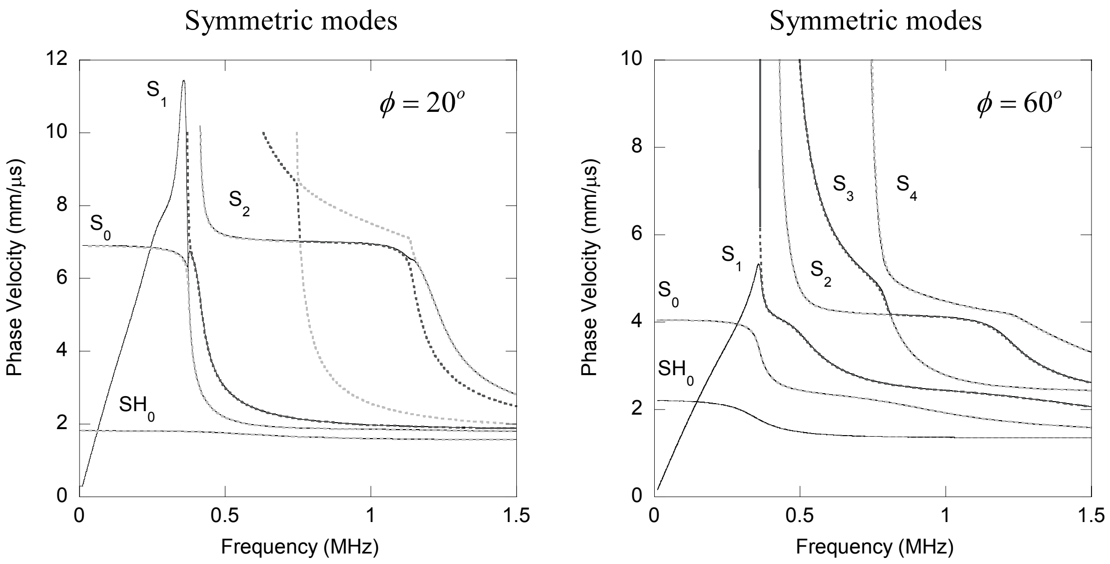
Symmetric modes

Symmetric modes

Figure 2.5: Mode connections. For 20 and 60 degrees phase direction (left and right hand side plots respectively), the Lamb modes dispersion curves are plotted in solid lines and labelled for the absorbing case, for the 3.6 mm thick carbon-epoxy plate (Hysteretic model). The modes displayed using dotted lines represent the Lamb modes in the purely elastic case.

It can be seen as well that the absorbing S_2 mode at 20 degrees (left plot) is a confluence of the purely elastic S_2, S_3 and S_4 modes. The same observation can be made for the 60 degrees phase direction (right plot), where the absorbing S_2 mode is an arrangement of purely elastic S_2 and S_3 mode fragments.

In addition to the dependence on the frequency, there is a well-pronounced angular dependence in the case of lossy anisotropic media. Like the phase velocity, the attenuation also varies with respect to the direction of the phase front. An illustration of this dependence is given in Fig.(2.6) for several frequencies.

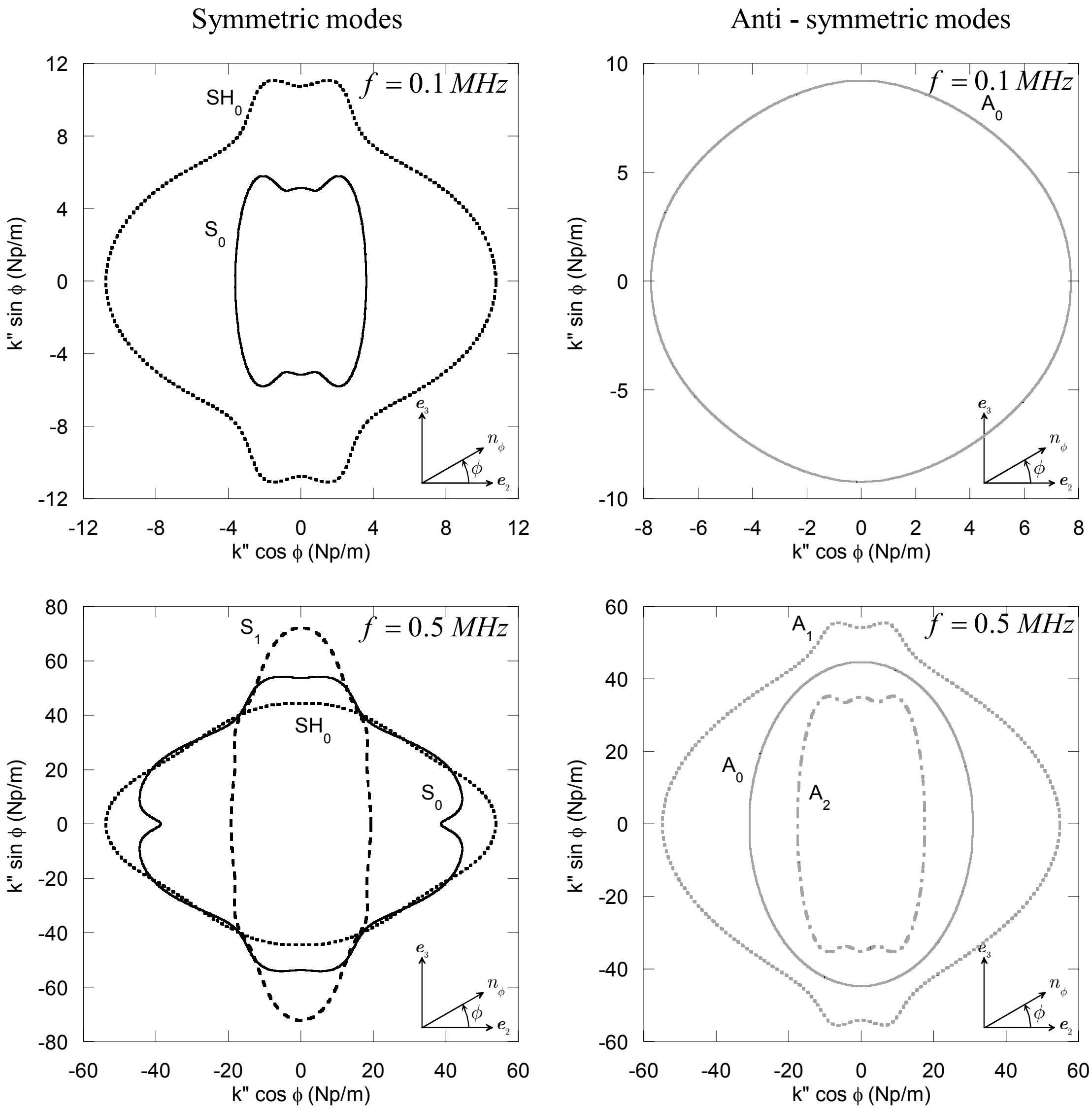

Figure 2.6: Attenuation of Lamb modes in polar coordinates, for the 3.6 mm thick carbon-epoxy plate (hysteretic model). The first row displays attenuation of the fundamental Lamb modes at 0.1 MHz. The second row displays attenuation of symmetric and anti-symmetric guided modes at 0.5 MHz, respectively on the left and right hand side of the figure.

On these polar plots representing the in-plane attenuation of Lamb modes as a function of the phase direction, it can be seen that the attenuation is affected by the anisotropy of the material. For instance at low frequency (0.1 MHz), the S_0 mode – mainly compressional at this frequency – is less attenuated in the direction of the fibres than in the 90 degrees direction, which is consistent with its mode shape. A similar comment can be made about the A_0 mode at the same frequency (when it is a bending mode) for which the attenuation is lower at 0 than at 90 degrees. At low frequency, i.e. with relatively simple mode shapes, this behaviour can be taken as a general rule. In the unidirectional carbon-epoxy example, the fibres act as a guide at 0 degree, whereas they act as scatterers in the perpendicular direction. This rule does not apply anymore at higher frequencies, with more complicated mode shapes.

To have a glance of all dependencies of the attenuation of one Lamb mode, the 3D view is again a useful tool. The attenuation of A_0 and S_0 are shown, respectively on top and bottom of Fig.(2.7), in cylindrical coordinates, and are naturally associated with 3D views of A_0 and S_0 phase velocity. These latter plots are however not displayed because of their similarity to Fig.(1.6) of Chapter 1.

In the absorbing case, a mode is characterised by both the real and imaginary part of its slowness, at given frequency and phase front direction. The reading of Fig.(2.7) follows the same rule as the other previously displayed 3D views. The in-plane coordinates are polar, i.e. the polar modulus stands for the attenuation and the azimuthal angle as the phase direction. The elevation is the frequency, just as in the other 3D plots. What has been shown with 2D polar plots is also visible in these figures; the attenuation of the A_0 mode is substantially higher in the 90 degrees direction than along the fibres. The dependence of its attenuation is rather smooth both with the frequency and the phase direction. For the S_0 mode however, the behaviour is not so straightforward. At low frequency it is more attenuated at 90 than at 0 degree, but when the frequency increases the variation of attenuation in high dispersion zones becomes steeper than for the A_0 mode.

2.5 Conclusion

This chapter summed up the modifications induced by the viscoelasticity on the phase velocity and attenuation. It has been seen that the viscosity causes very little changes to the magnitude of the phase velocity of the guided modes. However, the remarkable phenomenon of mode connections may be encountered for anisotropic absorbing plates.

The dependence of the attenuation of guided modes with the frequency is naturally strongly affected by the choice of a rheological model.

For simplicity and to follow the trend of many authors working on composites, the choice has been made to use the hysteretic model, where C''_{ijkl} does not depend on the frequency. Nevertheless, it is to be noted that all the development carried out in this work is applicable to any rheological model.

Similarly to the guided modes velocities for the non-absorbing case, the attenuation is shown in 3D plots, highlighting its dependence on both the frequency and the phase direction.

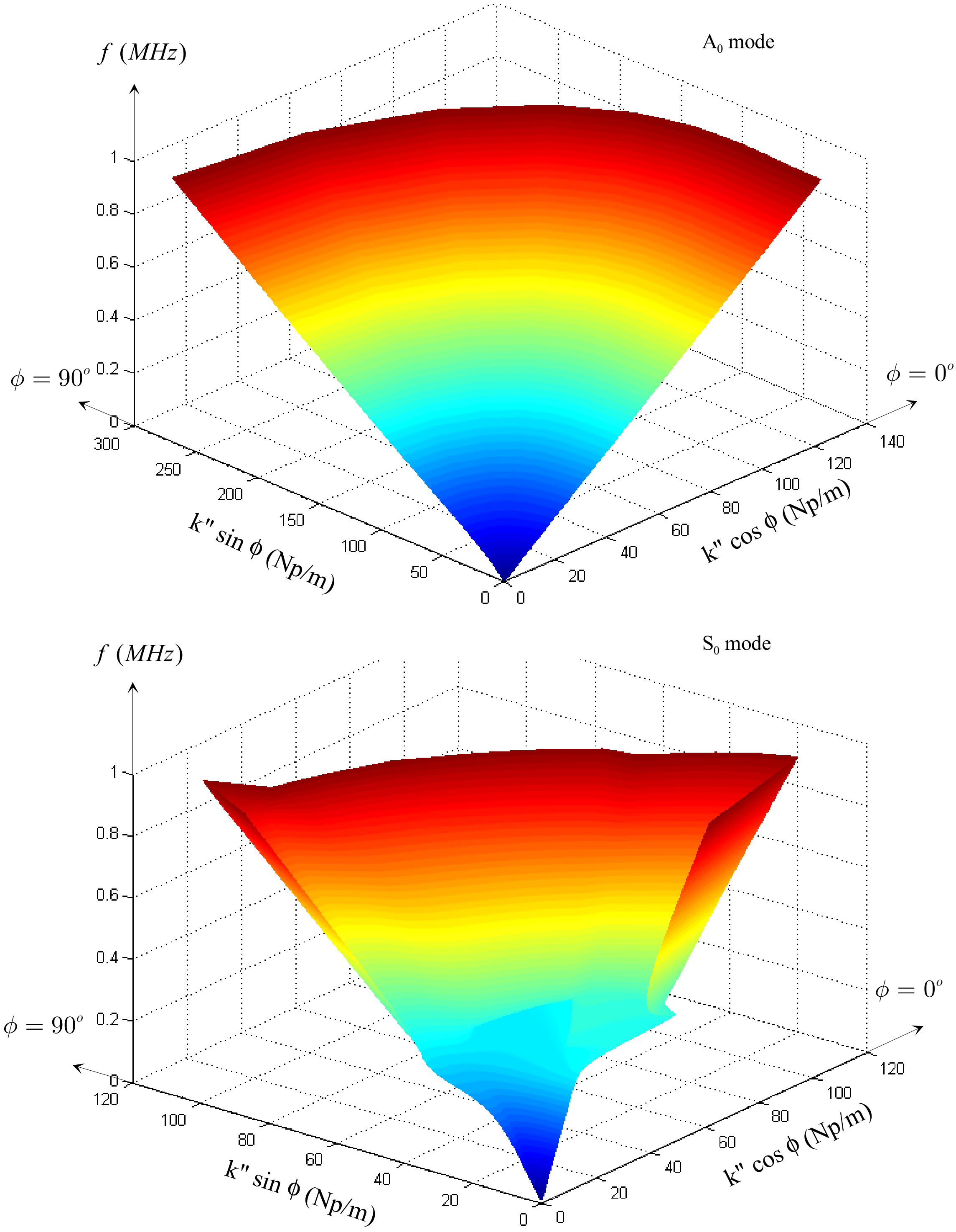

Figure 2.7: 3D view of the attenuation of A_0 (top figure) and S_0 (bottom figure), for the 3.6 mm thick carbon-epoxy plate. The coordinate system is cylindrical: the polar modulus is the attenuation (Np/m), the azimuthal angle is the phase direction (degrees), and the elevation is the frequency (MHz).

This chapter encompasses therefore the properties of Lamb modes caused jointly by the anisotropy and the viscoelasticity of the insonified material.

A limitation, reserved in this part, is that the phase velocity and attenuation have only been described; consequences of the viscosity on the group and energy velocity of guided modes have not been investigated yet. This more general subject is the topic of the next chapter.

Chapter 3

Energy velocity and attenuation along the ray direction

3.1 Introduction

Lamb waves are attractive for the non destructive testing industry. They can propagate in many materials for which quality control or the knowledge of the material properties is needed (Lowe, M.J.S. and Cawley, P., 1994; Challis, R.E., Bork, U. et al., 1996; Ghosh, T., Kundu, T. et al., 1998; Kundu, T., Maji, A. et al., 1998; Bonnin, A., Huchon, R. et al., 1999; Lowe, M.J.S. and Diligent, O., 2001). With conventional ultrasound techniques the scanning of a large structure is very long and tedious. The advantage of the guided waves is that they can propagate over large distances, thus reducing the time of the structure scan. The aim of an industrial application of Lamb waves is therefore to make a fast scan of large structures, spotting roughly the defect zones. A complementary conventional scan should then be performed in the area determined by the fast guided wave scan, if more precision is needed. The prerequisite for this task is the knowledge of all the propagation properties of the Lamb waves.

In some cases, it is possible to use Lamb modes knowing their phase information only. With the spectrum method (Sachse, W. and Pao, Y.-H., 1978; Castaings, M. and Hosten, B., 2001), the experimental phase velocity dispersion curves can be gained, performing several adjacent measurements with the receiving transducer. The change in phase between two adjacent measurements is expressed by the phase of the transfer function, which is defined by the Fourier transform of one signal divided by the Fourier transform of its adjacent one. Knowing the distance between the two measurement points Δx and the change in phase $\Delta\Phi$, the phase velocity can be deduced using the following relation:

$$V_{ph} = \frac{2\pi f \Delta x}{\Delta\Phi}. \tag{3.1}$$

Performing this routine automatically for several frequencies, it is possible to obtain experimental phase velocity dispersion curves and therefore to infer information on the plate integrity.

There are however many cases when dealing with dispersive waves requires not only the knowledge of their phase quantities but also of their energy quantities. In a point source- point receiver configuration for instance, with measurement at a single location, the received signal contains explicitly the energy information and is measured in an observation direction that is the ray direction or the energy direction. In the non-absorbing case, the group velocity is equal to the energy velocity, see Chapter 1. However with viscoelasticity taken into account, the definition of the group velocity in viscoelastic media becomes obscure. Even a choice for an approximate definition poses difficulty. The derivative of the angular frequency with respect to the real part? To the imaginary part? To the modulus of the wave vector? None of these would be rigorously meaningful. The first suggestion is however often used as an approximation of the group velocity; see discussion about this in (Bernard, A., Deschamps, M. et al., 1999). At the same time, the definition of the energy velocity is physically clear: it is the ratio of the averaged Poynting vector and the total energy density of the system, in other words the velocity of the energy travelling across the plate section. Moreover, as shown in (Bernard, A., Deschamps, M. et al., 1999), the comparison between the approximation of the group velocity, the energy velocity and experimental measurements concludes that the approximation of the group velocity is only valid when the attenuation is relatively small, whereas the energy velocity of the guided modes propagating in a viscoelastic medium is in accordance with the measurements.

The aim of the forthcoming study is to bring understanding to a new topic: the energy velocity and attenuation dispersions of a guided mode in the direction of observation. Some interesting analytical features of these quantities are investigated. This chapter consists of three sections. In the first one, all the energy terms are described and the complex Poynting vector is defined. The energy velocity is derived from the complex Poynting vector. In the second section the scalar product of $\boldsymbol{S}_{//}$ and the energy velocity vector is derived and the resulting terms are interpreted. This section intends to elucidate the attenuation of guided modes in their energy direction, as opposed to the phase attenuation or simply the attenuation in the previous chapter (Caroll, N.L., Humphrey, V.F. et al., 2002). Finally, in the third section the concept of frequential dispersion of both the energy velocity and the attenuation along the observation direction is introduced. As has been illustrated in the first chapters, the energy velocity dispersion curves need to be linked to the dispersion of their associated steering angle. It is believed that the display of these dispersions for a given energy direction which is presented here is novel. In contrast, the usual group velocity dispersion plots displayed in the literature are computed for a given phase front direction.

3.2 Energy contributions

As said earlier, the viscoelastic tensor has complex components. Hence the stress tensor can be decomposed into two contributions: the elasticity stress σ_{ij}^{e} and the viscosity stress tensor σ_{ij}^{d} (where *e* stands for elastic and *d* for dissipation).

$$\begin{aligned} \sigma_{ij} &= \sigma_{ij}^{e} + i\,\sigma_{ij}^{d}, \\ \sigma_{ij}^{e} &= C'_{ijkl}\varepsilon_{kl}, \\ \sigma_{ij}^{d} &= C''_{ijkl}\varepsilon_{kl}. \end{aligned} \tag{3.2}$$

In consequence, the potential energy e_p and the dissipation energy e_d densities for time-harmonic waves, can be expressed in terms of the complex formulation. The energy carried by a wave is indeed the average in time of the product of two sinusoidal quantities. This product can be expressed using the conjugate of one of the two associated complex terms. Taking into account the fact that products $\sigma_{ij}^{e}\varepsilon_{ij}^{*}$ and $\sigma_{ij}^{d}\varepsilon_{ij}^{*}$ are real (Royer, D. and Dieulesaint, E., 1996), the time-averaged energy densities can be expressed as:

$$\begin{aligned} \left\langle e_p \right\rangle_t &= \frac{1}{4}\sigma_{ij}^{e}\varepsilon_{ij}^{*}\,, \\ \left\langle e_d \right\rangle_t &= \frac{1}{4}\sigma_{ij}^{d}\varepsilon_{ij}^{*}\,, \end{aligned} \tag{3.3}$$

where $\langle\ \rangle_t$ stands for the average over a time period, and * for the complex conjugate. The mean kinetic energy density is given by:

$$\left\langle e_k \right\rangle_t = \frac{1}{4}\rho V_i V_i^{*}. \tag{3.4}$$

With regards to the Lamb waves, these averaged energy densities can be integrated over the thickness of the plate to obtain the spatially averaged energy terms. Let E_n be the averaged energy in time and in space:

$$E_n = \frac{1}{h}\int_{-h/2}^{+h/2} \left\langle e_n \right\rangle_t \, dx_1, \tag{3.5}$$

where n designates the type of energy $(n = p, d, k)$. Let us introduce the local complex Poynting vector, according to (Auld, B.A., 1973):

$$\left\langle P_i \right\rangle_t = -\frac{1}{2}\sigma_{ij}V_j^{*}, \tag{3.6}$$

The in-plane projection of the power flow is define as:

$$\boldsymbol{\Phi}_{//} = \frac{1}{h}\int_{-h/2}^{+h/2} \boldsymbol{P}'_{//} \, dx_1, \tag{3.7}$$

where $\boldsymbol{P}'_{//}$ is the real part of the in-plane component of the complex Poynting vector. This quantity represents the energy flow carried along the energy direction, in the azimuthal plane.

From these power-flow and energy quantities, the energy velocity is defined as the following ratio:

$$\boldsymbol{V}_e = \frac{\boldsymbol{\Phi}_{//}}{E_p + E_k}, \tag{3.8}$$

It is to be noted that this quantity is real and represents the speed at which the energy is carried by a guided mode in an anisotropic absorbing plate. This definition is physically clear in terms of energy contributions, as opposed to the group velocity in such a case. In practical terms, this is the velocity that is going to be measured in the experimental illustration. The description of the energy propagation is however incomplete, since this term does not take into account the energy attenuation. The study of the attenuation of guided modes along the energy direction is the topic of the next section.

3.3 Energy attenuation of guided modes

The derivation of this section is largely based on theory from (Auld, B.A., 1973; Royer, D. and Dieulesaint, E., 1996) dealing with the case of a piezoelectric purely elastic wave guide, and from (Carcione, J.M., Cavallini, F., 1993) in the case of viscoelastic bulk modes. The aim of the derivation is to determine the scalar product of the energy velocity vector with the complex slowness vector, in the case of a viscoelastic anisotropic wave guide. As will be seen later, the physical interpretation of the involved terms casts light on the properties of the attenuation of guided modes in viscoelastic plates. Manipulating the equation of motion Eq.(1.2) leads to the the following relation:

$$\boldsymbol{S}_{//}.\boldsymbol{P}_{//} = 2\left\langle e_k \right\rangle_t + \frac{i}{2\omega} V_i^* \sigma_{i1,1} \,. \tag{3.9}$$

The derivation to find Eq.(3.9) is detailed hereafter. First we note that multiplying Eq.(1.2) by V_i^* leads to:

$$V_i^* \sigma_{ij,j} = i\omega\rho V_i V_i^* = 4i\omega \left\langle e_k \right\rangle_t \,. \tag{3.10}$$

The left hand side term can be expanded this way.

$$\begin{aligned}
V_i^* \sigma_{ij,j} &= V_i^* \left(\partial_1 \sigma_{i1} - ik_2 \sigma_{i2} - ik_3 \sigma_{i3} \right); \\
V_i^* \sigma_{ij,j} &= V_i^* \partial_1 \sigma_{i1} - ik_2 V_i^* \sigma_{i2} - ik_3 V_i^* \sigma_{i3}; \\
V_i^* \sigma_{ij,j} &= V_i^* \partial_1 \sigma_{i1} + 2i\left(k_2 P_2 + k_3 P_3 \right); \\
V_i^* \sigma_{ij,j} &= V_i^* \partial_1 \sigma_{i1} + 2i\boldsymbol{k}_{//} \cdot \boldsymbol{P}_{//},
\end{aligned} \tag{3.11}$$

which, according to Eq.(3.10), leads to,:

$$2i\boldsymbol{k}_{//}\cdot\boldsymbol{P}_{//} = 4i\omega\left\langle e_k\right\rangle_t - V_i^*\partial_1\sigma_{i1}. \tag{3.12}$$

On expressing the wave vector as a function of the slowness vector Eq.(3.9) is obtained. On the other hand, the strain-displacement relationship can be time-derived to get:

$$i\omega\,\varepsilon_{ij} = V_{i,j}. \tag{3.13}$$

Multiplying this equation by σ_{ij}^* gives:

$$\boldsymbol{S}_{//}.\boldsymbol{P}_{//}^* = 2\left\langle e_p\right\rangle_t - 2i\left\langle e_d\right\rangle_t + \frac{i}{2\omega}\sigma_{i1}^*V_{i,1}. \tag{3.14}$$

The relation (3.14) is obtained through the following steps.

$$\begin{aligned}
\sigma_{ij}^*V_{i,j} &= i\omega\sigma_{ij}^*\varepsilon_{ij} = i\omega\left(\sigma_{ij}^e + i\sigma_{ij}^d\right)^*\varepsilon_{ij};\\
\sigma_{ij}^*V_{i,j} &= i\omega\sigma_{ij}^{e*}\varepsilon_{ij} + \omega\sigma_{ij}^{d*}\varepsilon_{ij};\\
\sigma_{ij}^*V_{i,j} &= 4i\omega\left\langle e_p\right\rangle_t + 4\omega\left\langle e_d\right\rangle_t;
\end{aligned} \tag{3.15}$$

Expanding the left hand side term of the last expression leads to:

$$\begin{aligned}
\sigma_{ij}^*V_{i,j} &= \sigma_{i1}^*\partial_1V_i - ik_2\sigma_{i2}^*V_i - ik_3\sigma_{i3}^*V_i;\\
\sigma_{ij}^*V_{i,j} &= \sigma_{i1}^*\partial_1V_i + 2i\left(k_2P_2 + k_3P_3\right);\\
\sigma_{ij}^*V_{i,j} &= \sigma_{i1}^*\partial_1V_i + 2i\boldsymbol{k}_{//}.\boldsymbol{P}_{//}^*,
\end{aligned} \tag{3.16}$$

which gives:

$$2i\,\boldsymbol{k}_{//}.\boldsymbol{P}_{//}^* = 4\omega\left\langle e_p\right\rangle_t - 4i\omega\left\langle e_d\right\rangle_t + i\sigma_{i1}^*\partial_1V_i. \tag{3.17}$$

Applying one more time the relation between the wave vector and the slowness vector, gives Eq.(3.14).

Adding Eqs.(3.14) and (3.9) leads to:

$$\boldsymbol{S}_{//}.\boldsymbol{P}'_{//} = \left\langle e_p\right\rangle_t + \left\langle e_k\right\rangle_t - \left\langle e_\omega\right\rangle_t - i\left\langle e_d\right\rangle_t - i\left\langle e_l\right\rangle_t, \tag{3.18}$$

where

$$\left\langle e_\omega\right\rangle_t = \frac{1}{2\omega}\operatorname{Im}\left(V_i^*\sigma_{i1,1}\right) \text{ and } \left\langle e_l\right\rangle_t = \frac{-1}{2\omega}P_{1,1}^*. \tag{3.19}$$

The energy term $\left\langle e_\omega\right\rangle_t$ can be understood, in the case of Lamb waves, as a dispersive energy, and $\left\langle e_l\right\rangle_t$ as the complex contribution of the leakage into the outside medium. These local equations can be integrated over the thickness of the wave guide. In the case of a plate in vacuum, that is to say in the case of a wave propagating without any loss due to leakage, the integration of $P_{1,1}$ over the thickness is zero. Integrating Eq.(3.18) over the thickness gives:

$$\boldsymbol{S}'_{//}.\boldsymbol{V}_e = 1 - \frac{E_\omega}{E_p + E_k}, \tag{3.20}$$

and

$$\boldsymbol{S}''_{//}.\boldsymbol{V}_e = \frac{E_d}{E_p + E_k}. \tag{3.21}$$

Eqs.(3.20) and (3.21) define respectively the projections of the phase slowness and the attenuation onto the energy velocity. Eq.(3.20) recalls the relation $\boldsymbol{S}'_{//}.\boldsymbol{V}_e = 1$, which is valid in the case of non-dispersive waves, as illustrated in Fig.(3.1). Let S_{n_e} be the projection of the phase slowness vector $\boldsymbol{S}_{//}$ onto the energy direction and S_e be the inverse of the energy velocity modulus; then this relation can be written as:

$$S_e = S_{n_e}, \tag{3.22}$$

As illustrated in Fig.(3.2), the phase fronts, separated by the phase wavelength $\lambda_{//}$ define a wavelength λ_{n_e} in the direction of observation. The time needed to cover these two distances is the same, as expressed by the following relation:

$$S_{n_e} \cdot \lambda_{n_e} = S'_{//} \cdot \lambda_{//}. \tag{3.23}$$

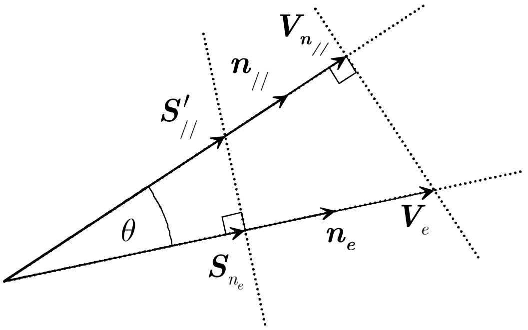

$$V_{\boldsymbol{n}_{//}} = V_{//}$$

$$S_{n_e} = S_e$$

Figure 3.1 : Phase and energy slowness and velocity projection for non-dispersive plane waves. $\boldsymbol{n}_{//}$ is the phase direction, $\boldsymbol{n}_e$ is the energy direction.

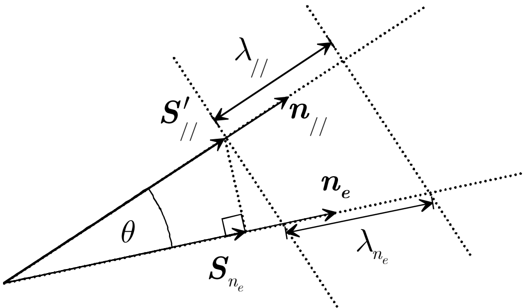

Figure 3.2 : Phase front (dotted lines) defining a wavelength along the energy direction $\boldsymbol{n}_e$.

In the case of the Lamb waves, Eq.(3.22) is modified by a dispersive energy component to form Eq.(3.20). This interpretation of E_ω can be approached using an analogy with the non-absorbing case. In this case, the group velocity is rigorously equal to the energy velocity, and Eq.(1.31) is verified. The right hand side of Eq.(1.32), that reads for the non-absorbing case only, refers to a frequential dispersion component. The analogy with Eq.(3.20) illustrates the interpretation of E_ω as a contribution responsible for frequential dispersion. Moreover the following relation, obtained from Eq.(3.20), relates E_ω to a characteristic of the dispersion, i.e. the difference between phase and energy velocities.

$$S_e - S_{n_e} = \frac{E_\omega}{\Phi_{//}}. \tag{3.24}$$

Indeed for dispersive waves, these two quantities are different, as seen in Fig.(3.3) illustrated by a grey zone between the slownesses along the energy direction, and the label ΔS. In the principal directions where no angular dispersion is present, it can be seen that the difference between the phase and energy velocity is completely expressed by the term E_ω and the in-plane power flow. This difference between slownesses can be expressed in velocities as well, illustrated by the grey zone and the label ΔV along the phase direction $\boldsymbol{n}_{//}$ in Fig.(3.3).

$$V_{n_{//}} - V_{//} = \frac{V_{//} E_\omega}{E_p + E_k}, \tag{3.25}$$

where $V_{n_{//}}$ is the projection of the energy velocity onto the phase direction and $V_{//}$ is the phase velocity modulus.

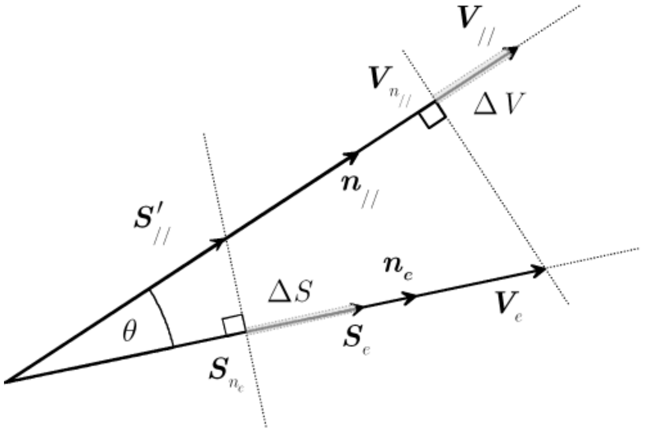

Figure 3.3: Phase and energy slowness and velocity projections for dispersive guided waves. ΔV is the difference between the projection of the energy velocity onto the phase direction and the phase velocity. Accordingly, ΔS is the difference between the projection of the phase slowness onto the energy direction and the energy slowness.

From Eq.(3.21), the projection of the phase attenuation onto the energy direction reads:

$$\boldsymbol{k}''_{//}.\boldsymbol{n}_e = \omega \frac{E_d}{\Phi_{//}}, \tag{3.26}$$

The term E_d is indeed expressed in [J.m^{-1}], it represents the dissipation energy per unit distance of the wave guide. The power flow $\Phi_{//}$ is expressed in [J.s^{-1}] and the frequency in [Hz]. The dimension of this ratio is therefore in [m^{-1}], consistent with an attenuation per unit distance. Eq.(3.26) shows the physical meaning of the projection of the phase attenuation along the ray direction (direction of the energy). This projection is equal to the ratio of the viscous dissipation energy to the average power flow in the azimuthal plane and therefore corresponds to the displacement field attenuation, along the energy direction (Deschamps, M. and Assouline, F., 1999). This quantity can be expressed as well in Nepers per wavelength which is obtained in multiplying the attenuation per unit distance by the wavelength. Using Eq.(3.23), the same attenuation in Nepers per wavelength may be referred to in the phase or in the energy direction, see Fig.(3.4). The attenuation along the ray direction is indeed obtained by multiplying the phase attenuation by the cosine of the steering angle whereas the wavelength in the energy direction is equal to the phase wavelength divided by the same cosine.

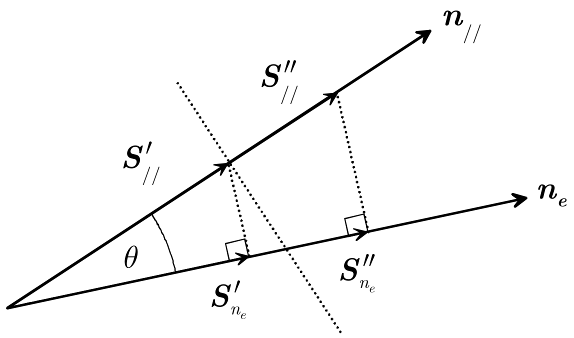

Figure 3.4: Projection of the phase slowness along the energy direction. θ is the deviation angle.

In this section, it has been seen that all guided mode properties appear differently whether the observer is in the phase or in the energy direction. Coming back to the point-source / point-receiver configuration, the point source is expected to excite modes in every phase directions, and the receiver is reading the energy information taking into account all the eventually different phase contributions. This matter is going to be illustrated in the next section, where the focus is put on the understanding of the direction of observation of guided modes in anisotropic media.

3.4 Lamb mode properties along the observation direction

As said earlier in Section 1.3, displaying the modulus of the energy velocity in a non-principal direction of an anisotropic media is an incomplete description. In Chapter 1, it has been explained and illustrated that those plots also need the associated steering angle. In this section, it is proposed to reverse the visualisation type, i.e. to represent the energy velocity dispersion in a chosen observation direction, whereas the phase velocity is to be displayed in modulus as a function of the frequency. To have the corresponding phase direction, the associated steering angle plot is still needed. The aim of such a visualisation is to get closer to a point-source - point-receiver experimental configuration, in which case the measured quantities are indeed the energy velocity and attenuation. This type of visualisation is useful in anisotropic media since quantities measured in a given direction might have been steered from a different phase direction. Moreover, in a cusp region, there is more than one signal received for the same mode at the same frequency. This is precisely what has been developed in this section.

The energy velocity of guided modes is calculated for a chosen observation direction. To the best of the author's knowledge, such a computation is novel. The principle of the calculation is as follows. From a dispersion curve of one Lamb mode (phase velocity as a function of the frequency) in a given phase direction, the slowness and wave surfaces are calculated at each frequency, using the classical dispersion plot values as initialisation. This information contains the direction of energy as well, or the direction of observation. At this point, phase directions (there can be more than one in a cusp region) corresponding to the chosen observation direction are searched on the slowness surface. For these particular phase directions, all quantities of the mode are calculated, i.e. the energy and the phase velocity, steering angle, phase and energy attenuation. This operation is then automatically repeated for the whole frequency range under consideration. This gives rise to multi-valued dispersion curves as opposed to the classical single-valued dispersion plots. An illustration of these calculations has been performed for guided modes SH_0, S_0, A_0, A_1, S_1 and S_2, in the example carbon-epoxy plate. In Fig.(3.5), their energy velocity dispersion is represented in the 50 degrees direction of observation.

As seen in Fig.(3.5), the energy velocity dispersion for most of the guided modes does alternate between single-valued and multi-valued curve types. This reveals the frequency-dependent arrival and vanishing of cusp of the wave surface in a sector enclosing the chosen direction. Looking at the S_0 mode for instance, it appears that there is no cusp until the frequency 0.4 MHz, then a cusp shows up in the 50 degrees direction, since there are three phase directions and velocities steering energy into the given direction of observation.

This cusp stays in this direction until the frequency 1.02 MHz, at which it moves away from the chosen observation direction. These features are summed up in Fig.(3.6), displaying waves surfaces of the S_0 mode for several frequencies.

In this figure, it can be seen that at 0.4 MHz, the intersection between the 50 degrees direction line and the S_0 wave surface does occur at three points. These three intersections predict the three different arrival times, which should be picked up experimentally.

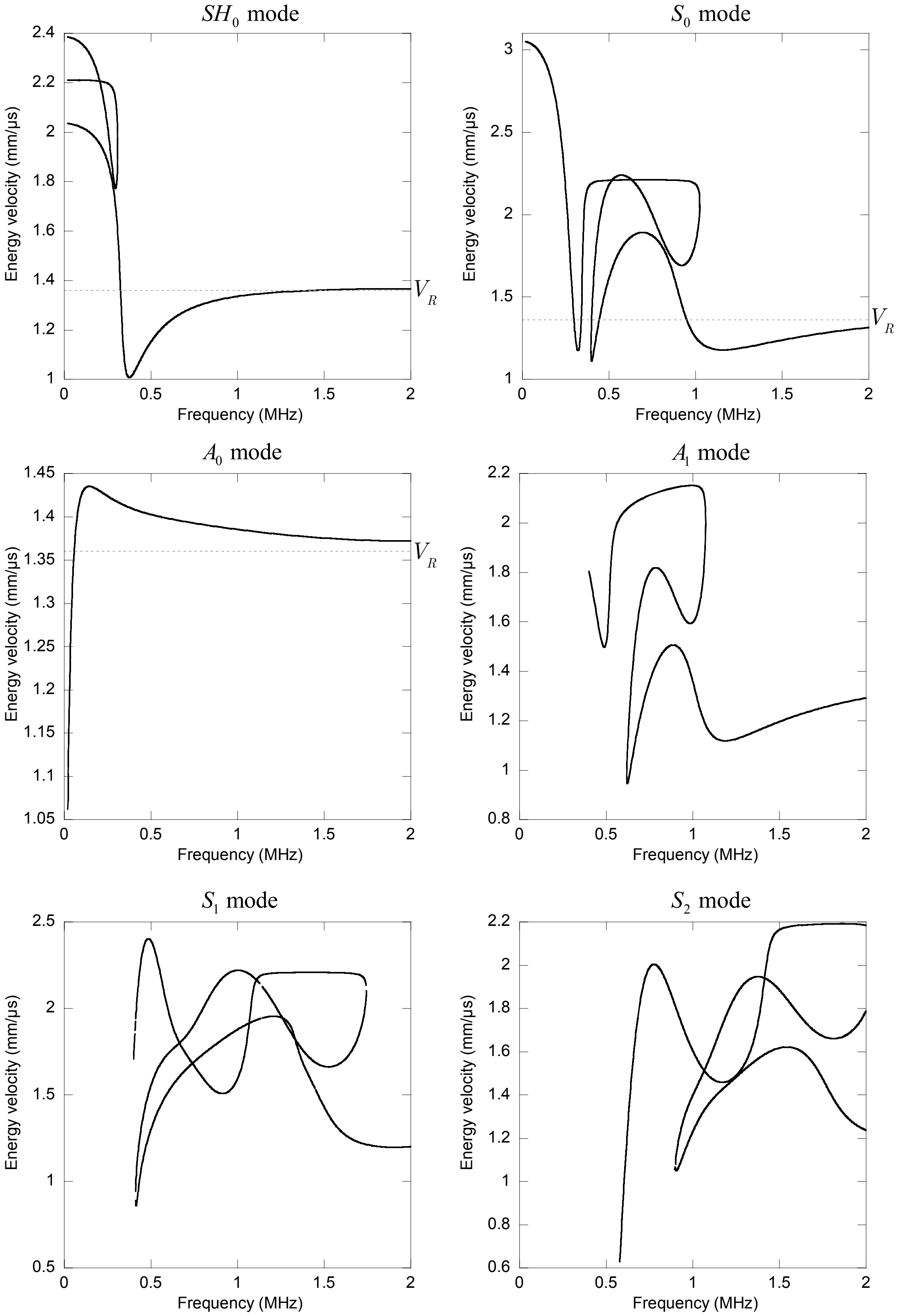

Figure 3.5: Energy velocity dispersion in the 50 degrees observation direction. SH_0, S_0, A_0, A_1, S_1 and S_2 modes. Plate is unidirectional carbon-epoxy, with material properties given in Table(2.3).

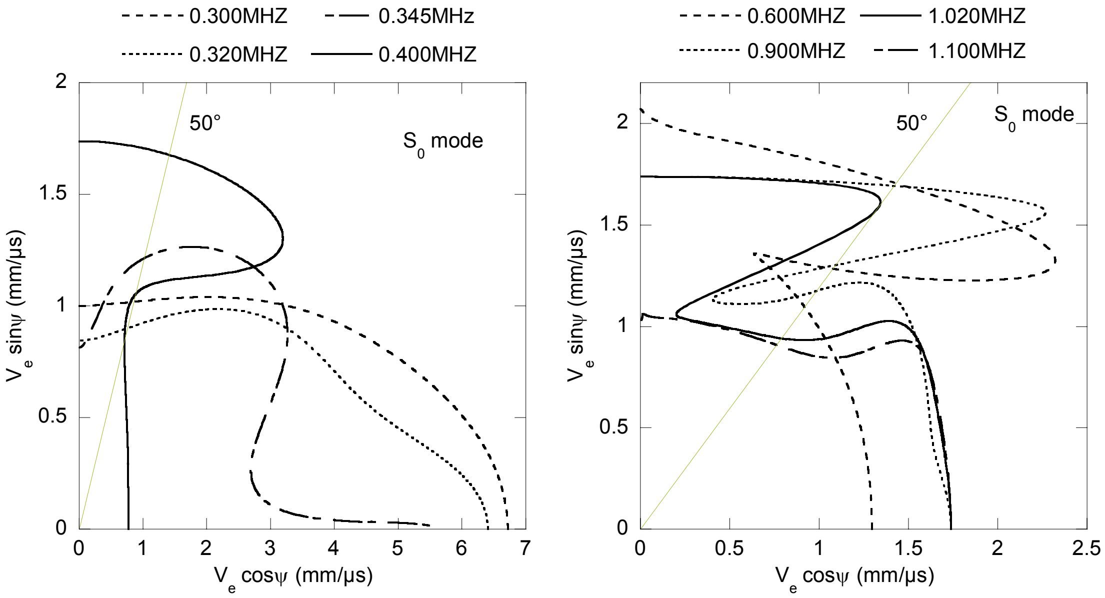

Figure 3.6: Azimuthal cuts of the wave surfaces of the S_0 mode at several frequencies. The 50 degrees direction is shown by the straight line. There is no cusp in this direction until 0.4 MHz, and then the cusp appears, remains present for a frequency bandwidth and disappears at 1.02 MHz.

In other words these three intersections correspond to three values of energy velocity of the S_0 mode, travelling in the same energy direction, despite the fact they have three different phase directions and velocities.

As opposed to non dispersive wave surfaces, for which the cusp of the shear mode is sharp (Every, A.G., Kim, K.Y. et al., 1997), it is observed in Fig.(3.6) that the shape of the waves surfaces of the S_0 mode is smooth. The frequency dispersion component, defined in the previous section, soften the energy focusing region.

For frequencies between 0.4 and 1.02 MHz, there are still three intersections between wave surfaces of S_0 and the 50 degrees direction line, indicating the cusp presence within this frequency range.

At 1.02 MHz, only two intersections are observed. As seen in Fig.(3.6), it corresponds to a cusp tangent to the 50 degrees direction line. At higher frequency, the cusp still exists, but shifts away toward the 90 degrees direction. This behaviour is in accordance with Fig.(3.5) where the S_0 energy velocity dispersion in the 50 degrees direction becomes single-valued, after being multi-valued in the frequency range 0.4-1.02 MHz.

Similar conclusions can be inferred for the other modes displayed in Fig.(3.5). The general rule is that a single-valued dispersion zone means only one phase direction and velocity steering in the chosen observation direction Ψ, while a multi-valued dispersion zone of the energy velocity corresponds to several phase directions and velocities aligned along Ψ, thereby revealing a cusp region including the chosen observation direction.

The energy velocity plots may be complemented by the diagrams for the other quantities characterising a mode. The method to calculate the phase velocity, attenuation, steering and phase angle referred to a given observation direction, has been explained above. These complementary plots are given for the fundamental modes $A_{0,}$ SH_0 and S_0 in Figs.(3.7), (3.8) and (3.9) respectively. They represent a modulus versus frequency dependence. Note that the phase direction, referred to a fixed energy direction (the direction of observation) does indeed vary due to the frequency dispersion. This variation should be recovered from the phase direction plots, also presented below. In turn, concerning the attenuation, the plots display the attenuation of the phase projected on the energy direction. This quantity has been studied in the previous section and has been found to correspond physically to the energy attenuation, see Eq.(3.26). In Figs.(3.7), (3.8) showing the SH_0 and the S_0 mode, it appears difficult to distinguish the different attenuations per unit distance associated to different phase directions. The distinction between them is however much clearer if the attenuation value is displayed in Nepers per wavelength. Once more, it is to be noted that for all curves, the transition from multi-valued to single-valued zone or reciprocally, reveals the arrival and vanishing of the cusp area embracing the given direction of observation. Similar comments can be made on any quantity displayed for the $A_{0,}$ SH_0, and S_0 modes.

Consider the properties of the SH_0 mode, see Fig.(3.7). At low frequency, the difference between the phase directions steering in the same energy direction of 50 degrees is striking. The extent of the cusp area is very large.

According to the phase direction plot (top right), the phase directions steering in the 50 degrees direction at low frequency are roughly 32, 73 and 86 degrees, that is, the steering angles are +18, -23 and –36 degrees, respectively. Looking at the phase velocity curve (top left plot), it can be observed that the moduli of the different phase direction velocities are indeed distinct in the cusp zone.

Note in passing that it is the SH_0 mode (see mode labelling in Chapter 1) which tends to the Rayleigh energy velocity, along with A_0 at high frequency.

Similar analysis can be applied to the S_0 mode shown in Fig.(3.8). From this figure and Fig.(3.6), it is seen that, at low frequency, there is no cusp at all on the S_0 wave surface (contrary to the SH_0 mode). However, a cusp enclosing the observation direction evolves at a higher frequency and then it closes up with further frequency increase.

Consider the A_0 mode. Inspecting Fig.(3.9), it is seen that there are no cusps of the energy velocity for this branch within the frequency range examined.

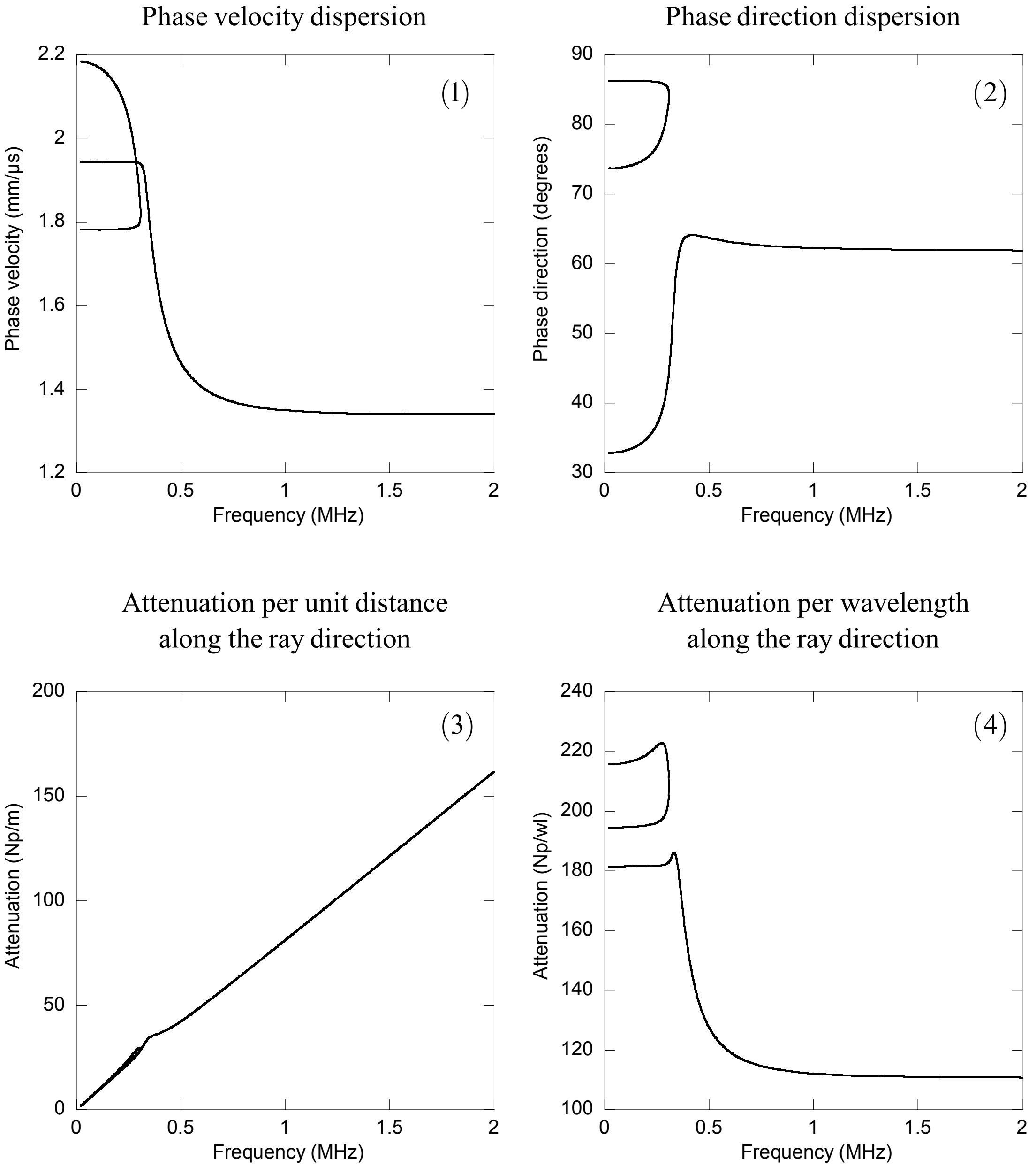

Phase velocity dispersion

Phase direction dispersion

Attenuation per unit distance along the ray direction

Attenuation per wavelength along the ray direction

Figure 3.7:Frequential dispersion of the parameters of the SH_0 mode, whose energy travels along the 50 degrees observation direction. The phase velocity dispersion is displayed in plot (1)*, the phase direction dependence on the frequency is displayed in* (2)*, the attenuation per meter and per wavelength are respectively shown by plots* (3) *and* (4)*.*

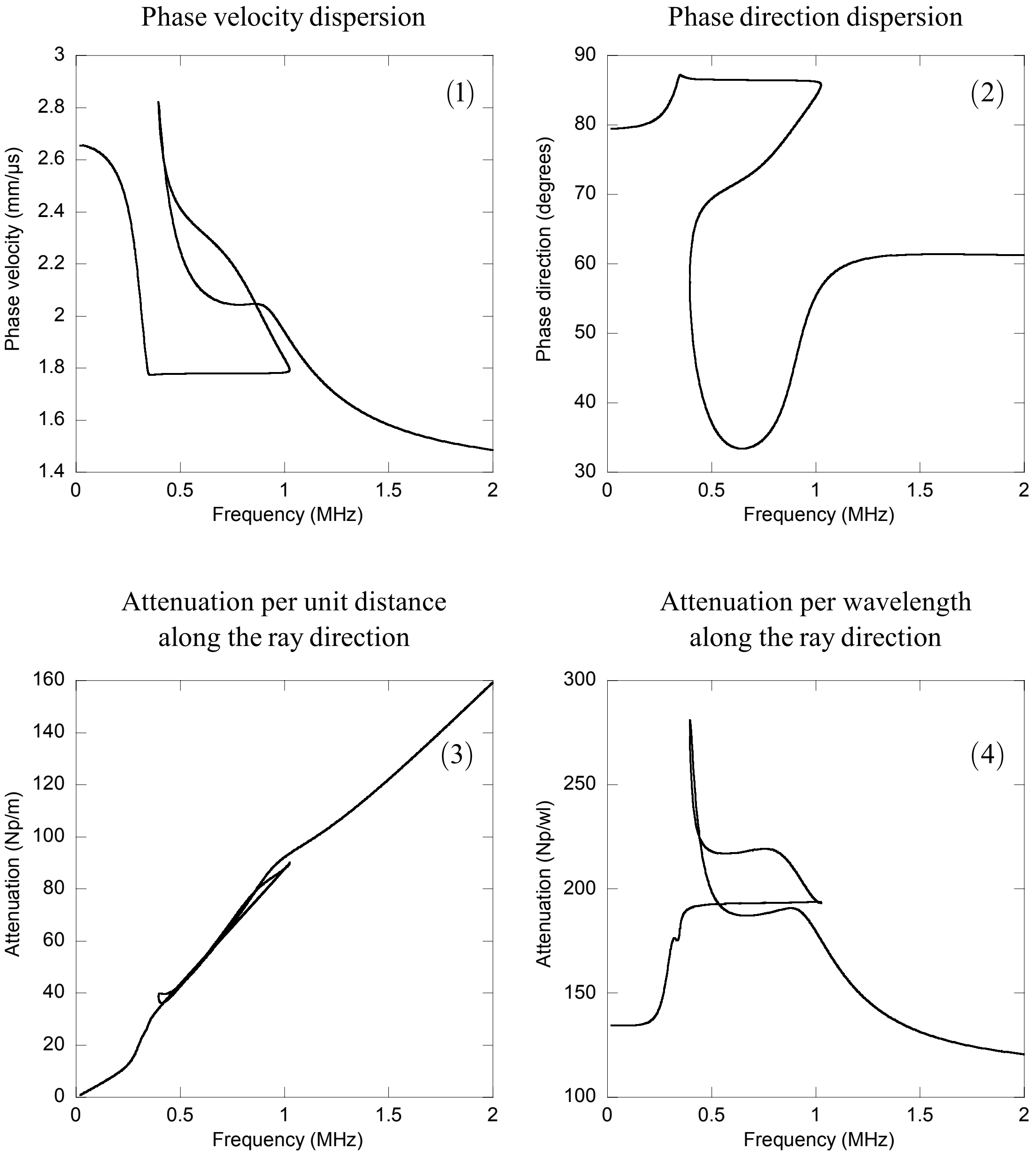

Figure 3.8: Frequential dispersion of the parameters of the S_0 mode, whose energy travels along the 50 degrees observation direction. The phase velocity dispersion is displayed in plot (1)*, the phase direction dependence on the frequency is displayed in* (2)*, the attenuation per meter and per wavelength are respectively shown by plots* (3) *and* (4)*.*

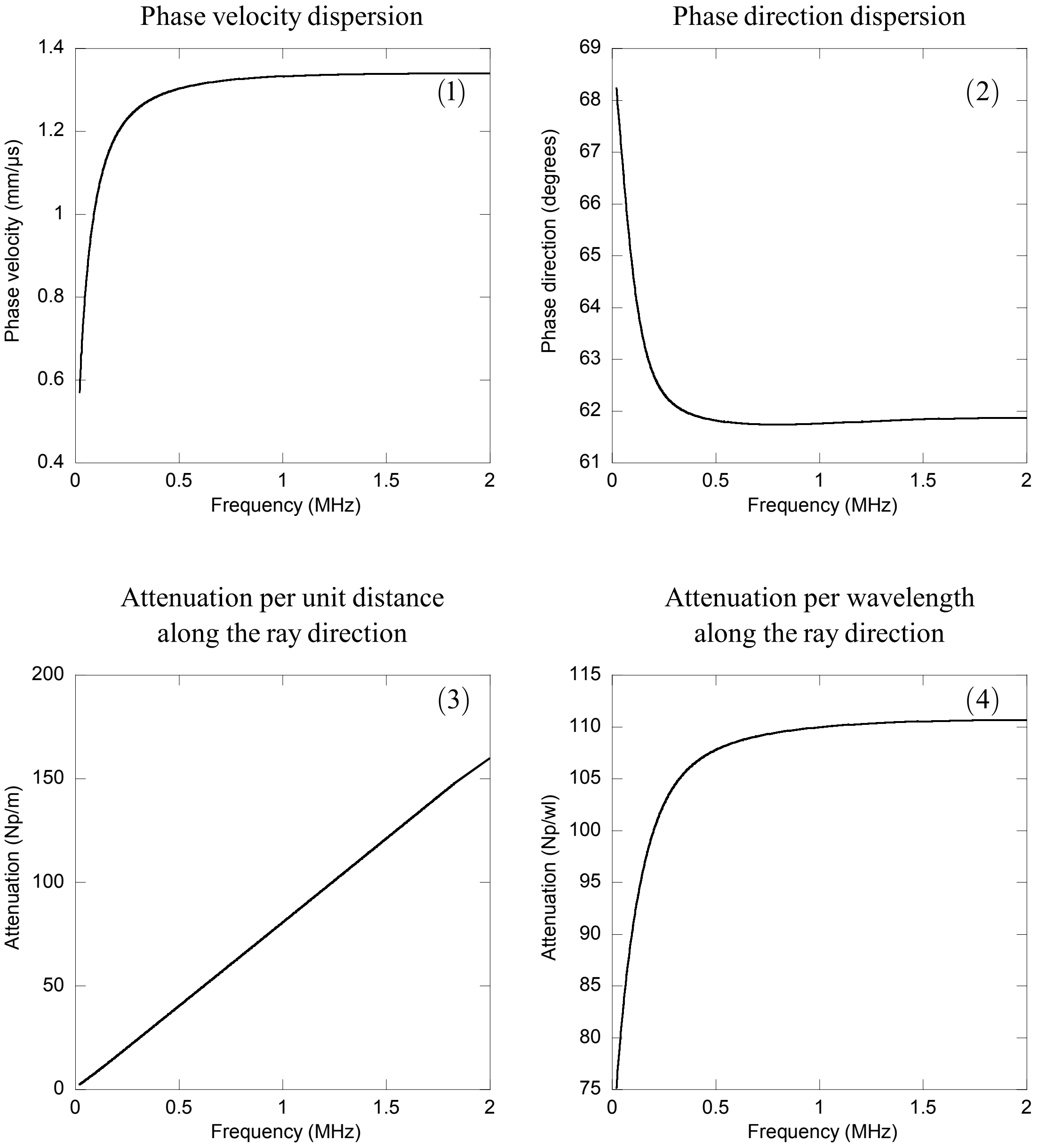

Figure 3.9: Frequential dispersion of the parameters of the A_0 mode, whose energy travels along the 50 degrees observation direction. The phase velocity dispersion is displayed in plot (1)*, the phase direction dependence on the frequency is displayed in* (2)*, the attenuation per meter and per wavelength are respectively shown by plots* (3) *and* (4).

In conclusion, we display the joint locus of the energy velocities, steering along the given 50 degrees observation direction, by the set of the considered modes SH$_0$, S$_0$, A$_0$, A$_1$, S$_1$ and S$_2$, in Fig.(3.10). This figure emphasises the complexity of the dispersion along the energy direction. Even though only six modes are displayed, it can be seen that, at some frequencies (e.g. 0.77 MHz), there are up to twelve energy velocities along the 50 degrees direction.

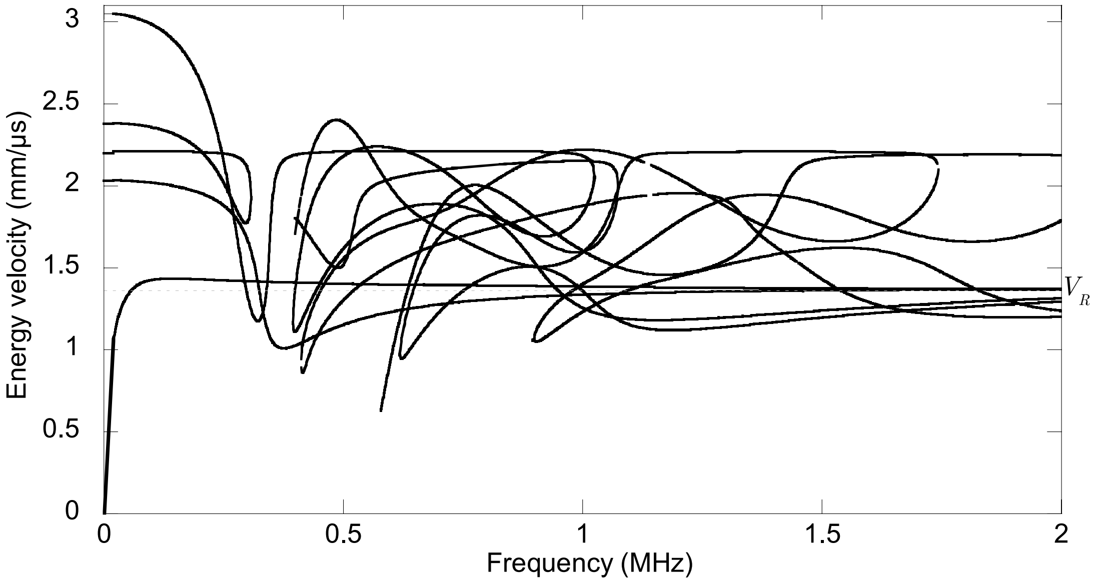

Figure 3.10: SH_0, S_0, A_0, A_1, S_1 and S_2 energy velocity versus frequency for the 50 degrees direction of observation, in the unidirectional carbon-epoxy plate.

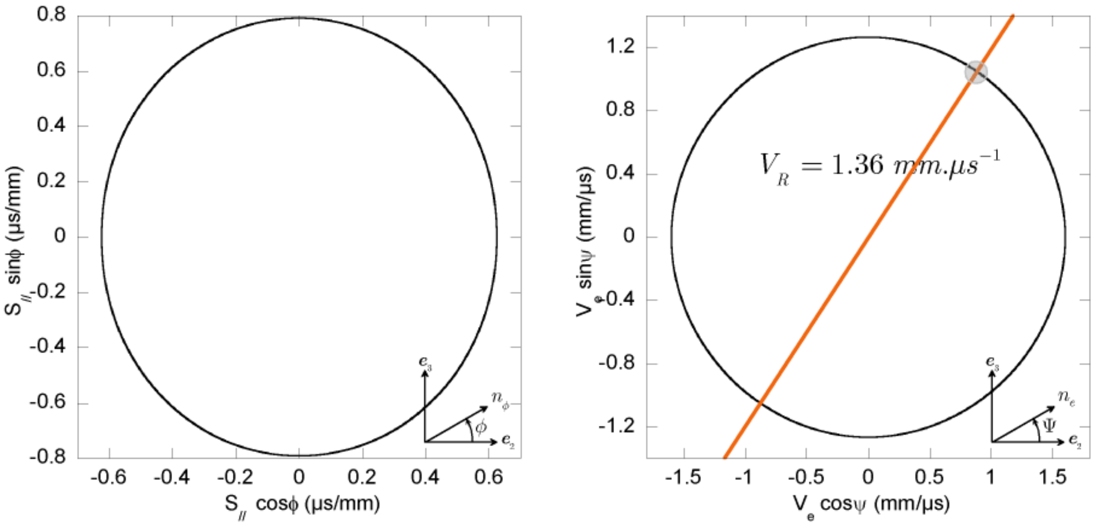

Figure 3.11: The Rayleigh slowness surface and wave surface in the carbon-epoxy material. At 50 degrees, direction indicated by the solid line, the energy velocity of the Rayleigh wave is 1.36 mm.µs^{-1}.

For this material the Rayleigh wave surface, displayed in Fig.(3.11) does not contain cusps. Therefore, below the bulk wave threshold, there is only one limit to which the energy velocity of the fundamental Lamb modes converges (Shuvalov, A.L., 2002). From Fig.(3.10), it can be seen that the A_0 and the SH_0 energy velocities in the direction 50 degrees approach the Rayleigh limit.

Another interesting point is that the energy velocities of all other modes in Fig.(3.10) must tend to the bulk velocity limits, as for the phase velocity dispersion curves. In order to observe this convergence towards the bulk velocity limits, the wave surface of the S_0 mode (that does not tend to the Rayleigh velocity) has been calculated at 5 MHz (18 MHz.mm). Results are displayed in Fig.(3.12), along with the bulk velocity wave surfaces. It is observed that the S0 mode converges towards the slow transverse (ST) bulk mode, and that it does this for all energy directions at 5 MHz.

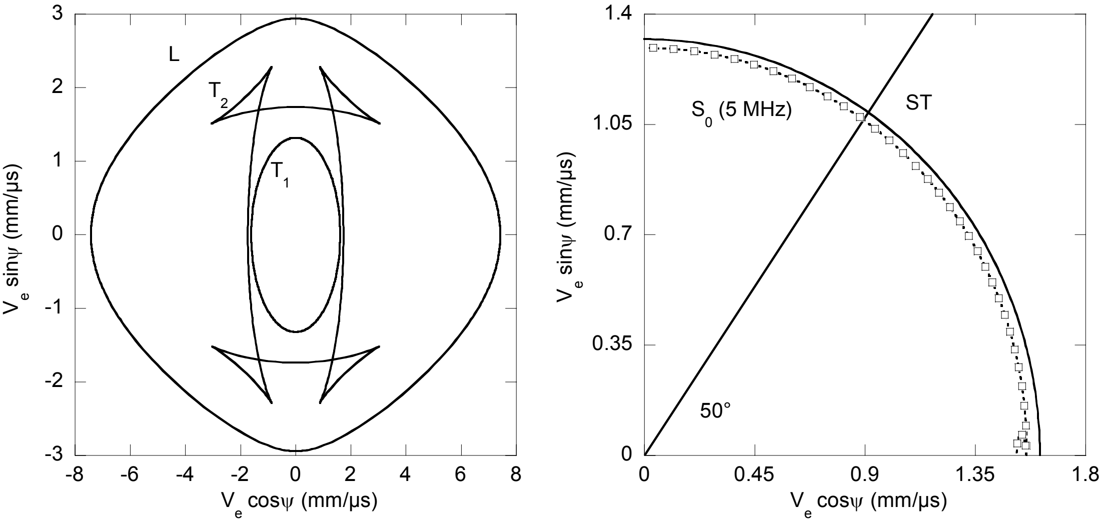

Figure 3.12: Bulk and S_0 wave surfaces of the carbon-epoxy plate, for which the material constants are given in Table (2.3). Left hand side plot: the non dispersive bulk modes are displayed using solid lines, labeled T_1 for the slow transverse mode, T_2 for the fast transverse and L for the longitudinal mode. Right hand side plot: the S_0 wave surface at 5 MHz is displayed using empty squares and compared with the T_1 wave surface. The straight line indicates the 50 degrees direction.

3.5 Calculations along the energy direction, alternative example

The aim of this section is to extend the study of the energy velocity of guided modes to another anisotropic material. The copper-like material has been chosen with the elasticity tensor displayed in Table (3.14). A particular feature of this material is a cuspidal shape of the

Rayleigh wave surface. In the 10 degrees direction, 5 distinct energy velocities of the Rayleigh wave can be observed, as illustrated by Fig.(3.15). Note in passing that the wave surface is not symmetrical. This is due to the fact that the considered material is not cubic, even though very similar to this symmetry. This feature emphasizes the strong dependence of the wave surface with the material properties.

Calculations have been performed up to 3.5 MHz for a 3.6 mm thick plate (12.6 MHz.mm) so that the limit of the guided modes can be observed. As expected, computations displayed in Figs.(3.16 and 3.17) illustrate that the energy velocities of the fundamental A_0 and SH_0 modes converge towards the Rayleigh energy velocities when the frequency tends to infinity. The limit of the S_0 mode, not reached at 3.5 MHz in Fig.(3.18), has been approached in calculating its wave surface at a higher frequency (9.55 MHz, corresponding to a frequency thickness product of 34.38 MHz.mm). As expected, its velocity tends to the bulk energy velocity. However, the limit is not reached for all directions. The convergence for all angles of observation is expected at higher frequency.

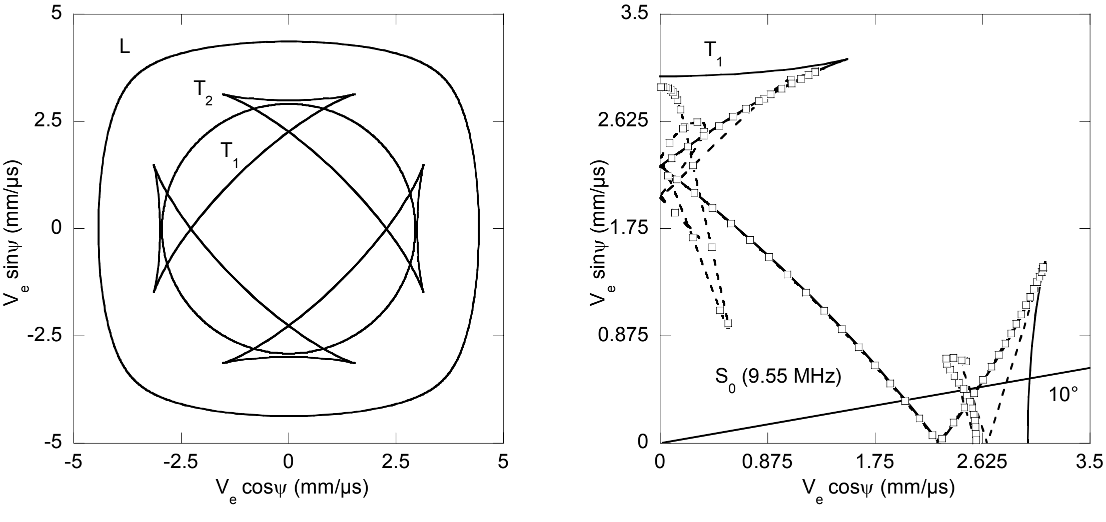

Figure 3.13: Bulk and S_0 wave surfaces of the copper plate, for which the material constants are given in Table (3.14). Left hand side plot: the non dispersive bulk modes are displayed using solid lines, labeled T_1 and T_2 for the transverse modes and L for the longitudinal mode. Right hand side plot: the S_0 wave surface at 9.55 MHz is displayed using empty squares and compared with the T_1 wave surface. The straight line indicates the 10 degrees direction.

Concerning the A_0 mode displayed in Fig.(3.16), the dispersion of its energy velocity in the 10 degrees direction varies from a single-valued to a multi-valued curve.

$C_{11} = 180$	$C_{12} = 110$	$C_{13} = 130$	0	0	0
	$C_{22} = 175$	$C_{23} = 120$	0	0	0
		$C_{33} = 170$	0	0	0
			$C_{44} = 80$	0	0
				$C_{55} = 75.5$	0
					$C_{66} = 77.5$

$\rho = 8.932\ g.cm^{-3}$
$e = 3.6\ mm$

Table 3.14: Copper-like material elastic constants, in GPa.

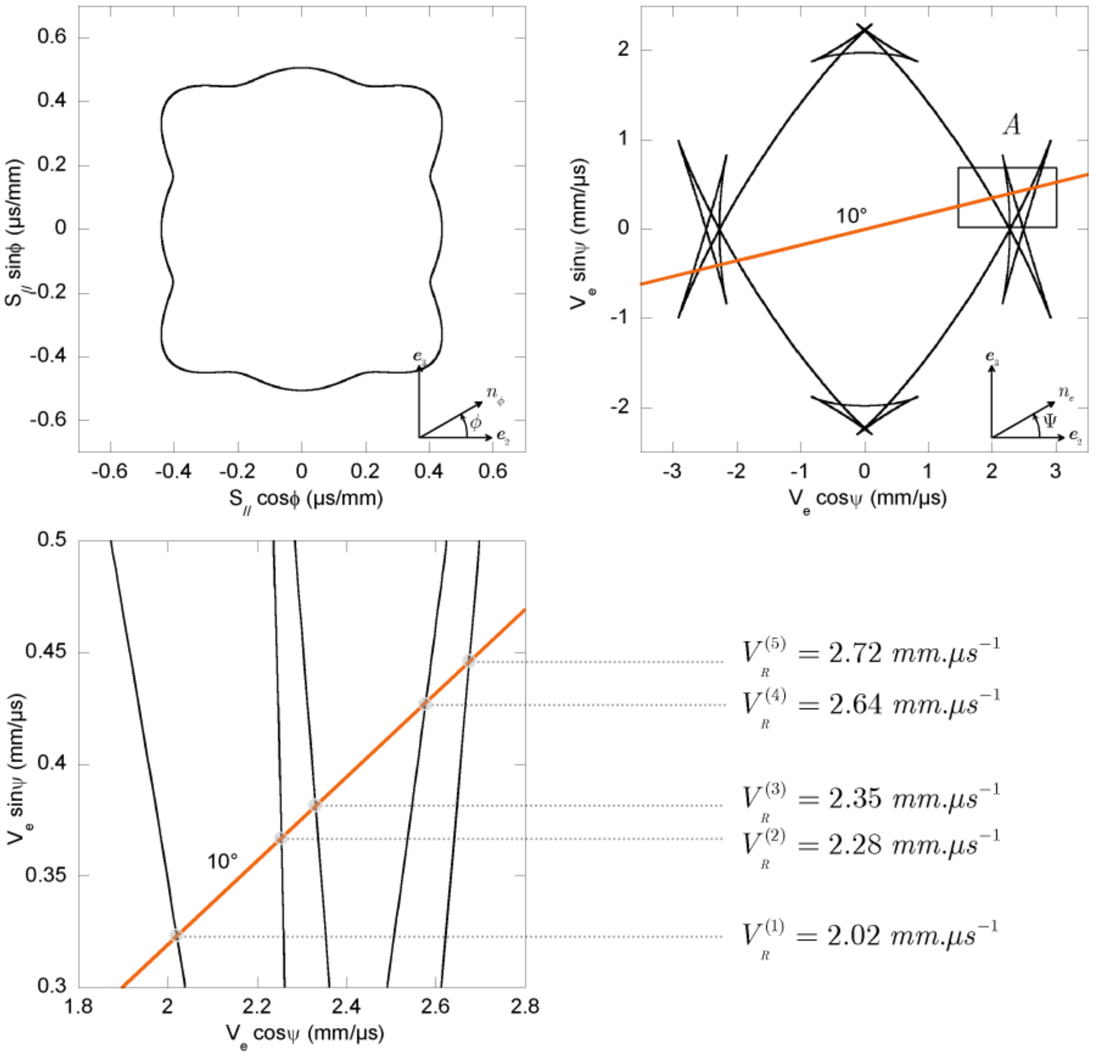

Figure 3.15: Rayleigh slowness (top left plot) and wave surfaces (top right plot) for the copper-like material. The straight line represents the 10 degrees direction. The bottom plot is a zoom of the wave surface around the 10 degrees direction, zone labeled "A" in the top right plot. The five values of Rayleigh energy velocities are reported.

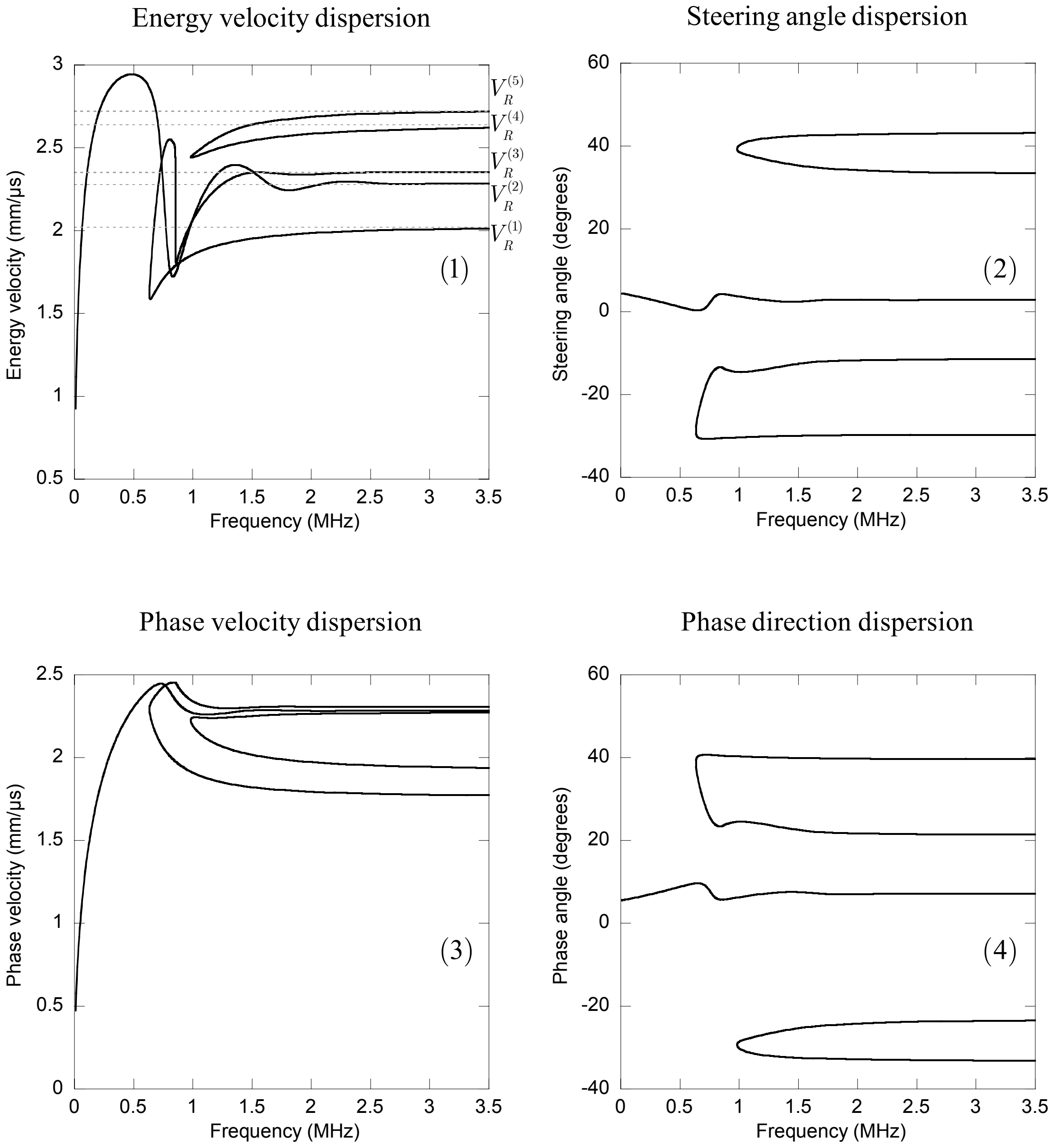

Figure 3.16: A_0 mode properties in the direction 10 degrees of a copper-like material, for which the properties are given in Table (3.14). The energy velocity dispersion is displayed in plot (1)*, the dependence of the phase velocity on the frequency is shown in plot* (3)*, and the dispersions of the steering angle and the phase direction are displayed respectively in plots* (2) *and* (4).

In these figures, complementary diagrams for the phase direction and the steering angle (their sum provides the direction of observation) are displayed for completeness, so that a reader can use one or the other type of visualization to interpret the deviation between phase and energy directions.

For the SH$_0$ mode at low frequency, shown in Fig.(3.17), comments are very similar to the carbon-epoxy case, but at high frequency, there are 5 energy velocities tending to the Rayleigh energy velocities, in accordance with the Rayleigh wave surface in the 10 degrees direction.

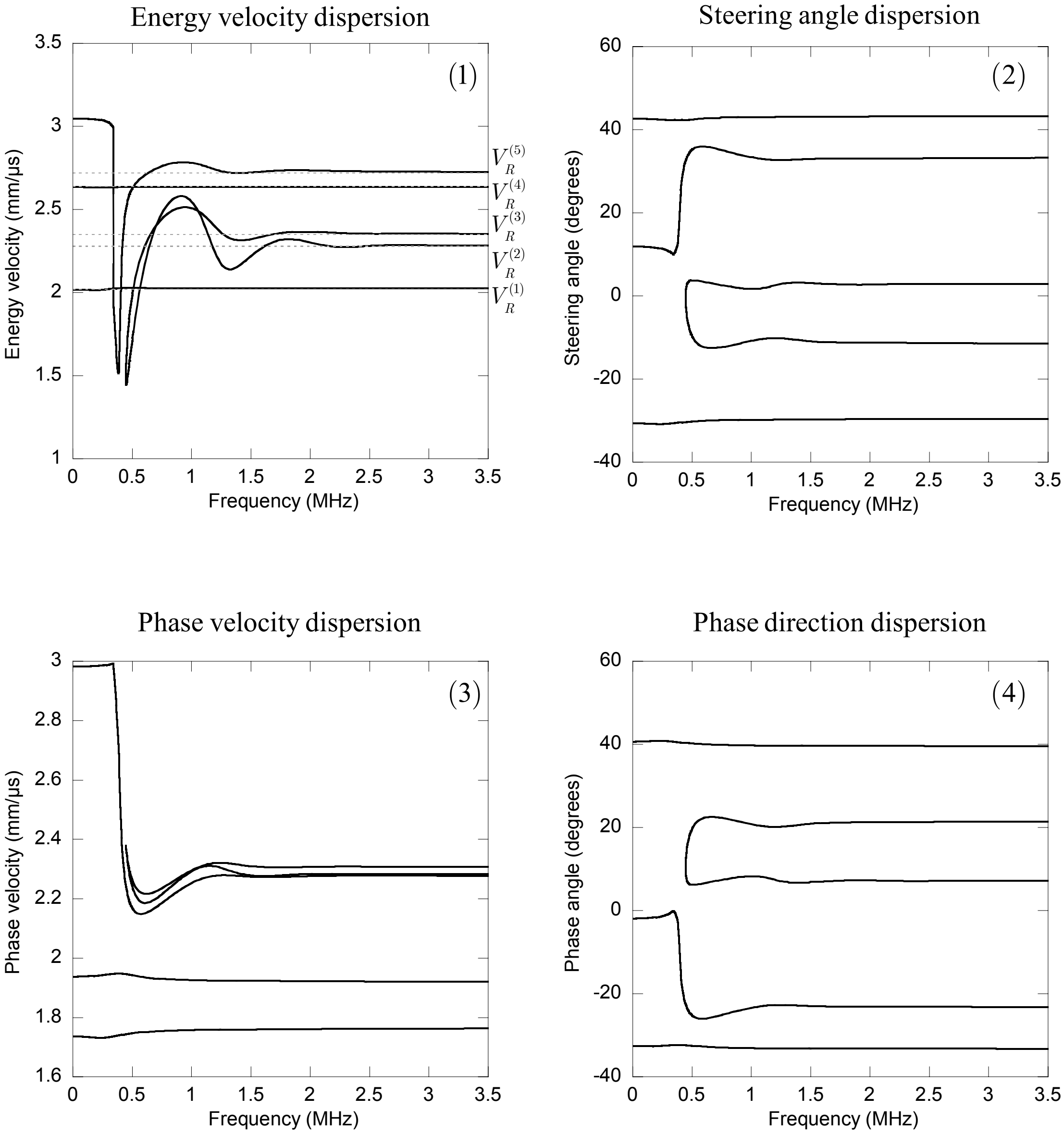

Figure 3.17: SH$_0$ mode properties in the direction 10 degrees of a copper-like material, for which the properties are given in Table (3.14). The energy velocity dispersion is displayed in plot (1)*, the dependence of the phase velocity on the frequency is shown in plot* (3)*, and the dispersions of the steering angle and the phase direction are displayed respectively in plots* (2) *and* (4)*.*

A specific phenomenon is manifested by the S$_0$ mode: two branches can arise and disappear, forming a closed curve identified by the label “A”, as seen between 1.3 and 1.6 MHz in Fig.(3.18). For a given frequency, two new phase front directions steering in the observation direction arise. What has not been seen yet is that these two directions merge at a higher frequency and cease together to steer in the chosen direction. This can be geometrically interpreted by the merging of two inflexion points of the associated slowness surface slice, occurring when the frequency increases.

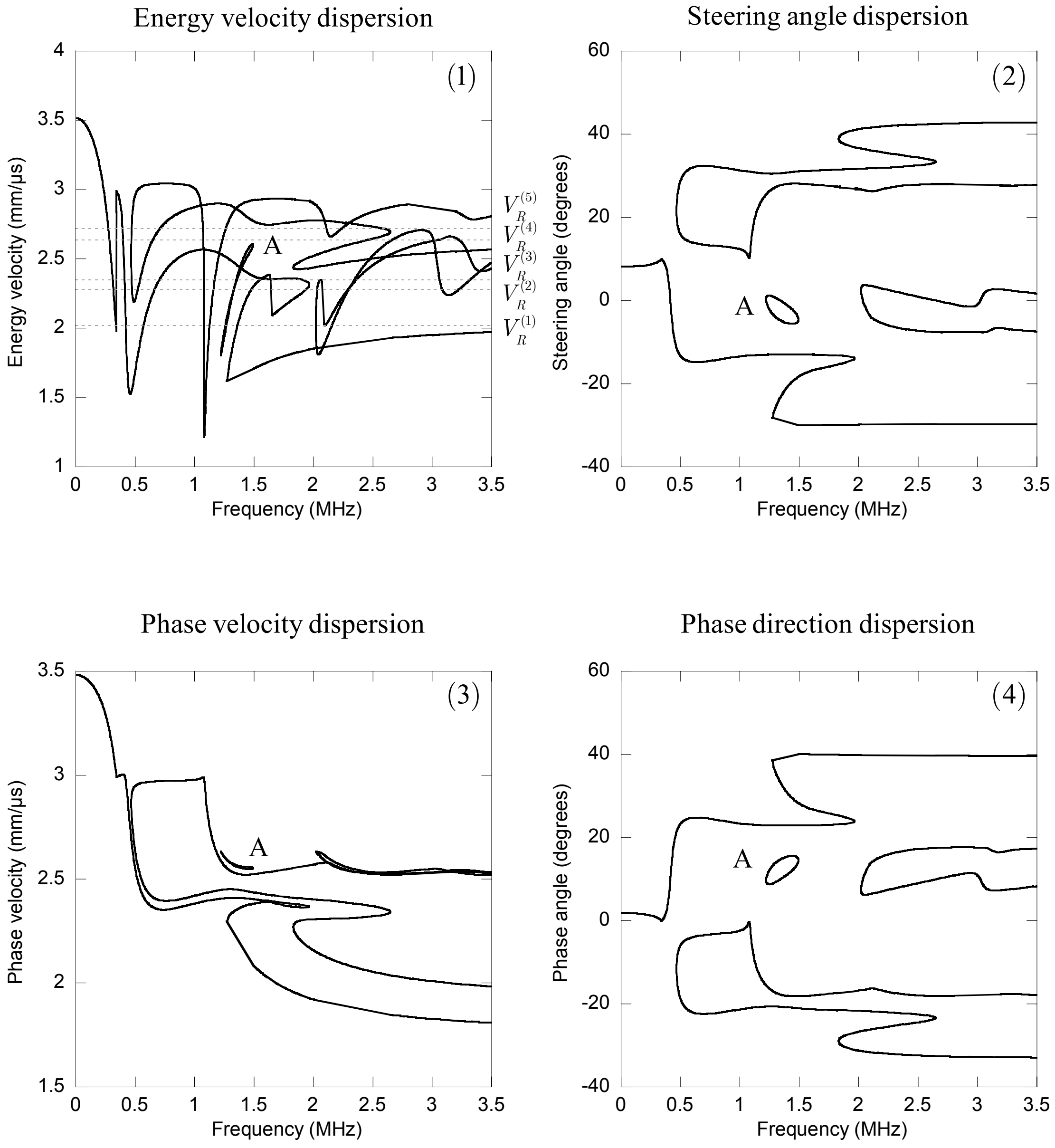

Figure 3.18: S_0 mode properties in the direction 10 degrees of a copper-like material, for which the properties are given in Table (3.14). The energy velocity dispersion is displayed in plot (1)*, the dependence of the phase velocity on the frequency is shown in plot* (3)*, and the dispersions of the steering angle and the phase direction are displayed respectively in plots* (2) *and* (4)*. The close curve zone is labeled "A".*

It is also noteworthy that the S_0 energy velocity exhibits the most intricate behaviour in comparison with the other fundamental modes in this material. In particular, there can be up to seven S_0 phase front directions steering in the 10 degrees direction of observation. A detailed description of this phenomenon happening around the frequency of 1.25 MHz is brought by wave surfaces of this mode shown in Fig.(3.19).

Displaying all the computed modes in one plot (see Fig.(3.20)) illustrates once again the complexity of the dispersion curves. Note that, in a small bandwidth around the 0.34 MHz frequency, the energy velocities curves of the S_0 and the SH_0 modes intersect, see zone labelled “A”, zoomed in plot (1) of Fig.(3.21). In order to confirm that this feature is not caused by a mode jump in the calculations, wave surfaces are displayed around the critical frequency of 0.34 MHz (for 0.338 and 0.345 MHz) in plot (2) of Fig.(3.21).

It is observed that the variations of these wave surfaces are consistent with the calculated dispersion of energy velocity in the 10 degrees direction. The variations of S_0 and SH_0 wave surfaces with the frequency are indeed very steep in this frequency region.

At the same time, we recall that the phase velocity dispersion curves cannot intersect, due to coupling (see Chapter 1), under the given conditions (non principal direction and no viscosity). A complementary phase dispersion plot is displayed to highlight the behaviour of the phase velocity in the vicinity of the energy velocities crossing (in Fig.(3.20), see plot (3) and its zoom in plot (4)). From these plots, it is possible to identify the phase direction that steer in the 10 degrees direction. This direction, which corresponds to the crossing of the SH_0 and S_0 energy velocities, has been found to be equal to 0.1 degree. The phase velocity dispersion in this particular direction has been calculated for the S_0 and SH_0 modes. As expected, these two modes exhibit a region where they are very close in velocity but do not cross (see zone labelled “B” in plot (4)), due to coupling (see Chapter 1).

3.6 Conclusion

In this chapter, a new feature has been put forward, which is displaying mode characteristics in a chosen observation (or energy) direction. The appropriate algorithm, proceeding from a fixed reference observation direction, has been implemented. This approach is essential for the point source – point receiver experimental configuration, which is of great importance for many practical applications. The obtained results represent multi-valued dispersion curves instead of the classical single-valued curves, thus revealing the presence of a cusp on the wave (energy velocity) surface. In particular, it was shown that a frequency dependent cuspidal form of the wave surface is a fairly common feature of the Lamb modes in anisotropic plates. It is evident that a prerequisite for a correct interpretation of the experimental data is the knowledge of how many arrival times will be detected in a given direction and at a given frequency. This kind of information is delivered by the developed approach. Among other properties of the guided modes, their attenuation in the observation direction has been described.

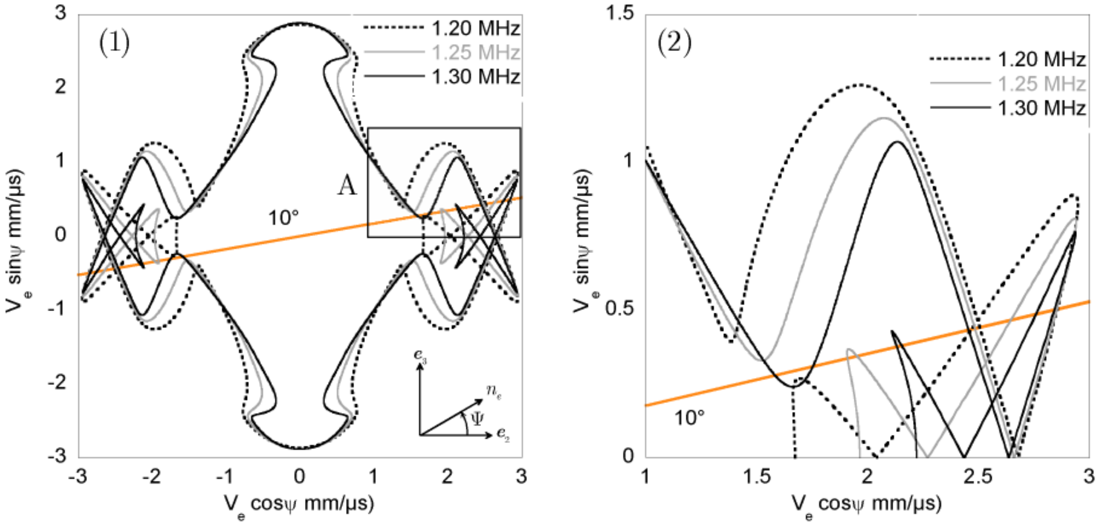

Figure 3.19: S_0 wave surfaces at frequencies for which successively 3, 5 and 7 phase directions steer in the 10 degrees direction, for the copper-like material. Left plot (1) *represents the wave surfaces of the S_0 mode for 1.20, 1.25 and 1.30 MHz. Right plot* (2) *is a zoom of the zone labelled "A" in the left plot. The straight line stands for the 10 degrees direction.*

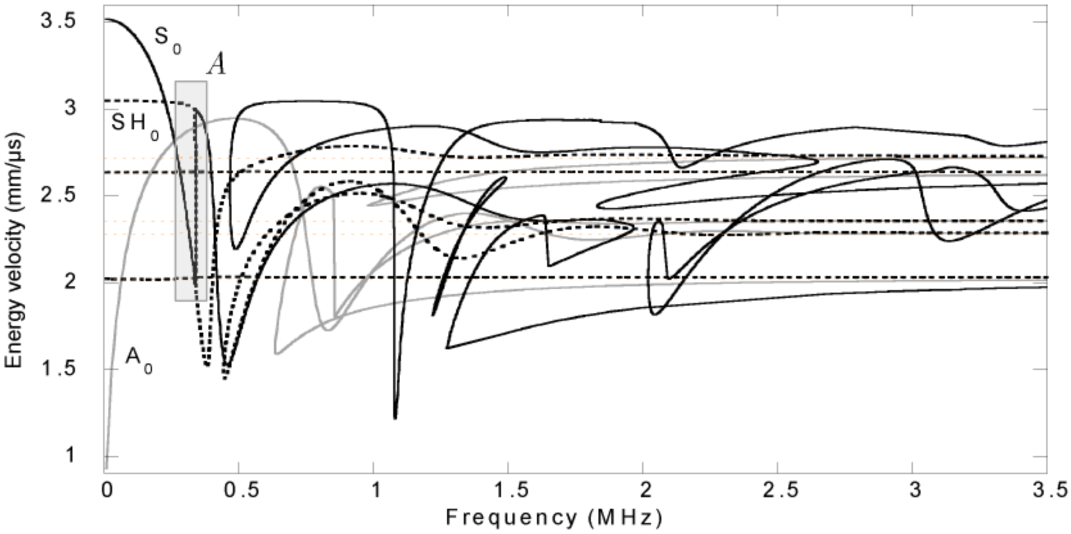

Figure 3.20: Energy velocity of the fundamental modes in the copper-like material propagating in the 10 degrees direction. Dotted straight lines represent the 5 Rayleigh energy velocities.

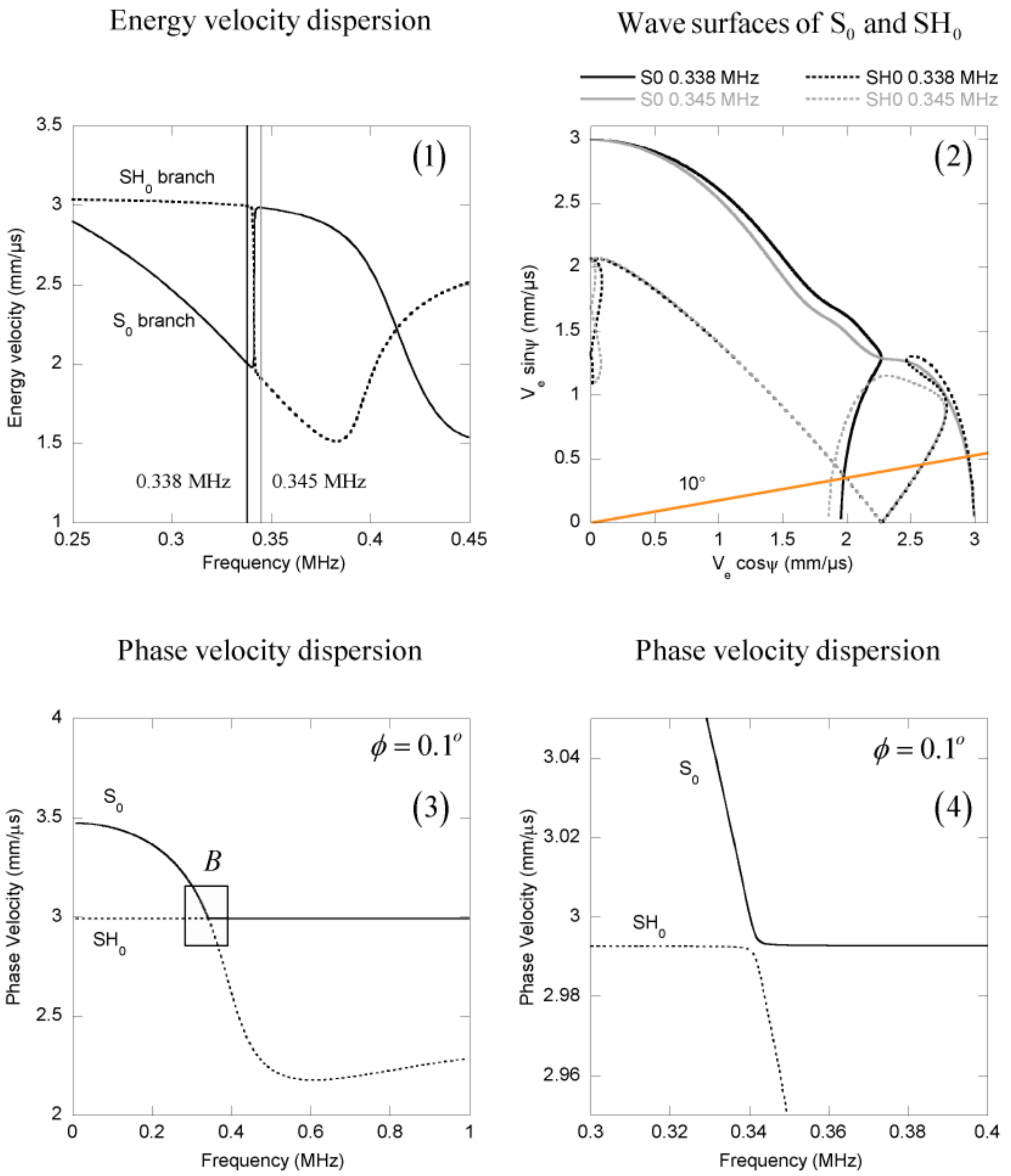

Figure 3.21: The top left plot (1) *zooms the energy velocity dispersion of Fig.(3.18) around the intersection of the* SH_0 *and* S_0 *energy velocities. The top right plot* (2) *shows the wave surfaces of these modes, for the two frequencies marked by straight lines in plot* (1). *In this plot, solid lines represent the* S_0 *mode, and dotted lines the* SH_0 *mode. The straight line indicates the 10 degrees direction. The bottom left plot* (3) *displays their associated phase dispersion at a phase angle that steers in the 10 degrees direction. The bottom right plot* (4) *zooms the dispersions of these two modes.*

Through the derivation of the involved energy terms and velocity, it has been shown that the projection of the phase attenuation onto the associated energy direction corresponds to a ratio of the dissipation energy to the total energy, which is physically meaningful.

These properties have been illustrated by theoretical calculations for the unidirectional carbon-epoxy plate and for a copper-like material. Computations for fundamental and higher order modes have given plentiful examples of cusp frequential dispersion. The next chapter deals with the experimental observation of the described phenomena, for unidirectional glass and carbon-epoxy plates.

Chapter 4

Experimental illustration

4.1 Introduction

Lamb waves are the subject of much applied research relating to the inspection of plate structures. They are used to test adhesively bonded components (Seifried, R., Jacobs, L.J. et al., 2002), for long range inspection of large structure (Cawley, P. and Alleyne, D., 1996), for the detection of delaminations (Tan, K.S., Guo, N. et al., 1995) or for material characterisation (Safaeinili, A., Lobkis, O.I. et al., 1996; Chimenti, D.E., 1997; Wu, T.T. and Liu, Y.H., 1999). The preceding discussion has brought to light different properties of the Lamb modes, which facilitate their application for non destructive evaluation and testing.

In this Chapter, an experimental illustration of the guided mode properties in lossy orthotropic plate is given. Measurements concern both the energy velocity and the attenuation of the Lamb modes. The aim is to provide experimental examples and validations of what has been described theoretically in the previous chapters. Bearing in mind the common difficulty of making ultrasound attenuation measurements, performing such experiments in an orthotropic plate is a challenging task. It embroils the problems coming from the experimental set-up, from the characterisation process and from the anisotropy of the material.

Three types of experiments are presented. The first one, described in the second section, is carried out using a point source-point receiver configuration, for a unidirectional glass-epoxy plate. This experiment is made under the assumption of a purely elastic material, in order to illustrate the validity of the group velocity considerations described in Chapter 1.

The second experiment has two goals. One of them is the observation of the steering angle phenomenon (for a given direction and frequency), the other is the illustration of the phase attenuation of a guided mode propagating in a non-principal direction. The experimental set up is performed on a unidirectional carbon-epoxy panel, using a line source and point receiver configuration. The set up is described in the third section, along with the obtained results.

In the fourth section, the experiment deals with measurements of the Lamb mode attenuation and velocities for all directions, at several fixed frequencies. For such an experiment, the point source – point receiver configuration has been applied, so that energy velocity and attenuation could be picked up in any direction. Measurements have been achieved for the unidirectional carbon-epoxy panel.

The type of signals obtained for all experiments were very close, so they have been post-processed using mostly the same tools. The changes made from one set-up to another one are related only to the size of the source transducers and the receiving method. The description of these processing tools, involving both the time of flight extraction, and the attenuation calculation from measured signals, is given in the first section.

4.2 Post-processing

The aim of this section is to describe the common post-processing of signals obtained from different experiments. To retrieve wave and attenuation data, different techniques are available. In order to get the energy velocity of a mode, it is necessary to determine precisely the time of flight of a given packet. Once the mode is recognised, it is possible to calculate its attenuation from several amplitude measurements at different distances.

There are different ways of determining the arrival time of a mode. The most instinctive way of looking at the data is actually to look at them in the time domain. When only a single mode is present, and when the frequency dispersion is small, a good way is simply to take the time corresponding to the maximum of the envelope of the signal. This can be done by taking the inverse Fourier transform of the Hilbert transform of the experimental signal (Max, J., 1977).

However, in other cases, the information given by the envelope can be erroneous because of the presence of more than one mode or more than one single frequency in the wave packet. Because the envelope is calculated for the centre frequency of the toneburst, this method is therefore approximate. For more precision, there is a need of a more powerful tool to extract experimental group velocity measurements. For that purpose, a wavelet post-processing computer routine has been developed. The wavelet transform of a signal is meant to separate packets arriving at the same time, but composed of different frequencies. The main advantage of the processing is to enhance the contrast of the arriving wave packets, in order to identify them and increase the precision concerning their arrival times. The wavelet transform is performed using a Morlet wavelet, with its centre frequency matching the experimental centre frequency, in order to perform the correlation with a signal very close to the experimental source. The wavelet transform of a function f (t) is defined as follows (Flandrin, P., 1993):

$$W_{\Psi}f(b,a) = |a|^{-\frac{1}{2}} \int_{-\infty}^{+\infty} \Psi^{*}(\frac{t-b}{a})f(t)\,dt. \tag{4.1}$$

In Eq.(4.1), Ψ is the basic wavelet used for the transformation. Ψ^{*} is its complex conjugate, and a and b stand for dilatation and translation factors, respectively. Ψ has to satisfy two conditions of admissibility. The first one corresponds to finite energy condition (normalised), and the second one imposes a zero average on the wavelet, implying some oscillations in the wavelet function. The Morlet wavelet is defined as follows:

$$\Psi(t) = \left(\frac{1}{\pi\, t_{0}^{2}}\right)^{\frac{1}{4}} \exp\left(-\frac{1}{2}\left(\frac{t}{t_{0}}\right)^{2} + 2i\pi\upsilon_{0}t\right). \tag{4.2}$$

To fit the centre frequency of the experimental source, υ_{0} was fixed at the experimental centre frequency, and to satisfy the conditions of admissibility, t_{0} is deduced from the condition $2\pi\upsilon_{0}\mathrm{t}_{0} = 5.43$ (Flandrin, P., 1993).

These two methods are illustrated in Fig.(4.1). They have been used on experimental data. It appears that, in the frequency range of the experiment where the fundamental modes are not very dispersive, the two methods give the same results. This provides a double check of the measured quantities.

There are also different ways of measuring the decay in amplitude. In the time domain, the amplitude of the maximum of the envelope corresponds to the amplitude of the mode. If taken at different distances from the source, this method leads to measurements of amplitude as a function of the distance. These measurements can be fitted with an exponential function, using the least squares method for instance, see Fig.(4.2). This function is simply related to the attenuation, and its value at a given frequency (the centre frequency of the wave packet) is obtained.

Repeating the same processing method for a range of several frequencies, it is possible to obtain the attenuation of a selected mode as a function of the frequency. This approach can work well if signals are moderately well separated and modes are non-dispersive. The significance of dispersion is that its accompanying modification of the shape of the signal envelope alters the measured amplitude, even in cases where there is no loss of energy (Wilcox, P., Lowe, M. et al., 2001).

Another way to look at the data is to look at them in the frequency domain, in a very similar way as is commonly used to determine transmission or reflection coefficients (Guo, N., Lim, M.K. et al., 1995). The closest signal to the source is set as the reference S_0. Another signal taken at a larger distance from the source is then set as the transmitted signal S_i. The ratio of the Fourier transforms (FFT) of these signals leads directly to the reduction of amplitude as a function of the frequency, for a given distance.

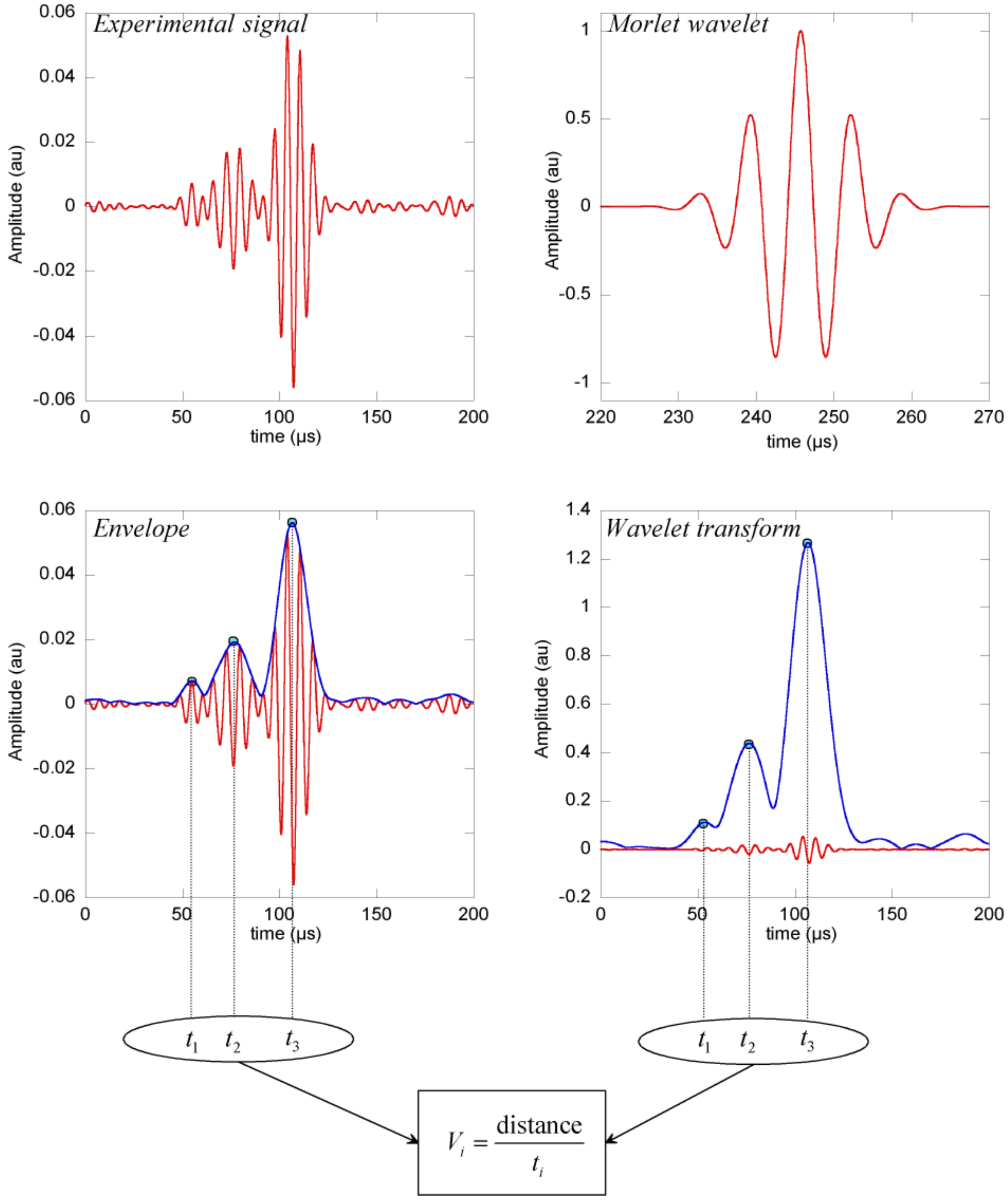

Figure 4.1: Velocity extraction from experimental data, using either the envelope or the wavelet transform.

Knowing the distance d, separating the two locations of measurements, this is simply converted to give the attenuation value $\alpha(f)$ as a function of the frequency, see Fig.(4.3):

$$\alpha(f) = -\frac{1}{d}\ln\left\|\frac{\tilde{S}_0(f)}{\tilde{S}_i(f)}\right\|, \tag{4.3}$$

where $\tilde{S}_0(f)$ and $\tilde{S}_i(f)$ are the Fourier transforms of the signals $S_0(t)$ and $S_i(t)$, respectively.

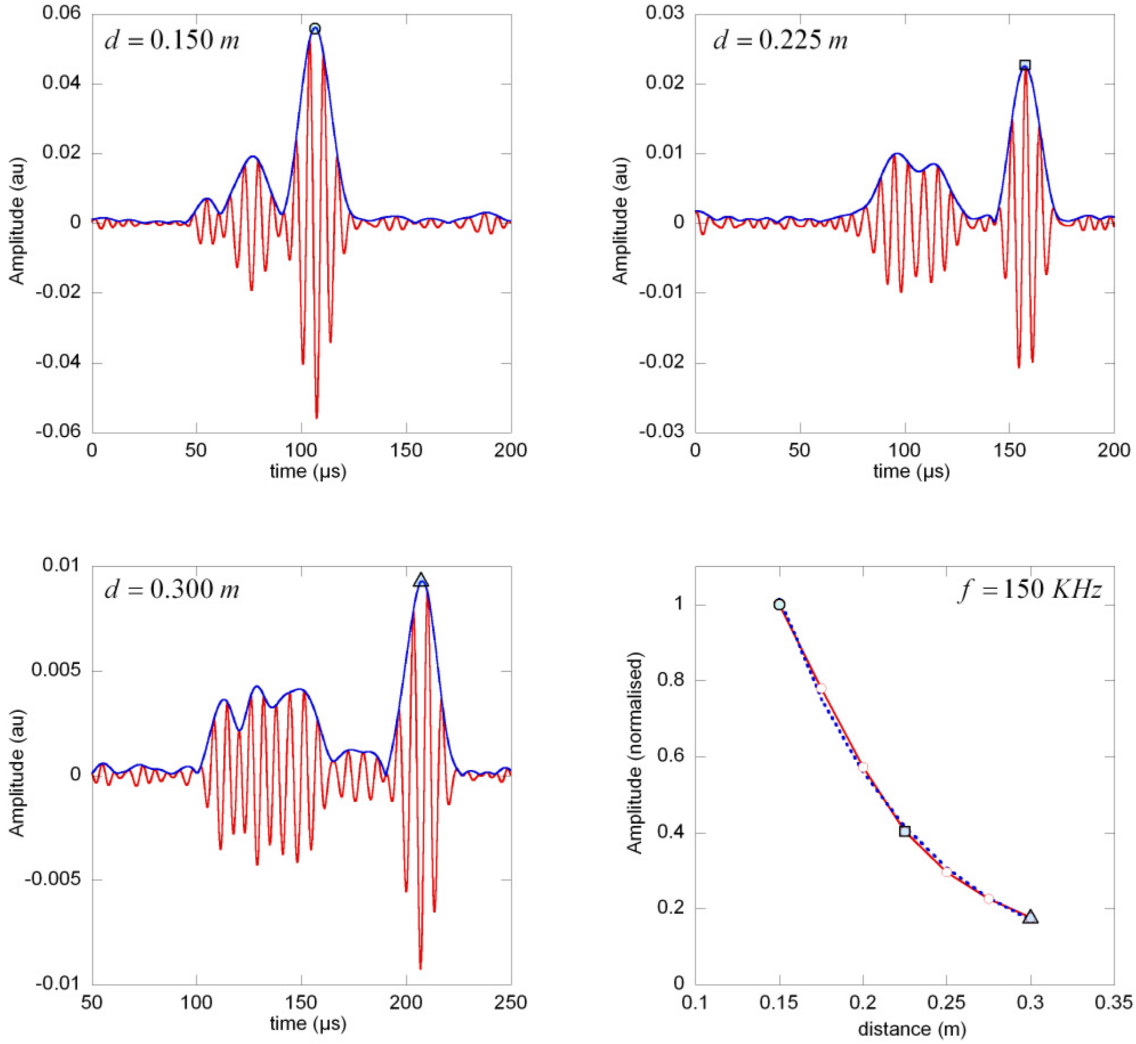

Figure 4.2: Attenuation extraction from experimental measurements. Amplitude of the selected mode are recorded for each distance, then fitted with an exponential function to obtain the attenuation at the experimental frequency (Example measurements are done for the carbon-epoxy plate, 55 degrees from the direction of the fibres, at 150 kHz).

Repeating this method for several distances, an average gives a reliable attenuation measurement of the selected mode. In this case the attenuation is not compromised by any dispersion of the signal, but on the other hand it becomes even more important to have good separation of signals.

Once again these two methods have been tried on the obtained experimental data, and it appears in these cases that they give the same results. All of the data which were processed were for modes and frequencies where there was little frequency dispersion.

One other issue which has not yet been discussed is the beam spreading. When a wave is excited from a localized source and it radiates out into the plate, energy considerations dictate that the amplitude must decay as the distance from the source, and thus the length of the wave front increases. For a point source generating the A_0 mode (for example) in an isotropic plate, the wave front is a circle with constant amplitude at all circumferential positions, and its length increases linearly with the distance from the source. The energy density must then decrease linearly with the distance and so the displacement amplitude decreases as the square root of the distance.

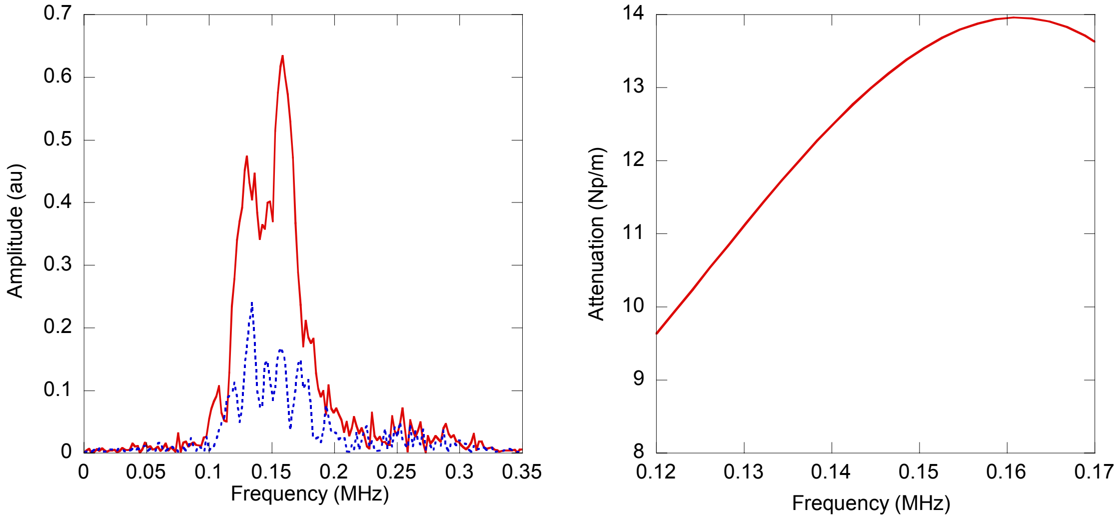

Figure 4.3: Attenuation extraction from experimental measurements, using ratio of spectra. Left hand side plot: spectra of the closest signal (solid line) and the most distant to the source(dotted line). Right hand side plot: Attenuation as a function of the frequency obtained from the ratio of the spectra, see Eq.(4.3).

In an anisotropic plate or in any circumstance in which the source has some form of polarization, such as the source for the SH_0 mode, the spreading function may be strongly related to the angular position and can be complex to establish. However one useful characteristic is that the effect of beam spreading diminishes at long distances from the source. Another way of viewing this is to consider that at large distances from the source the wave may be approximated as a plane-crested wave rather than a spherical-crested wave. Indeed this was the assumption which was made here. Thus it is expected that the error associated with beam spreading was smaller for the longer-distance locations than for the near locations. Nevertheless, in any case, the error associated with beam spreading is unlikely to be significant compared to that due to the uncertainties of the measured material constants.

4.3 Non-absorbing case: group velocity and frequential dispersion

Recalling the first chapter, it has been seen that group and phase velocities of guided modes are different. This difference comes from both spatial and frequential terms. The aim of the experiment presented in this section is to illustrate the group velocity formula of Eq.(1.27), that gives the group velocity of Lamb modes in anisotropic media.

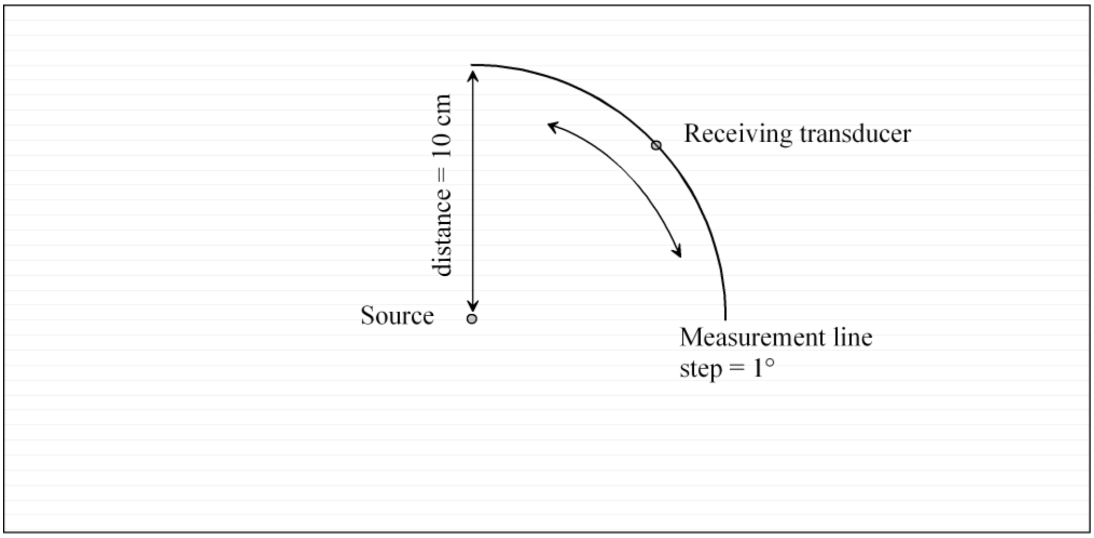

Figure 4.4: Experimental set-up. A fixed point source transducer is used as the source. The point source receiver describes a quarter of a circle around the source.

The experimental set up is briefly described in Fig.(4.4). The emitting transducer is a point-transducer developed by (Evans, M., Webster, J.R. et al., 2000) that remains still during the measurements. The signal, which is sent to the emitting transducer (Macro Design Ltd, U.), is a 5 cycles sinusoidal shaped signal, modulated by a Hanning window. The receiver, which is identical, is plugged to an amplifier and an oscilloscope (Lecroy 9410), linked with an IEEE card to a computer for data recording and post-processing. These transducers are lying on an unidirectional Glass-epoxy plate (30×30 cm), whose properties are given in Table.(4.5). Measurements were performed at each degree from the direction of the fibres to its perpendicular.

For every direction, the envelope and the wavelet transform have been calculated to extract group velocities of the excited modes. Associating a grey scale coefficient to each amplitude of the envelope, each signal can be represented by a grey scaled straight line as a function of the time.

$C_{11} = 17.78$	$C_{12} = 7.82$	$C_{13} = 5.96$	0	0	0
	$C_{22} = 41.50$	$C_{23} = 7.65$	0	0	0
		$C_{33} = 19.40$	0	0	0
			$C_{44} = 6.50$	0	0
				$C_{55} = 5.05$	0
					$C_{66} = 5.60$

$\rho = 1.940\ g.cm^{-3}$
$e = 3.195\ mm$

Table 4.5: C_{ij} table for the unidirectional glass-epoxy panel, used for the calculations. The whole elasticity tensor is given in GPa.

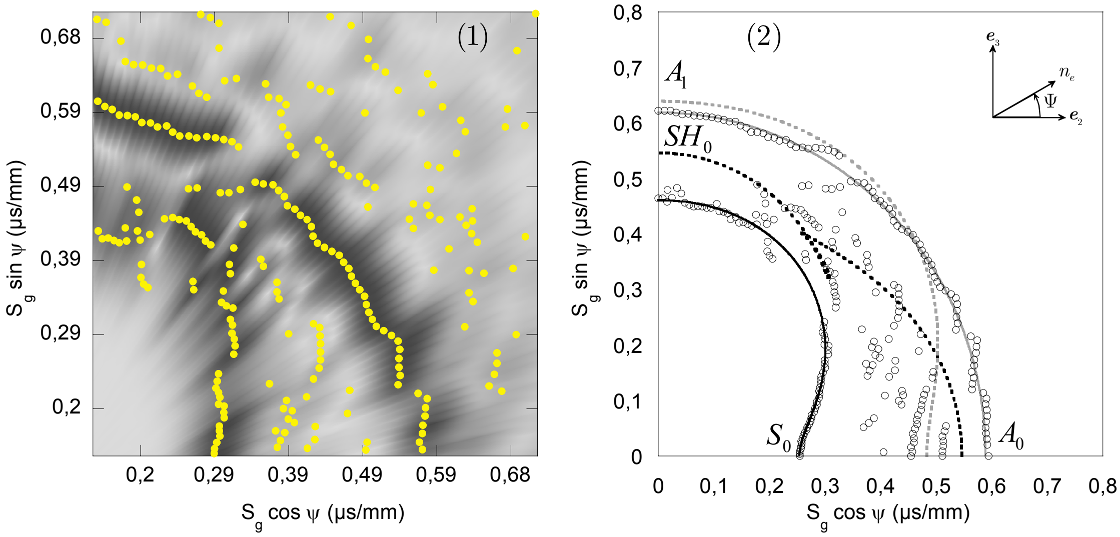

Figure 4.6: Experimental results for group slowness of Lamb modes in glass-epoxy plate. Left hand side plot (1): grey scale image interpolation of measurements envelopes and associated maximum values (solid discs). Right hand side plot (2): group slowness of Lamb modes present at 0.3 MHz. Solid and dotted line represent the theoretical prediction, empty discs are experimental measurements. For both plots the horizontal axis represents the direction of the fibres.

Dividing the time values by the distance between the two transducers, one can visualise the Lamb wave slowness fronts. This has been performed using an interpolated image of the measurement lines, displayed in Fig.(4.6(1)). On top of this image the extracted slownesses have been overlaid.

Bearing in mind that the characterisation of anisotropic material is a difficult matter, the confidence interval of the elasticity components is rather large. The reader has to be aware that the material's C_{ij} have been slightly adjusted in order to fit experimental measurements in principal directions. Thus the glass-epoxy constants have been modified to provide the best fit to the measurements of the A_0 and S_0 modes at 0 and 90 degrees. The original C_{ij} set issued from the characterisation process is displayed in Table (4.7) along with its modification in percentage. In accordance with the characterisation method, the set of in-plane components of the elasticity tensor is the least reliable and therefore the one which needs the greatest adjustments to match fundamental mode velocities in principal directions. Thus C_{22}, C_{13}, C_{23} and C_{44} are the most affected components. The rest of the characterisation remains in a 10% confidence interval.

$C_{11} = 19.71$	$C_{12} = 8.68$	$C_{13} = 9.86$	0	0	0
	$C_{22} = 50.45$	$C_{23} = 8.60$	0	0	0
		$C_{33} = 21.44$	0	0	0
			$C_{44} = 5.70$	0	0
				$C_{55} = 5.13$	0
					$C_{66} = 5.79$

9.8%	9.9%	23.9%	0	0	0
	17.7%	11.0%	0	0	0
		9.5%	0	0	0
			14.0%	0	0
				1.5%	0
					3.2%

Table 4.7: Material constants in GPa issued from the characterisation procedure at 1 MHz (Castaings, M. and Hosten, B., 2000) (top table), associated modification (bottom table).

The experimental measurements are then compared with theoretical prediction using Eqs.(1.27-1.29). The results are displayed in Fig.(4.6(2)). Note that points whose slowness were greater than the slowest mode (A_0) have been discarded. The plate used was only 30×30 cm and multiple reflections from edges occurred during the experiment. Points with a greater slowness than A_0 are therefore understood as edge reflections of other modes and cannot be compared with the computed prediction. Now aware of all post experiment procedures, the obtained results can be discussed.

As seen in Fig.(4.6(2)) the agreement for the A_0 and S_0 group slowness is excellent for all directions. Concerning the SH_0 mode however, measurements do not agree with theoretical computations. Due to the excitation and receiving method (the point transducers work predominantly with out of plane motions), this mode has not been well generated in all directions and its amplitude is much lower than the S_0 one. The mode shape of SH_0 being in-plane in principal directions, it makes sense not to try to observe it at 0 and 90 degrees with this experimental set up. In non-principal directions however, its mode shape becomes more complicated and involves some out of plane components. But negating this advantage for its detection, its velocity becomes closer to the S_0 velocity and the interferences induced by this proximity make the separation between these two modes difficult. As seen on Fig.(4.6(2)) points measured around the SH_0 cusp zone are the result of this phenomenon. Moreover it can pointed out that despite the fact that the material has been considered non-absorbing for the calculations, there is some absorption occurring.

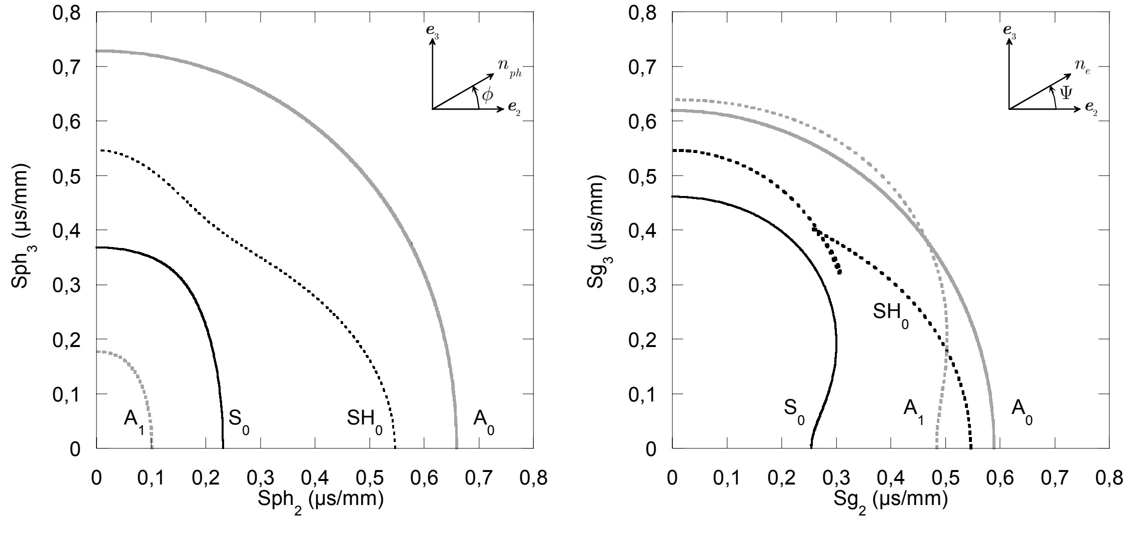

Figure 4.8: Slowness and wave surfaces of Lamb modes in the Glass-epoxy plate at 0.3 MHz. The horizontal axis represents the direction of the fibres.

It is expected that the attenuation is stronger in the direction perpendicular to the fibres. In accordance with this remark, more unwanted reflections and interferences are observed in the 0 degree direction rather than in the 90 degrees direction, where the attenuation is so high that the amplitude of edge reflections are not detected. Looking at the A_1 mode in Fig.(4.6(2)), it is believed that this mode is not observed experimentally. Some experimental measurements are very close to this mode slowness but they are actually S_0 edge reflection measurements.

These experimental data illustrate the group velocity formula for guided modes in an anisotropic plate (see Chapter 1, section 1.4, Eq.(1.27)). In this formula, the dispersion terms can be emphasised by comparing the slowness and the wave surfaces of the Lamb modes displayed in Fig.(4.8). The group velocity formula includes both angular and frequency dispersion contributions. In principal directions, where there is no spatial dispersion and the energy and the phase travel in the same direction, the magnitudes of the group and the phase velocity differ. This difference is therefore due solely to the frequential dispersion. In Fig.(4.8) the distinct phase and group slownesses of A_1 for instance illustrate this feature.

This experimental illustration of the computation of the energy velocity of the guided modes, which has been carried out for all directions of observation, has enabled results to be displayed in polar coordinates. However this form of data masks the dependence of the group direction on the phase front direction. One goal of the following section is to concentrate on a single mode in a particular phase direction and to measure its associated steering angle. Moreover, the viscosity of the material has not been taken into account yet, so the second goal of the next experiment is to illustrate the attenuation of a single Lamb mode in an absorbing anisotropic plate.

4.4 Steering angle and phase attenuation

As mentioned above, the present experiment aims to excite a single guided mode at a particular phase front direction and to take viscosity into account. For these purposes, a panel bigger than the previous one is appropriate. The Lamb modes can indeed propagate over long distances and amplitude measurements over a long range are better suited for attenuation evaluation. Thus a large panel of unidirectional carbon-epoxy material has been prepared. Its dimension are 1.14 by 0.94 m, its thickness is 3.6 mm. The plate was constructed at the Department of Aeronautics at Imperial College, from 24 pre-preg plies in parallel alignment. The material was supplied by S.P.Systems (material reference: Pre-preg SE84HT/HEC/150/400/35%+or- 3% ; Order code: PC53-1051). The viscoelasticity tensor of this plate has been evaluated using a smaller sample of the same material and is displayed in Table (2.3), (Castaings, M. and Hosten, B., 2000; Castaings, M., Hosten, B. et al., 2000).

A classic method used in ultrasonics for Lamb wave propagation is to have two transducers coupled to the sample as described in the previous section. One works as an emitter, the other as a receiver. This method is very efficient for the measurement of the velocity of guided modes, which is achieved simply by taking two measurements with different separation distances. However, it is not very suitable for attenuation measurements because of the variability of the coupling conditions when the transducer is positioned on the plate. It is difficult to have a constant coupling with any kind of contact method. The contact between the transducer and the plate can change (improve) with the time, and therefore raise the amplitude of the received signal. For a gel-coupled transducer, it is obvious that the coupling is dependent on the temperature of the gel and the extent to which it may have dried out, as well as the contact layer thickness and the solid contact with any surface asperities. These problems can be improved with a rigorous experimental protocol, but cannot be avoided. Furthermore, regardless of the kind of transducer, the Lamb waves spread as they travel along the plate, and this in itself reduces their amplitude, even in the absence of material attenuation. Clearly it is therefore very difficult to obtain measurements of the attenuation due to the material damping.

The problem can be minimised by keeping one of the transducers in contact in the same position throughout the duration of the experiments, while moving the other. This is the approach which was undertaken. For the moving transducer (the receiver), a laser interferometer sensor was used (POLYTEC). The laser measurements do not depend at all on coupling with the plate.

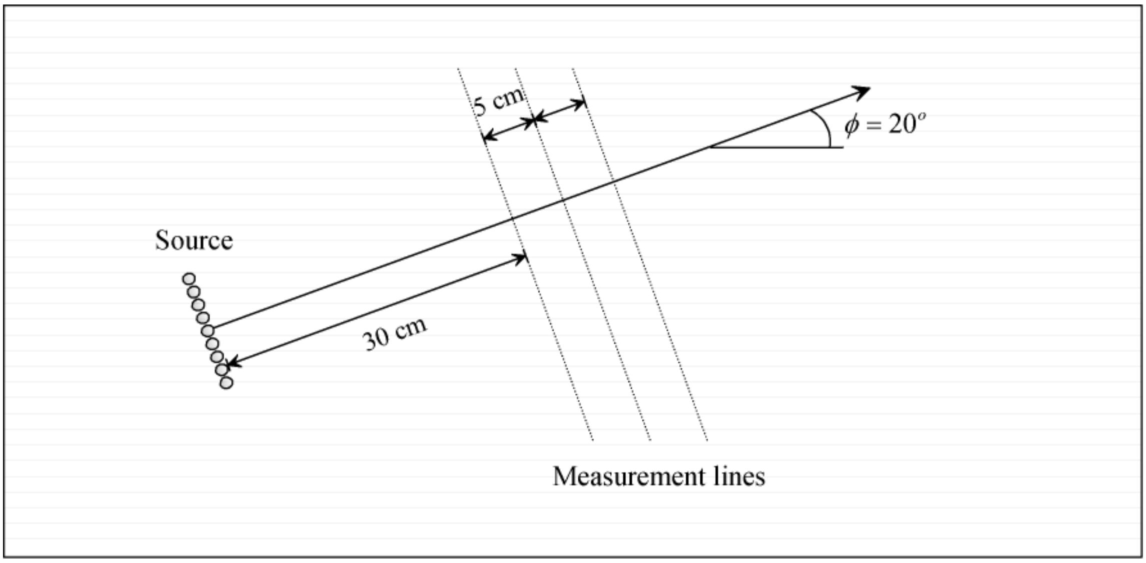

Figure 4.9: Experimental set-up. The line source is fixed to the panel. A laser interferometer is used to perform measurements along the dotted lines. Horizontal lines represent the fibres direction.

However, there is still a significant difficulty in that the sensitivity of the laser sensor is very much lower than that of a conventional piezoelectric transducer. This required a great deal of effort in maximizing the signal from the transmitting transducer and in setting up of both the emitter and the receiver. To get the most of the laser interferometer, a reflective tape has been used on the measurements spots. Fortunately it was still possible to make a good number of measurements, but this issue of sensitivity was a limiting factor in the range of what could be measured. The experimental set up is illustrated in Fig.(4.9). The line source is oriented with a 20 degrees angle with the fibres direction (0 degree). Measurements are performed every half centimetre at respectively 30, 35 and 40 cm away from the source.

Another issue is to find a source that can send approximately a plane guided wave in a particular direction. To play this role, a row of nine piezoelectric discs (1 mm thick and 10 mm wide each, from Morgan Matroc) has been utilised. The signal, which is sent to the source *via* a wave generator (Macro Design Ltd, U.), is a 5 cycles sinusoidal shaped signal, modulated by a Hanning window. Its directivity has been evaluated on an isotropic aluminium plate with the same experimental set up. The source was positioned in the 0 degree direction. Measurements were performed every centimetre, 35 centimetre away from the source, using the same interferometer as in the previous section.

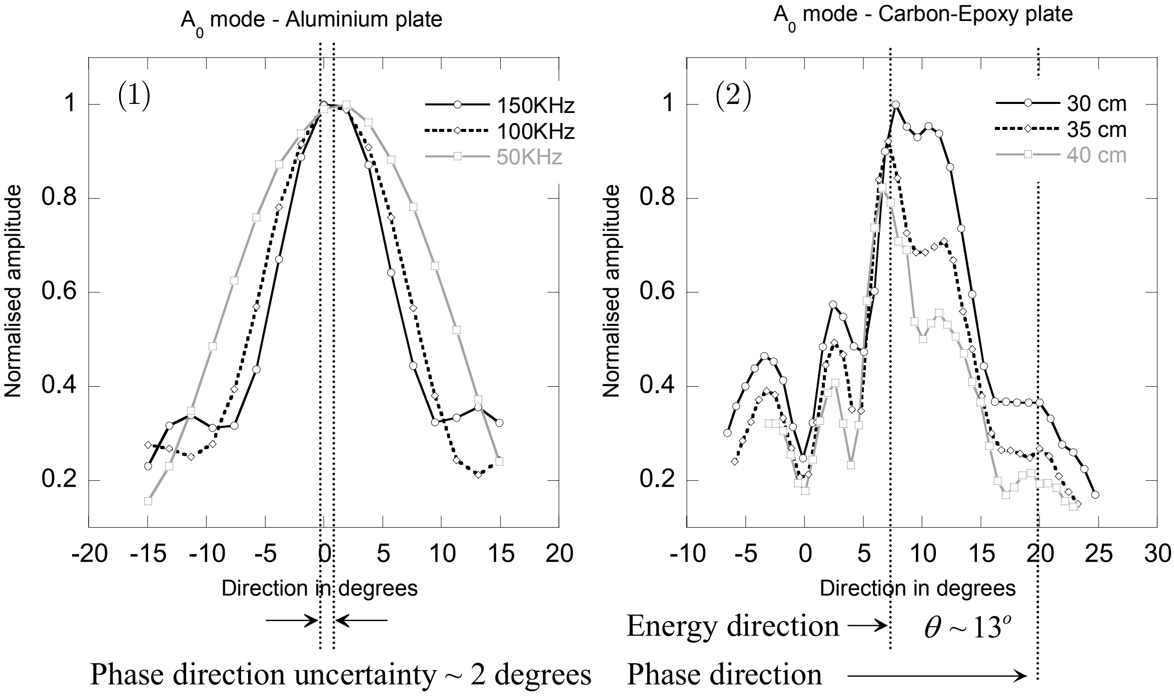

Figure 4.10: Directivity of the line source on aluminium plate (left hand side plot (1)*) after a propagation over 30 cm, and steering angle on Carbon-epoxy plate (right hand side plot* (2)*) at 50 kHz. All amplitudes have been normalised by the highest value of the received signals.*

The A_0 mode was identified using its energy velocity and its envelope amplitude was measured for several frequencies and displayed as a function of the direction of the observation. It appears on the left plot of Fig.(4.10(1)) that the line source can excite the A_0 mode in a chosen direction within 2 degrees of uncertainty. Moreover it can be seen that phase and energy travel in the same direction. Having illustrated the diffraction pattern associated to the A_0 mode in aluminium, results of the experiment on the carbon-epoxy panel can be interpreted. In Fig.(4.10(2)) the envelope amplitude of the A_0 mode excited at 50 kHz is displayed as a function of the direction of observation, for the three distances described above. The peak of amplitude is observed in the 7 degrees direction for all measurement lines, implying the 13 degrees steering angle since the main phase excitation direction is 20 degrees. This value is to be compared with the predicted steering angle which is 11 degrees. The discrepancy with the measured value is totally explained by the uncertainty of the source directivity. The agreement of the steering angle is therefore excellent and the phenomenon understood and illustrated.

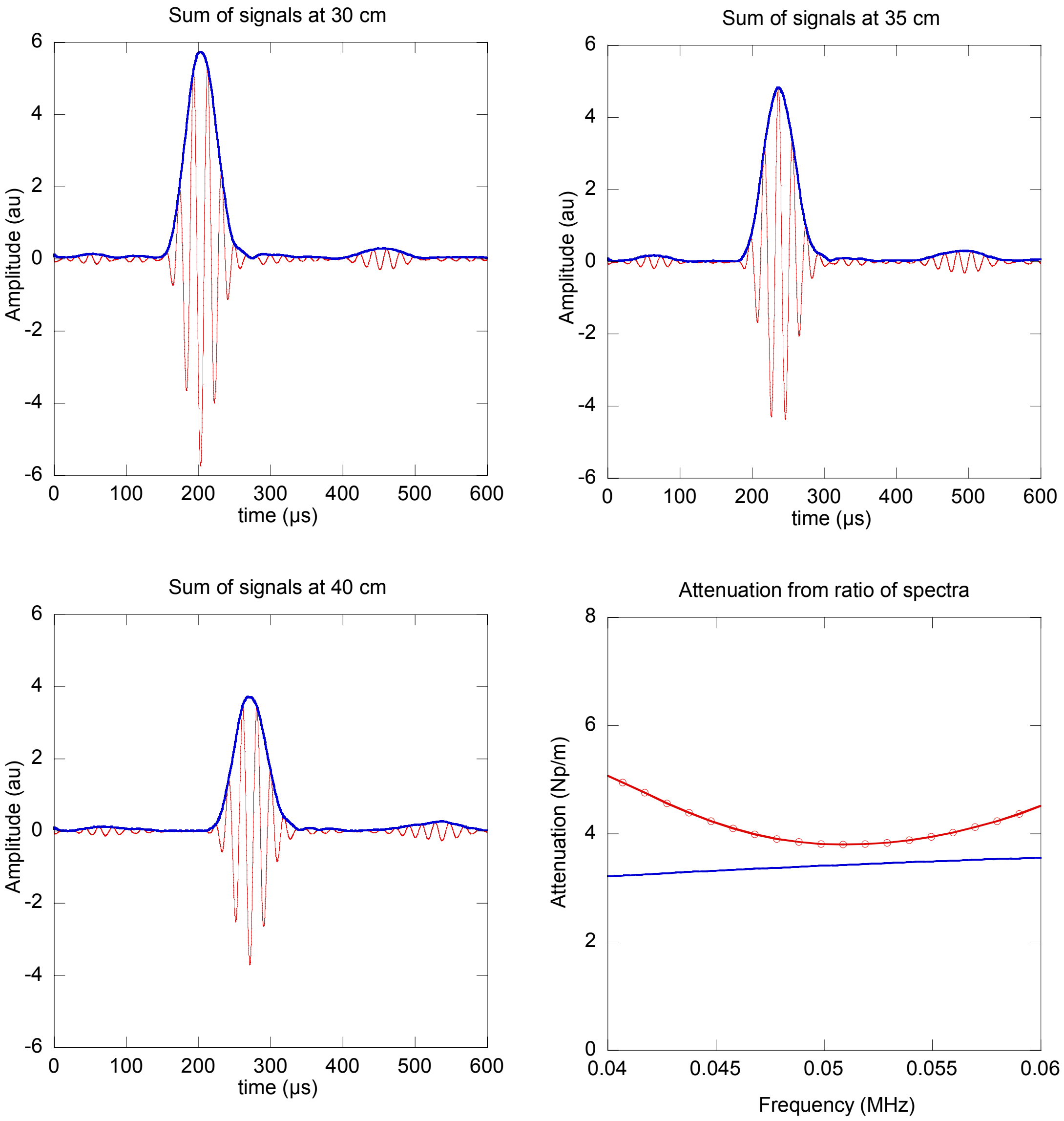

Figure 4.11: Sum of signals for the three measurement lines, respectively at 30, 35 and 40 cm away of the line source. The bottom right figure compares the computed prediction (solid line) with the experimentally obtained phase attenuation (lines and empty discs).

The aim of the second part of this section is to illustrate the attenuation of the A_0 mode in a non-principal direction (20 degrees). Using the sum of the signals on each row (measurement line described in Fig.(4.9)), it is possible to obtain a signal whose phase is close to the chosen phase direction. When summing all the signals of one row, interferences occur. All phase terms are constructive in the 20 degrees direction and destructive for the other directions. The resulting signal represents therefore a plane A_0 mode with the desired phase direction. This summation acts as an inverse Fourier transform of the emitted signal. Instead of summing all the wave number contributions to obtain the physical signal as a function of the coordinates and the time, the summation pulls out the wave number component corresponding to the chosen phase direction. In other words, the harmonic associated to the 20 degrees direction is extracted by the summation over the row.

This task was performed for the three distances of the experiment in order to compare their spectrum amplitudes. To get the phase attenuation of the A_0 mode, the spectrum division appears to be better suited than an exponential fit because of the small number of distance measurements. The summed signals and the comparison between prediction and measurements of the A_0 phase attenuation are shown in Fig.(4.10). As expected, the amplitude of the summation decreases with the distance. The attenuation measurement is obtained with the spectrum ratio described in the first section of the chapter, between lines at 30 and 40 cm away from the source. Bearing in mind that uncertainties on the imaginary parts of the viscoelasticity tensor are large, it is reasonable that the observed agreement between measured and computed phase attenuation is not ideal. Moreover, the summation over the lines has not been carried out over infinite lines but over a finite number of measurements. However attenuation values in the spectrum bandwidth of the experiment (around 50 kHz) describe reasonably the behaviour of the A_0 mode attenuation at low frequency.

With this experimental set up, it has been possible to observe quite precisely the beam deflection phenomenon, and to recover the phase attenuation of a fundamental Lamb mode. An interesting feature is also to evaluate the attenuation of a guided mode along its energy propagation direction. This is the aim of the next experiment described in the following section.

4.5 Attenuation and velocity along the energy direction

As stated in the introduction to this chapter, the overall motivation is for the practical use of guided modes in composites materials. For illustration and to see how detectable Lamb waves in composite are, another experimental set-up has been developed. The aim of this procedure is to measure the velocities and attenuations of selected guided modes in an anisotropic plate. The experimental program focused on the fundamental modes for a number of reasons. The attenuation of many of the modes is very high, in which case they are difficult or impossible to measure, the separation of multi-mode signals of the higher order modes is difficult, and the fundamental modes remain in any case the modes of greatest practical interest for structural monitoring.

A stack of two 5 mm diameter PZT discs (from Morgan Matroc) has been constructed for the transmitter (source). The two PZT discs were connected together electrically so that the power was amplified compared to only one disc. The source transducer was applied at the centre of the plate and was connected to a wave generator (Macro Design Ltd, U.). A laser interferometer (POLYTEC) was used as the receiver. The set up is shown in Fig.(4.12) and a detailed view of the source transducer is shown in Fig.(4.13).

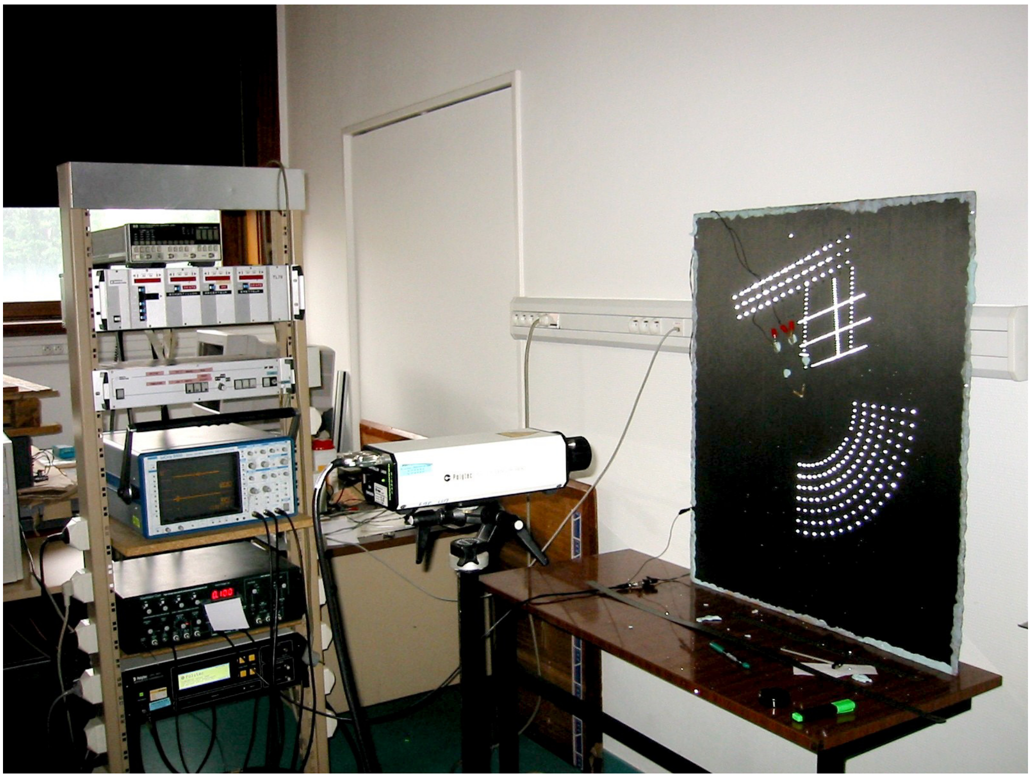

Figure 4.12: Point source-point receiver experimental set-up. The source is fixed to the unidirectional Carbon-epoxy panel. The laser interferometer can be moved to perform measurements on the 7 circle quarters described by the reflective tape spots in the picture.

The signal, which was sent to the emitting transducer, was a 5 cycles sinusoidal shaped signal, modulated by a Hanning window. The laser sensor was positioned so that the focusing of the laser beam could be precisely adapted to the spot on which it was aiming. The source always remained located at the same position. The measurements were made for two main frequencies 0.1 and 0.15 MHz. During the experiments, the laser sensor was moved from 150 mm to 300 mm away from the source, with a 25 mm step. The signal received from the laser sensor was visualised on an oscilloscope. Signals were then averaged before being recorded on a computer. The number of recorded signals was thus substantial, therefore a software routine was developed to treat these data efficiently and reliably (see the post-processing section).

The first thing to do before measuring attenuation was to recognise the guided modes. To identify a Lamb mode, the energy velocity has to be determined. Once the mode is identified, it is possible to follow it at several distances from the source and at different frequencies.

Theoretical computations have been performed at the same frequencies as the experiment was carried out. In Fig.(1.5) of Chapter 1, the slowness surfaces of the modes A_0, S_0 and SH_0 are shown.

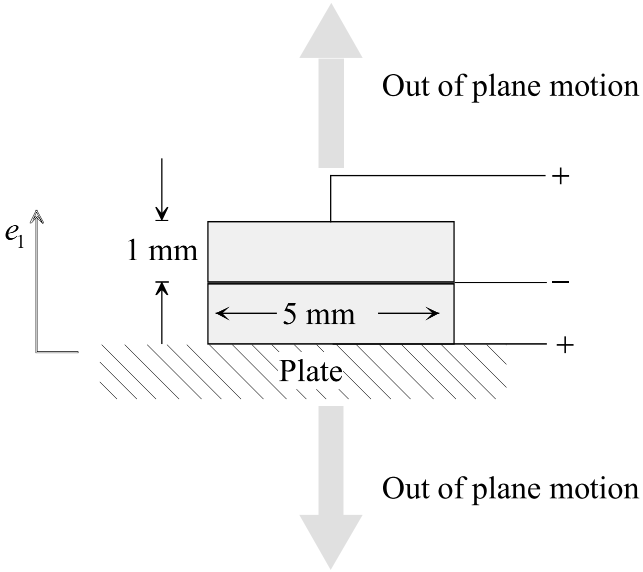

Figure: 4.13 Schematic of the source. Its dimension are small compared to the wavelength and the distance of propagation so that it can be assimilated to a point source.

Having the phase slowness and attenuation, it has been possible to calculate wave surfaces and attenuations along the ray direction for these modes. Velocity measurements are shown in Fig.(4.14) at 0.1 and 0.15 MHz. Not only the agreement is good, but it is also possible to see the diffraction of the SH_0 mode at the edge of the cusp. The accordance between predicted and measured energy velocity is excellent for the A_0 mode.

In Fig.(4.14), for energy angles above 70° (after the cusp), there are still experimental measurements of the SH_0 velocity, interfering with S_0. In the SH_0 cusp area, it was also possible to separate two or three arrival times for the same mode, but steered from different phase directions.

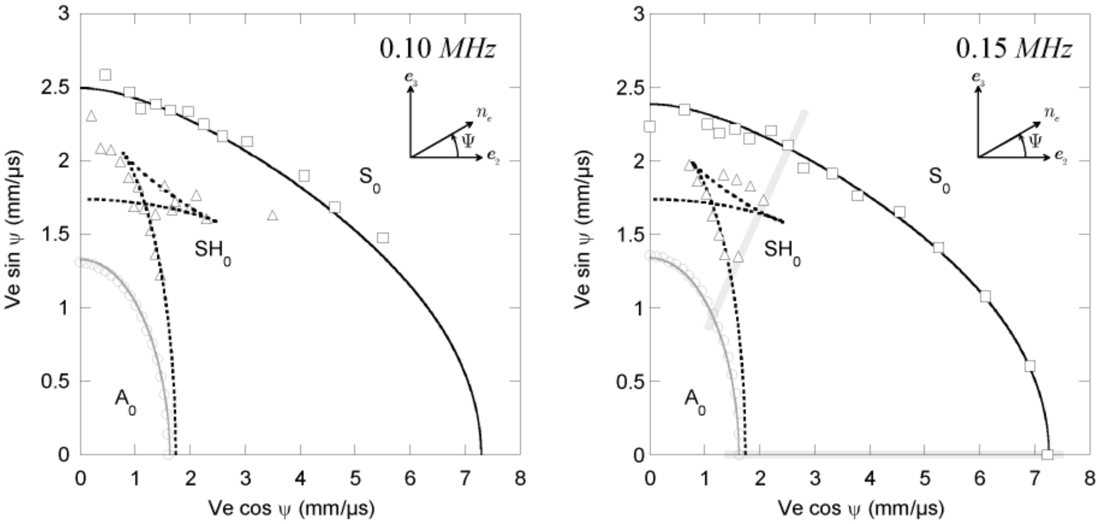

Figure 4.14: Experimental measurements of energy velocity and wave surfaces of fundamental modes. The horizontal axis represents the direction of the fibres. Shadowed zones correspond to 0 and 40 degrees direction, to be associated with signals displayed in Fig.(4.15).

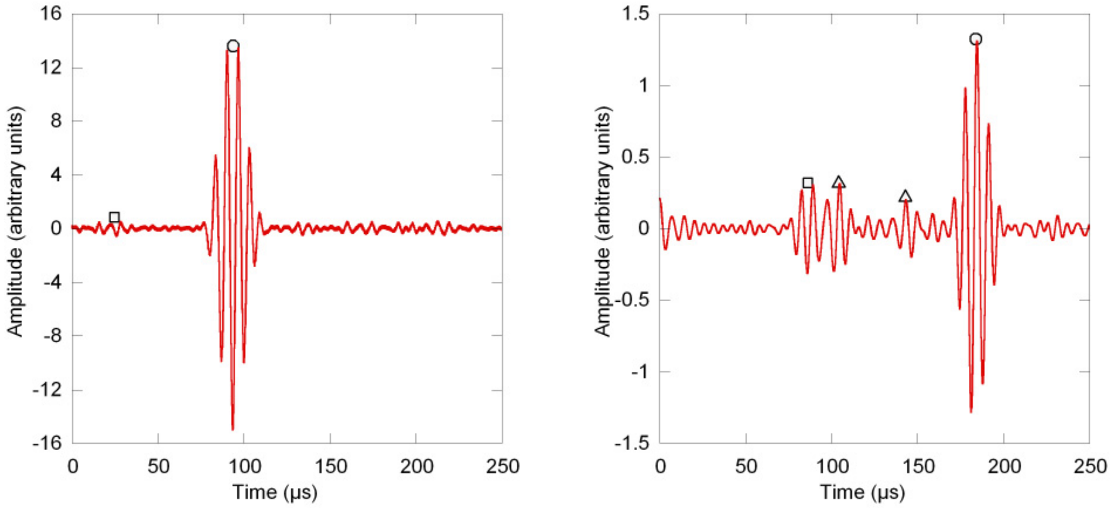

Figure 4.15: Experimental signals at 0.15 MHz. On the left hand side, the signal is quite powerful, in the 0 degree direction, 15 cm away from the source. On the right hand side, it is weaker and more complicated in the 40 degrees direction, 27.5 cm away from the source. Discs, squares and triangles denote the arrival time of A_0, S_0 and SH_0 respectively, to be associated with the polar measurements of Figs.(4.14) and (4.17).

Thus, despite the fact that only three branches of guided modes are present at 0.1 and 0.15 MHz, five different arrival times should be seen in directions that are within the cusp range. This means that, whereas the experimental signal is quite simple in the fibres direction, see Fig.(4.15), it becomes more complex in the cusp range.

With the post-processing described earlier, it has been possible to extract four of those five arrival times of the signal, and therefore four velocities. They have been indicated in Fig.(4.14). Such observations, which visualise the wave surface cusps, are well known for bulk waves, but believed to be novel for Lamb waves in lossy orthotropic plates.

The rheological model which was assumed was the hysteretic model, in which the imaginary part of the viscoelastic tensor is independent of the frequency. It appears that neither this model nor the Kelvin-Voigt model, described in Chapter 2, represents correctly the dependence of the guided mode attenuation with the frequency. The choice of the rheological behaviour is made on a model in which the C''_{ij} depend linearly by parts on the frequency. They are ruled by the following relation:

$$C''_{ij}(f) = C''^{0}_{ij} + \eta_{ij}\ \omega, \tag{4.4}$$

where C''^{0}_{ij} and η_{ij} are the coefficients of the straight line representing the dependence on the frequency of the C''_{ij}. The C''_{ij} have therefore been fitted, using experimental attenuation measurements of the A_0 mode, both at 0.1 and 0.15 MHz, they are shown in Table (4.16). In this adjusted model, the imaginary parts of the C''_{ij} depend linearly with the frequency, only for the considered bandwidth. Outside this region, the frequency dependence of the viscoelastic components is not modelled.

$f = 0.10$ MHz	$f = 0.15$ MHz
$C''_{11} = 0.280$	$C''_{11} = 0.300$
$C''_{12} = 0.600$	$C''_{12} = 0.650$
$C''_{13} = 0.250$	$C''_{13} = 0.260$
$C''_{22} = 7.500$	$C''_{22} = 7.600$
$C''_{23} = 0.300$	$C''_{23} = 0.320$
$C''_{33} = 0.600$	$C''_{33} = 0.610$
$C''_{44} = 0.280$	$C''_{44} = 0.200$
$C''_{55} = 0.100$	$C''_{55} = 0.085$
$C''_{66} = 0.120$	$C''_{66} = 0.135$

Table 4.16: Frequency dependent C''_{ij} of the carbon-epoxy plate, in GPa.

Results concerning attenuations are presented in Fig.(4.17), for 0.1 and 0.15 MHz. For the SH_0 mode, measurements are difficult to perform. In directions close to the principal directions, it has a small out of plane component, and is therefore not easily detectable. The amplitude of reception of this mode is much higher in the cusp region, but it has many arrival times, with different phase components. Because these components are very close in velocities, they interfere together and make attenuation measurements hardly possible. That is the reason why only a few attempts are shown in Fig.(4.17) for the SH_0 mode. As regards the S_0 mode, its amplitude was also too small or mixed with the SH_0 mode to perform reliable measurements, see Fig.(4.15). However, for the A_0 mode, which has a larger out of plane component than the other modes, it was possible to realize attenuation measurements.

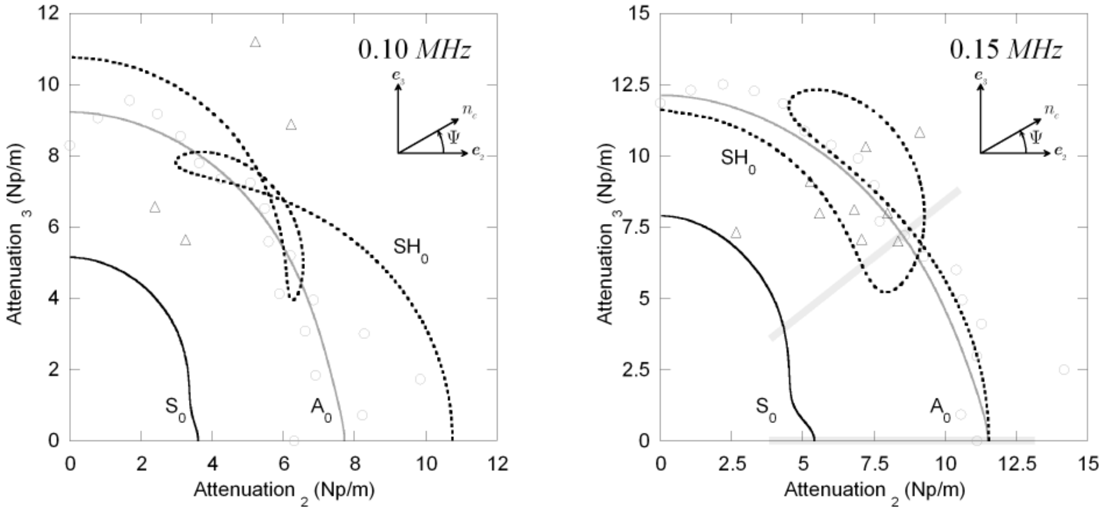

Figure 4.17: Experimental measurements and theoretical predictions of attenuation of fundamental guided modes. The horizontal axis is the direction of the fibres. Consistently with Figs.(4.14) and (4.15) the 0 and 40 degrees directions are shadowed.

Results agree with the projection of the phase attenuation along the ray direction, in polar coordinates, as seen in Fig.(4.17), and as a function of the frequency as seen in Fig.(4.18). Fig.(4.17) shows the attenuation of A_0 as a function of the frequency, along the observation directions 0, 35, 50 and 60 degrees respectively. These measurements demonstrate the dependence of the energy attenuation on the observation direction, as well as on the frequency.

Due to the back fitting realised on the C''_{ij} set of the material, these experimental measurements cannot be interpreted as a quantitative validation of this rheological model.

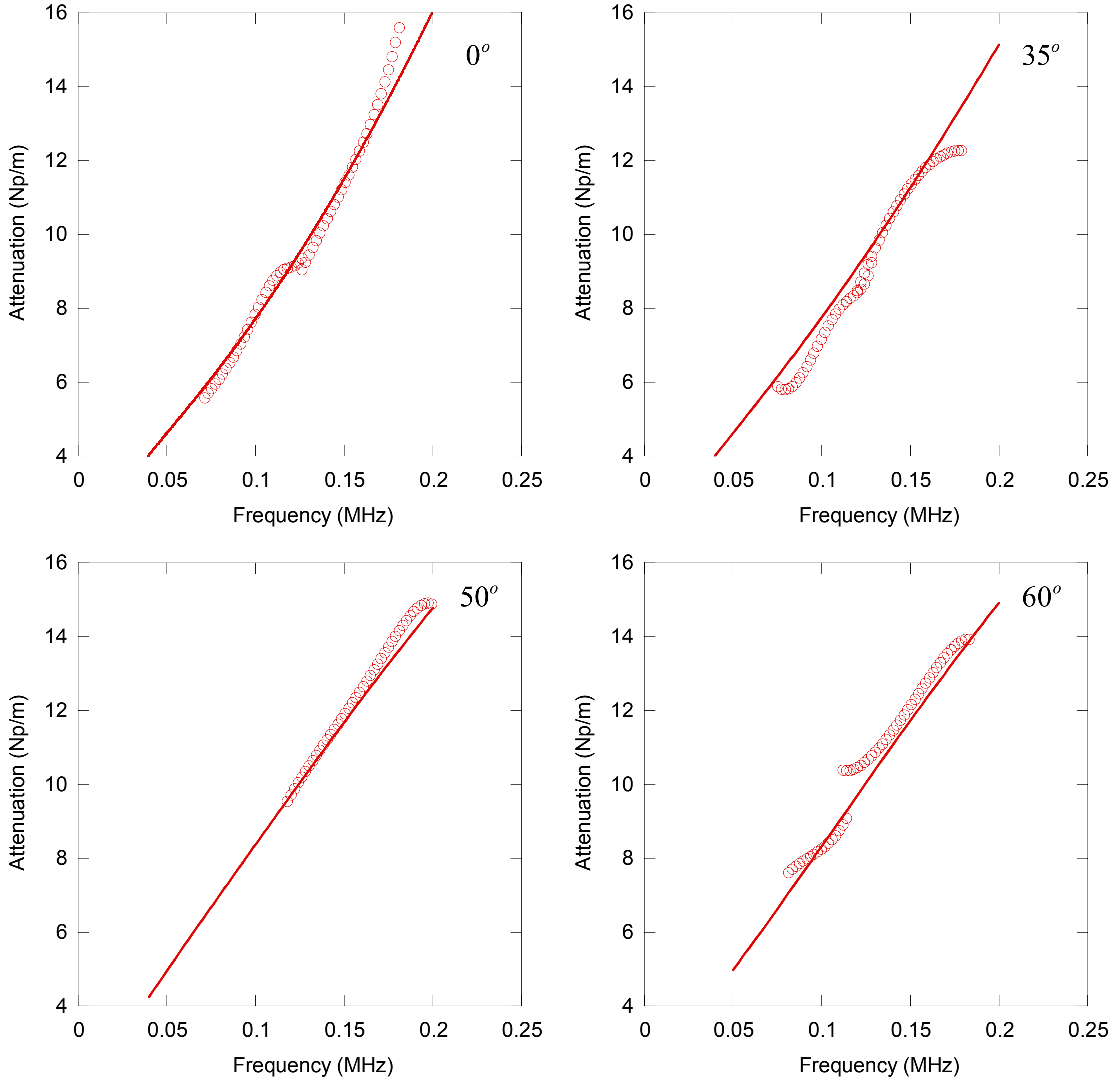

Figure 4.18: Attenuation along the observation direction for the A_0 mode. Empty discs are the measured attenuation in Np/m and the solid lines are the predictions made using the modified rheological model.

However, the adjustment concerns only the rheology of the material and does not compromise the qualitative understanding of the attenuation of the guided waves. As a proof, once the behaviour of the material has been set, the attenuation measurements agree with the predicted calculations, both as a function of the direction and the frequency. In any case, this experiment demonstrates that Lamb waves may offer good possibilities for characterising viscoelastic anisotropic materials.

4.6 Conclusion

In this experimental study, the focus has been put on understanding the properties of guided modes along the energy (observation) direction. An experimental illustration has been given for the fundamental modes propagating in unidirectional carbon and glass-epoxy plates. Concerning the energy velocities, good agreement has been found for all modes at low frequency. The beam deviation measurements of a single Lamb mode also proved to be in accordance with the computed predictions. It is believed that the experimental observation of the cuspidal features, manifested by the SH_0 plate mode, is a novelty for the Lamb waves.

This energy attenuation has been viewed as the projection of the phase attenuation onto the ray direction. For a point source-far field configuration, the theoretical derivation developed in Chapter 3, showed that this quantity is physically clear: this is the ratio of the dissipation energy due to viscosity and the total energy of the mode, i.e. the sum of both kinetic and elastic energies. Attenuation measurements have been realized for the A0 mode, demonstrating the potential of using Lamb modes for material characterisation.

This study emphasizes the need for dispersion curves representing the energy velocity in a chosen observation direction rather than for a fixed phase direction. A development of this work is viewed to be based on involving analytical dispersion curves for fundamental modes at low frequency (Shuvalov, A.L., 2000). This would make the computation faster and also facilitate the inverse problem for material characterization. This method should be an efficient way to determine complex viscoelastic components involved in low-frequency guided modes.

Conclusion

In this thesis, the properties of Lamb waves propagating in any direction of an orthotropic viscoelastic plate have been studied. The theoretical framework started with the solving of the dispersion equation for the purely elastic case. The derivative of the Lamb determinant was formulated analytically, and was shown to be valuable for the calculation of the phase slowness, the frequency and the phase direction, providing the numerical precision required for the following of a mode. Moreover, it enabled the frequency and angular dispersions of the phase velocity of the Lamb modes to be obtained quickly, as well as their associated group velocity. For non-principal directions in anisotropic plates, it is well-known that the phase front direction differs from the direction of the energy transport. The study of the group velocity is therefore only complete when both the modulus and the direction are determined. The frequency dispersion of the deviation angle has therefore been calculated and associated to the frequency dispersion of the modulus of the group velocity. The dependence of the properties of the Lamb modes on the frequency and the phase direction has been summed up in 3D plots.

The model was extended to take into account the viscosity of the insonified material, allowing the calculation of the wave attenuation caused by the material absorption. This attenuation depends on the frequency and on the phase front direction. A global 3D view, representing the dependence of the attenuation on these variables was given .

Another novelty brought by this work was the representation of the Lamb waves dispersion curves for the direction of observation. All the properties, i.e. the dependence on the frequency of the phase velocity, the energy velocity, the phase attenuation, the attenuation along the ray direction, and the deviation angle, were represented for a chosen energy direction. As opposed to the display of these properties for a fixed phase direction, this representation enabled the frequency dependence of the cusps of the wave fronts to be observed.

The attenuation along the ray direction, defined as the projection of the phase attenuation along the chosen observation direction, was also obtained. The study of this quantity has shown its physical interpretation: this is the ratio of the dissipation energy (caused by the viscosity) to the power flow carried by the Lamb wave (flow of the Poynting vector). A numerical application of these theoretical considerations has been achieved using the material data of a unidirectional carbon-epoxy plate and of a copper plate.

Finally, an experimental illustration of the described properties is presented in the last chapter. The validation of the group and energy velocity formulas (direction and modulus) is offered for the glass-epoxy plate. The beam skewing, predicted for the A_0 mode propagating in a carbon-epoxy plate, has been shown to correspond to the measured values. Complementary energy velocity measurements have been performed on the carbon-epoxy plate. The cusps of the SH_0 wave front have been observed at low frequencies in these measurements.

Experimental measurements of the attenuation of the guided modes as a function of the frequency and of the phase direction is a challenging task, because of the difficulty of obtaining the C_{ij} constants of the material, and in particular their imaginary parts. Initially the constants were measured using a bulk wave characterisation method. Then a rheological model that is valid in the experimental frequency bandwidth was chosen, and the imaginary parts were modified to fit to a few measured data for Lamb wave attenuation. This has been achieved for the A_0 mode propagating at relatively low frequency in the carbon-epoxy plate.

A valuable perspective of this work concerns the material characterisation. It has indeed been shown that, from a viscoelastic tensor obtained from the conventional method using bulk waves (at high frequency, compared to the frequency of the Lamb modes that can be easily detected), it is possible to refine the complex components of the tensor, and furthermore, for several frequencies. A rheological model involving a dependence of the attenuation on the frequency, which is a combination of several locally valid models, could therefore be empirically determined. To begin with, the assumption of low frequency or small thickness can be made, in order to obtain an explicit analytical formulation of the dispersion of the fundamental Lamb modes. With such a formulation, the inversion problem for which the aim is to obtain the constants as a function of the energy velocity, can be considered.

It is to be noted that the Lamb modes which are good candidates for easy excitation and propagation over large distances, are the fundamental modes at low frequency. Therefore, the range of NDE applications on composite structures is not restricted by this low frequency-thickness assumption.

From a more academical point of view, the calculation of the dispersion curves for a given energy direction can be optimised. The developed algorithm enables the computations of all the properties of a Lamb mode for a selected energy direction, from the frequency and angular dispersions of the phase velocity and the phase attenuation. An interesting research topic would be to obtain directly all the properties of the guided waves along the energy direction, for a faster inversion.

Conclusion

Dans cette thèse les propriétés des ondes de Lamb se propageant dans une direction quelconque d'une plaque orthotrope viscoélastique ont été étudiées. L'étude théorique porte d'abord sur la résolution de l'équation de dispersion pour le cas purement élastique. L'importance de l'expression analytique des dérivées du déterminant de Lamb, en fonction de la lenteur de phase, de la fréquence et de la direction de phase, se révèle dans la précision numérique nécessaire au suivi de mode. De plus, elle permet d'obtenir rapidement les dispersions fréquentielle et angulaire de la vitesse de phase des ondes de Lamb, ainsi que le calcul des vitesses de groupe associées. Pour les directions non-principales d'une plaque anisotrope, il est connu que la direction de phase des ondes guidées diffère de la direction du transport d'énergie. L'étude des vitesses de groupe n'est donc complète que si le module et la direction sont déterminés. La dispersion fréquentielle de l'angle de déviation a donc été calculé et associé à la dispersion fréquentielle du module de la vitesse de groupe. Les variations des propriétés des ondes de Lamb avec la fréquence et la direction de phase a été résumée dans des graphiques en trois dimensions.

La prise en compte de la viscosité dans le matériau insonifié permet le calcul de l'atténuation des ondes guidées causée par l'absorption du milieu. Cette atténuation dépend de la fréquence et de la direction de phase. Une vue globale en trois dimension des variations de l'atténuation avec ces paramètres est également présentée.

Une nouveauté apporté par ce travail est la représentation de la dispersion des ondes de Lamb pour une direction d'observation donnée. Toutes les propriétés, à savoir l'évolution des vitesses de phase, vitesse d'énergie, angle de déviation, atténuation de phase, atténuation le long du rayon, en fonction de la fréquence, sont représentées pour une direction de propagation d'énergie sélectionnée. Par opposition à la considération de ces quantités pour une direction de phase donnée, cette représentation permet par exemple d'observer l'évolution fréquentielle des cornes des surfaces d'ondes et se rapproche de la configuration expérimentale source et récepteur ponctuels. L'atténuation le long de la direction du rayon, définie comme la projection de l'atténuation de phase le long de la direction d'observation choisie, est également obtenue. L'étude de cette quantité a exhibé son sens physique: il s'agit du rapport énergie de dissipation (perte due à la viscosité) sur le flux de puissance transporté par l'onde (flux du vecteur de Poynting). L'application numérique des ces considérations théoriques a été réalisée sur un matériau composite de carbone-époxy unidirectionnel et un cristal de cuivre.

Enfin, une illustration expérimentale des propriétés décrites est proposée dans le dernier chapitre. La validation des formules de vitesse de groupe et d'énergie (direction et norme) est proposée pour une plaque de verre-époxy. D'autre part, la déviation du faisceau, calculée pour le mode A_0 se propageant dans une plaque de carbone-époxy, s'est avérée correspondre aux mesures réalisées sur ce matériau. Des mesures complémentaires de vitesse d'énergie ont été réalisées sur le carbone-époxy. L'observation de cornes présentes sur la surface d'onde du mode guidé SH_0 a pu être vérifiée expérimentalement.

En ce qui concerne les mesures d'atténuation, elles ont servies à choisir un modèle rhéologique valide dans la bande fréquentielle utilisée. A partir de ce modèle, les constantes viscoélastiques complexes, obtenues en premier lieu par une méthode de caractérisation utilisant les ondes de volumes, ont été réajustées sur les mesures expérimentales. Tenant compte de la difficulté de telles mesures, alliant à la fois les problèmes causés par l'anisotropie et ceux liés aux mesures d'atténuation, quantifier l'atténuation de modes guidés en fonction de la fréquence et de la direction de propagation est un réel défi. Il a été relevé pour le mode A_0 se propageant à relativement basse fréquence dans le carbone-époxy.

Une perspective importante de ce travail se situe dans le domaine de la caractérisation de matériau. Il a en effet été montré qu'à partir d'un tenseur de viscoélasticité obtenu par des méthodes conventionnelles utilisant les ondes de volumes (à haute fréquence, comparé à la fréquence des ondes de Lamb détectables), il est possible d'utiliser les ondes guidées pour affiner les constantes complexes, et ce, pour plusieurs fréquences. Un modèle rhéologique impliquant une atténuation dépendant de la fréquence par morceaux pourrait donc être déterminé de façon empirique. Dans un premier temps, il est envisageable de faire l'approximation de faible fréquence ou faible épaisseur dans le but d'avoir une expression analytique explicite de la dispersion des modes guidés fondamentaux, afin de pouvoir inverser le problème et d'obtenir les constantes en fonction des vitesses d'énergie.

Il est à noter que les modes de Lamb susceptibles d'être utilisés aisément sont les modes fondamentaux à basse fréquence. Cette approximation de faible fréquence-épaisseur n'apparaît donc pas restrictive quant aux applications de contrôle non-destructif.

Sur un plan plus fondamental, il semble intéressant de se concentrer sur l'obtention des courbes de dispersion pour une direction d'énergie choisie. L'algorithme développé calcule toutes les propriétés des ondes de Lamb pour une direction d'observation, à partir des dispersions fréquentielle et angulaire de la vitesse et l'atténuation de phase. L'obtention directe des paramètres des ondes guidées selon la direction d'énergie est un thème de recherche intéressant pour une inversion plus rapide.

References

Alleyne, D.N. and Cawley, P., (1991), "*The quantitative measurement of Lamb wave interaction with defects* ", Ultrasonics International, pp. 491-494.

Audoin, B., Baste, S. and Castagnède, B., (1991), "*Estimation de l'intervalle de confiance des constantes d'élasticité identifiées à partir des vitesses de propagation ultrasonores*", C.R. Acad. Sci. Paris Mécanique des Solides, 2, pp. 679-686.

Auld, B.A., (1973), "*Acoustic fields and waves in solids*", (1), Wiley-Interscience publication.

Auld, B.A., (1973), "*Acoustic fields and waves in solids*", (2), Wiley-Interscience publication.

Balasubramaniam, K. and Ji, Y., (2000), "*Skewing of the acoustic wave energy vector in stacked 1-3 anisotropic material systems*", Journal of Sound and Vibrations, 236, (1), pp. 166-175.

Balasubramaniam, K. and Whitney, S.C., (1996), "*Ultrasonic through-transmission characterization of thick fibre-reinforced composites*", NDT & E International, 29, (4), pp. 225-236.

Bar-Cohen, Y. and Mal, A.K., (1990), "*Characterisation of adhesive bonding using leaky Lamb waves*", Review of Progress in Quantitative NDE, Plenum Press, New York, pp. 1271-1277.

Bernard, A., Deschamps, M. and Lowe, M., (1999), "*Energy velocity and group velocity for guided waves propagating within an absorbing or non-absorbing plate in vacuum*", Review of Progres in Quantitative NDE, 18, pp. 183-190.

Bescond, C. and Deschamps, M., (1998), "*Dynamical surface response of a semi-infinite anisotropic elastic medium to an impulsive force*", J Acoust Soc Am, 103, (1), pp. 114-124.

Biot, M.A., (1952), "*The Interaction of Raleigh and stoneley waves in the Ocean Bottom*", Seismological Society of America, 42, pp. 81-93.

Biwa, S., Watanabe, Y. and Ohno, N., (2001), "*Modelling of ultrasonic attenuation in unidirectional fiber-reinforced plastics*", Nondestructive Characterization of Materials, 10, pp. 223-230.

Bonnin, A., Huchon, R. and Deschamps, M., (1999), "*Ultrasonic waves propagation in absorbing thin plates application to paper characterization*", Ultrasonics, 37, pp. 555 - 563.

Carcione, J.M., Cavallini, F., (1993), "*Energy balance and fundamental relations in anisotropic-viscoelastic media*", Wave Motion, 18, pp. 11-20.

Carcione, J.M., Cavallini, F., (1995), "*Attenuation and quality factor surfaces in anisotropic visco-elastic media*", Mechanics of Materials, 19, pp. 311-327.

Caroll, N.L., Humphrey, V.F. and Smith, J.D., (2002), "*Energy and phase velocity considerations required for attenuation and velocity measurements of anisotropic composites*", Ultrasonics, 40, pp. 525-530.

Castagnède, B., Kim, K.Y., Sachse, W. and Thompson, M.O., (1991), "*Determination of the elastic constants of anisotropic materials using laser-generated ultrasonic signals*", Journal of Applied Physics, 70, (1), pp. 150-157.

Castaings, M. and Hosten, B., (2000), "*Air-coupled Measurement of Plane Wave, Ultrasonic Plate Transmission for Characterizing Anisotropic, Viscoelastic Materials*", Ultrasonics, 38, pp. 718-786.

Castaings, M. and Hosten, B., (2001), "*Lamb and SH waves generated and detected by air-coupled ultrasonic transducers in composite material plates*", NDT & E International, 34, pp. 249-258.

Castaings, M., Hosten, B. and T., K., (2000), "*Inversion of Ultrasonic, Plane-Wave Transmission Data in composite Plates to infer Viscoelastic Material Properties*", NDT & E International, 33, pp. 377 - 392.

Cawley, P., (1987), "*The sensitivity of mechanical impedance method of non-destructive testing*", NDT International, 20, (4), pp. 209-215.

Cawley, P. and Alleyne, D., (1996), "*The use of Lamb waves for the long range inspection of large structures*", Ultrasonics, 34, pp. 287-290.

Challis, R.E., Bork, U. and Todd, P.C.D., (1996), "*Ultrasonic NDE of adhered T-joints using Lamb waves and intelligent signal processing*", Ultrasonics, 34, pp. 455459.

Chandra, R., Singh, S.P. and Gupta, K., (1999), "*Damping studies in fiber-reinforced composites-a review*", Composites Structures, 46, pp. 41-51.

Chimenti, D.E., (1997), "*Guided waves in plates and their use In materials characterization*", Applied Mechanical Review, 50, (5), pp. 247-284.

Christoffel, E.B., (1877), Ann. Mat. Pura Appl. 8, pp. 193.

Chu, Y.C. and Rokhlin, S.I., (1994), "*Analysis of composite elastic constant reconstruction from ultrasonic bulk wave velocity data*", Review of Progress in Quantitative NDE, Plenum Press, New York, pp. 1165-1172.

Dayal, V. and Kinra, V.K., (1989), "*Leaky Lamb waves in an anisotropic plate. 1:An exact solution and experiments*", J Acoust Soc Am, 85, (6), pp. 2268-2276.

Deschamps, M. and Assouline, F., (1999), "*Attenuation along the poynting vector direction of inhomogeneous olane waves in absorbing and anisotropic solids*", Acta Acustica, 86, pp. 295-302.

Ditri, J.J. and Rose, J.L., (1994), "*Excitation of guided waves in generally anisotropic layers using finite sources*", Journal of Applied Mechanics, 61, pp. 330 - 338.

Dorman, J., Ewing, M. and Oliver, J., (1960), "*Study of shear-velocity distribution in the upper mantle by mantle Rayleigh waves*", Bulletin of the Seismological Society of America, 50, (1), pp. 87-115.

Evans, M., Webster, J.R. and Cawley, P., (2000), "*Design of self-calibrating simulated acoustic emission source*", Ultrasonics, 37, pp. 589-594.

Every, A.G., Kim, K.Y. and Maznev, A.A., (1997), "*The elastodynamic response of a semi-infinite anisotropic solid to sudden surface loading*", J Acoust Soc Am, 102, (3), pp. 1346-1355.

Flandrin, P., (1993), "*Temps-Fréquence*", Hermes, Paris.

Gan, T.H., Hutchins, D.A., Billson, D.R. and Schindel, D.W., (2001), "*The use of broadband acoustic transducers and pulse-compression techniques for air-coupled ultrasonic imaging*", Ultrasonics, 39, pp. 181-194.

Ghosh, T., Kundu, T. and Karpur, P., (1998), "*Efficient use of Lamb modes for detecting defects in large plates*", Ultrasonics, 36, pp. 791 - 801.

Gruber, J.J., Smith, J.M. and Brochelman, R.H., (1988), "*Ultrasonic velocity C-scans for ceramic and composite material characterisation*", Materials Evaluation, 46, pp. 90-96.

Guo, N. and Cawley, P., (1993), "*The interaction of Lamb waves with delaminations in composite laminates*", J Acoust Soc Am, 94, pp. 2240-2246.

Guo, N., Lim, M.K. and Pialucha, T., (1995), "*Measurement of attenuation using a normalized amplitude spectrum*", Journal of Non-destructive Evaluation, 14, pp. 9-19.

Hosten, B., (1989), "*Anisotropic materials characterisation by single or double transmission ultrasonic method*", Ultrasonics International, pp. 31-35.

Hosten, B., (1991), "*Bulk heterogeneous plane wave propagation through viscoelastic plates and stratified media with large values of frequency domain*", Ultrasonics, 29, pp. 445-450.

Hosten, B., Deschamps, M. and Tittmann, B.R., (1987), "*Inhomogeneous wave generation and propagation in lossy anisotropic solids Application to the characterisation of viscoelastic composite materials*", J Acoust Soc Am, 82, (5), pp. 1763-1770.

Kundu, T., Ehsani, M., Maslov, K.I. and Guo, D., (1999), "*C-scan and L-scan generated images of the concrete/GFRP composite interface*", NDT&E international, 32, pp. 61-69.

Kundu, T., Maji, A., Ghosh, T. and Maslov, K., (1998), "*Detection of Kissing Bonds By Lamb Waves*", Ultrasonics, 35, pp. 573 - 580.

Lakes, R.S., (1999), "*Viscoelastic solids*", Franck A. Kulacki, university of Minnesota.

Lamb, H., (1917), "*On waves in an elastic plate*", Conference of the Royal Society, London, pp. 114-128.

Leclezio, E., (2002), "*Diffraction des ondes de Lamb par des fissures verticales*", Thesis, university of Bordeaux 1, n° 2472.

Leymarie, N., Aristégui, C., Audoin, B. and Baste, S., (2002), "*Identification of complex stifness tensor from waveform reconstruction*", J Acoust Soc Am, 111, (3), pp. 1232-1244.

Leymarie, N., Aristégui, C., Audoin, B. and Baste, S., (2002), "*Viscoelastic property identification from waveform reconstruction*", Review of Quantitative Nondestructive Evaluation, 21, pp. 1431-1438.

Lowe, M., (1995), "*Matrix techniques for modelling ultrasonic waves in multilayered media*", IEEE Transactions on Ultrasonics, Ferroelectrics and Frequency control, 42, (4), pp. 525-542.

Lowe, M.J.S., (1993), "*Plate Waves for the NDT of Diffusion Bonded Titanium*", Mechanical Engineering, London, Imperial College of Science Technology and Medicine, pp 300.

Lowe, M.J.S. and Cawley, P., (1994), "*The applicability of plate wave techniques for the inspection of adhesive and diffusion bonded joints*", Journal of Non-destructive Evaluation, 13, (4), pp. 185-199.

Lowe, M.J.S. and Diligent, O., (2001), "*The low frequency reflection characteristics of the fundamental symmetric Lamb wave S0 from a rectangular notch in a plate*", J Acoust Soc Am, (Submitted), pp.

Lowe, M.J.S. and Pavlakovic, B., N., (2001), "*DISPERSE User's manual version 2.0*".

Macro Design Ltd, U., "*"Wavemaker" general purpose function generator and receiver*".

Max, J., (1977), "*Méthodes et techniques de traitement du signal et applications aux mesures physiques*", Masson.

Maznev, A.A. and Every, A.G., (1995), "*Focusing of acoustic modes in thin anisotropic plates*", Acta Acustica, 3, (5), pp. 387-391.

Nagy, P.B., (1994), "*Leaky guided wave propagation along imperfectly bonded fibers in composite materials*", Journal of Non-destructive Evaluation, 13, (3), pp. 137-145.

Nagy, P.B. and Adler, L., (1989), "*Adhesive joint characterisation by leaky guided interface waves*", Review of Progress in Quantitative NDE, Plenum Press, New York, pp.

Nayfeh, A.H., (1995), "*Wave propagation in layered anisotropic media*", (39), Elsevier.

Nayfeh, A.H. and Chimenti, D.E., (1988), "*Ultrasonic wave reflection from liquid-coupled orthotropic plates with application to fibrous composites*", Journal of Applied Mechanics, 55, pp. 863-870.

Pavlakovic, B., Lowe, M., Alleyne, D. and Cawley, P., (1997), "*Disperse : a general purpose program for creating dispersion curves*", Review of Progress in Quantitative NDE, 16A, pp. 155-192.

POLYTEC, "*Model OFV 2700*".

Poncelet, O., Deschamps, M. and Lowe, M., (2000), "*Célérité de groupe des ondes de Lamb dans une plaque anisotrope*", Proceedings of the 5th Congress on Acoustics, pp. 169-172.

Potel, C., Gatignol, P. and Belleval, J.F., (2001), "*Deviation of the modal waves excited by an ultrasonic monochromatic beam in an anisotropic layer*", C.R. Acad. Sci, 329, (2b), pp. 815-822.

Potel, C., Gatignol, P. and Belleval, J.F., (2002), "*A stationary phase argument for the modal wave beam deviation in the time-space domain for anisotropic multilayered media*", Ultrasonics, 40, pp. 549-553.

Rayleigh, L., (1885), "*On waves propagating along the plane of an elastic solid*", Proc. London Math. Soc., 17, pp.

Rokhlin, S., (1979), "*Interaction of Lamb waves with elongated delaminations on thin sheets*", International Advances in Non-destructive Testing, 6, pp. 263-285.

Rose, J.L., (1999), "*Ultrasonic Waves in Solid Media*", Cambridge University Press ed.

Royer, D. and Dieulesaint, E., (1996), "*Ondes élastiques dans les solides*", Masson, Paris.

Sachse, W. and Pao, Y.-H., (1978), "*On the determination of phase and group velocities of dispersive waves in solids*", Journal of Applied Physics, 49, (8), pp. 4320-4327.

Safaeinili, A., Lobkis, O.I. and Chimenti, D.E., (1996), "*Quantitative materials characterization using air-coupled leaky Lamb waves*", Ultrasonics, 34, pp. 393-396.

Seifried, R., Jacobs, L.J. and Qu, J., (2002), "*Propagation of guided waves in adhesive bonded components*", NDT & E International, 35, (5), pp. 317-328.

Shuvalov, A.L., (2002), "*Theory of plane subsonic elastic waves in fluid-loaded anisotropic plates*", Proceedings of the Royal Society of London, 458, pp. 1323-1352.

Simon, C., (1997), "*Propagation des ondes de Lamb dans un matériau composite stratifié; application à la detection de délaminages*", Université de Paris 7.

Simon, C., Kaczmarek, H. and Royer, D., (1997), "*Elastic Wave Propagation Along Arbitrary Directions In Free Orthopic Plates Application To Composite Materials*", Proceedings of the 4th Congress on Acoustics, pp. 715-718.

Solie, L.P. and Auld, B.A., (1973), "*Elastic waves in free anisotropic plates*", J Acoust Soc Am, 54, (1), pp. 50-65.

Sun, K., J., and Johnston, P., H.,, (1995), "*Effect of rivet rows on propagation of lamb waves in mechanically fastened two-layer aluminum plates*", Review of Progress in Quantitive Nondestructive Evaluation, 14, pp. 1569-1577.

Szabo, T.L. and Wu, J., (2000), "*A model for Longitudinal and Shear Wave Propagation in viscoelastic Media*", J Acoust Soc Am, 107, pp. 2437 - 2446.

Tan, K.S., Guo, N. and Wong, B.S., (1995), "*Experimental evaluation of delaminations in composite plates by the use of Lamb waves*", Composites Science and Technology, 53, pp. 77-84.

Tan, K.S., Guo, N., Wong, B.S. and Tui, C.G., (1995), "*Comparison of Lamb waves and pulse in detection of near-plate surface defects in laminate plates*", NDT and E International, 28, (4), pp. 215-223.

Wilcox, P., Lowe, M. and Cawley, P., (2001), "*The effect of dispersion on long-range inspection using ultrasonic guided waves*", NDT&E international, 34, pp.

Wolfe, J.P., (1998), "*Imaging Phonon*", C.U.P. Cambridge.

Wu, T.T. and Liu, P.L., (1998), "*Adancement on the non-destructive evaluation of concrete using transient elastic waves*", Ultrasonics, pp. 197-204.

Wu, T.T. and Liu, Y.H., (1999), "*On the measurement of anisotropic elastic constants of fiber-reinforced composite plate using ultrasonic bulk wave and laser generated Lamb wave*", Ultrasonics, 37, pp. 405-412.

Résumé

Les propriétés de la propagation des ondes de Lamb en milieu anisotrope viscoélastique sont étudiées. Les variations de la vitesse de phase, de l'atténuation, de la vitesse d'énergie et de la déviation de faisceau sont décrites en fonction de la fréquence et de la direction de propagation du front de phase. Les considérations énergétiques prises en compte permettent d'étudier plus précisément la propagation de l'énergie des modes de Lamb. Ainsi, les courbes de dispersion ne sont plus décrites pour une direction de phase imposée, mais selon la direction d'observation. L'atténuation des ondes guidées le long du rayon est également détaillée. Une illustration expérimentale des propriétés décrites (vitesses de phase et d'énergie, angle de déviation, atténuation) est apportée en prenant l'exemple de plaques de carbone-époxy unidirectionnels, ainsi que de verre-époxy unidirectionnels.

Abstract

The properties of the Lamb waves propagating in viscoelastic anisotropic media are studied. The dependences of the phase velocity, the attenuation, the energy velocity, and the beam deviation on the frequency and on the phase front direction are described. The energy considerations taken into account enable a more precise study of the energy propagation of the Lamb modes. Thus, the dispersion curves are not plotted any longer for a given phase front direction, but for a chosen observation direction. The attenuation of the guided waves along the ray direction is also detailed. An experimental illustration of the described properties (energy and phase velocities, skewing angle, attenuation) is carried out on unidirectional carbon-epoxy and glass-epoxy plates.